

University of Montana

ScholarWorks at University of Montana

Graduate Student Theses, Dissertations, &
Professional Papers

Graduate School

2020

Dynein Light Chain 1 Functions as a Cofactor for Post-Transcriptional mRNA Regulation and RNA Granule Assembly

Nicholas Day

University of Montana, Missoula

Follow this and additional works at: <https://scholarworks.umt.edu/etd>



Part of the [Cell Biology Commons](#), and the [Developmental Biology Commons](#)

Let us know how access to this document benefits you.

Recommended Citation

Day, Nicholas, "Dynein Light Chain 1 Functions as a Cofactor for Post-Transcriptional mRNA Regulation and RNA Granule Assembly" (2020). *Graduate Student Theses, Dissertations, & Professional Papers*. 11624.

<https://scholarworks.umt.edu/etd/11624>

This Dissertation is brought to you for free and open access by the Graduate School at ScholarWorks at University of Montana. It has been accepted for inclusion in Graduate Student Theses, Dissertations, & Professional Papers by an authorized administrator of ScholarWorks at University of Montana. For more information, please contact scholarworks@mso.umt.edu.

Dynein Light Chain 1 Functions as a Cofactor for Post-Transcriptional mRNA
Regulation and RNA Granule Assembly

By

Nicholas John Day

BA, University of San Diego, San Diego, CA, 2015

Dissertation

Presented in partial fulfillment of the requirements for the degree of

Doctor of Philosophy
In Cellular, Molecular, and Microbial Biology

The University of Montana
Missoula, MT

June 2020

Approved by:

Scott Whittenberg
Graduate School Dean

Ekaterina Voronina
Division of Biological Sciences

Mark Grimes
Division of Biological Sciences

Jesse Hay
Division of Biological Sciences

Brent Ryckman
Biochemistry Program

Bruce Bowler
Biochemistry Program

Dynein Light Chain 1 Functions as a Cofactor for Post-Transcriptional mRNA Regulation and RNA Granule Assembly

Chairperson: Jesse Hay

Gene regulation is essential for ensuring maintenance, proliferation, and proper development of a cell. RNA binding proteins (RBPs) regulate gene expression by targeting and binding mRNAs to control their translation and often localize to cytoplasmic assemblies of protein and RNA called RNA granules to facilitate post-transcriptional mRNA regulation. Using *C. elegans* as a model organism, we report on the function of dynein light chain 1 (DLC-1), a subunit of the dynein motor complex, in post-transcriptional mRNA regulation in the gonad. Previous work suggests that DLC-1 is an RBP cofactor that functions independent of the dynein motor. It is unknown how widespread this regulatory role for DLC-1 may be or what direct interactions between DLC-1 and RBPs make mRNA regulation possible. The work presented in this dissertation suggests that DLC-1 is an important contributor to post-transcriptional mRNA regulation as well as RNA granule assembly. First, we used RNA immunoprecipitation coupled with high throughput sequencing (RIP-seq) to identify the mRNAs associated with DLC-1 through its interaction with RBPs. We found that DLC-1 is involved in post-transcriptional regulation of the oogenic transcriptome and demonstrated that DLC-1-associated transcripts depend on DLC-1 for regulation of their expression in the germline. From this work we identified the RBP OMA-1 as a new interactor of DLC-1 by an *in vitro* pulldown. Furthermore, we developed a protocol for application of *in situ* Proximity Ligation Assay (PLA) for use in *C. elegans* to probe for protein-protein interactions across developmental stages. This allowed us to detect formation of DLC-1/OMA-1 complexes in the gonad. Finally, we used a bioinformatic scan to find additional *C. elegans* RBPs that might interact with DLC-1. Using *in vitro* pulldowns, we verified predicted direct interactions between DLC-1 and 4 core RBP components of P granules, which are a subtype of RNA granule. Knockdown or knockout of *dlc-1* disrupts embryonic P granule assembly, suggesting that DLC-1 has an important role in this process. As a whole, this work expands upon the alternate and emerging functions of dynein light chains and suggests that cofactors like DLC-1 play critical roles in promoting mRNA regulation.

Acknowledgements

I would like to express my gratitude to:

Katya Voronina: for your encouragement and guidance as I pioneered my way through new techniques in the lab. Your enduring patience and ability to quickly resolve or troubleshoot different problems has helped me to be successful. During my time as a graduate student, I have learned so much about critical thinking, data analysis and interpretation, scientific writing, and many other things. I am grateful to have been able to work in this lab and receive such valuable training.

My committee members: for your helpful discussion and advice through the years.

Voronina lab members, past and present: for maintaining a collaborative environment that was a vibrant and friendly place to work in as a grad student.

My wife, Le: for your unending support and understanding of the woes of grad school and science, even during late nights or long weekends in the lab.

Friends and family, near and far: your continued enthusiasm for me as I pursued my degree, even if it was difficult to understand why I spent so much time studying worms.

The *C. elegans* community: your dedication to making information, resources, and worm strains accessible to others has made this model organism a great tool for biology.

| Table of Contents | Page |
|---|-------------|
| Abstract | II |
| Acknowledgements | III |
| List of Figures and Tables | V |
| Abbreviations | VII |
| | |
| Chapter 1: Introduction | |
| 1.1: Post-Transcriptional Control of Gene Expression | 1 |
| 1.1.1: Protein-RNA Interactions | 2 |
| 1.1.2: Biochemical and Computational Approaches to Identify RBPs | 3 |
| 1.1.3: Assembly of RNA Granules and Their Role in PTR | 5 |
| 1.2: Using <i>C. elegans</i> as a Model Organism to Study RBPs and PTR | 9 |
| 1.2.1: mRNA Regulatory Pathways that Govern Germ Cell Development | 10 |
| 1.2.2: Germ Granules in <i>C. elegans</i> Development | 16 |
| 1.3: Dynein Motor Complex | 17 |
| 1.4: Dynein Light Chain in Protein Complex Assembly and mRNA Regulation | 19 |
| 1.4.1: Dynein Light Chains in Protein Complex Assembly | 19 |
| 1.4.2: Dynein Light Chain in mRNA Regulation | 22 |
| | |
| Chapter 2: <i>C. elegans</i> DLC-1 Associates with Ribonucleoprotein Complexes to Promote mRNA Regulation | 25 |
| Introduction | 26 |
| Materials and Methods | 28 |
| Results | 32 |
| Discussion | 51 |
| | |
| Chapter 3: <i>In Situ</i> Detection of Ribonucleoprotein Complex Assembly in the <i>C. elegans</i> Germline using Proximity Ligation Assay | 55 |
| Introduction | 56 |
| Materials and Methods | 61 |
| Results | 64 |
| Discussion | 68 |
| | |
| Chapter 4: P Granule Components Interact with and Require DLC-1 for their Subcellular Localization | 73 |
| Introduction | 74 |
| Materials and Methods | 79 |
| Results | 84 |
| Discussion | 112 |
| | |
| Chapter 5: Conclusions and Future Directions | 120 |
| References | 133 |

| List of Figures and Tables | Page |
|---|-------------|
| Chapter 1 | |
| Figure 1.1: <i>C. elegans</i> Germline Development | 14 |
| Chapter 2 | |
| Figure 2.1: Expression and immunopurification of 3xFLAG::DLC-1 | 33 |
| Figure 2.2: Identification and characterization of DLC-1-associated RNAs | 36 |
| Figure 2.3: 3'UTR Motifs in mRNAs associated with DLC-1 | 42 |
| Figure 2.4: DLC-1 promotes expression control of its targets | 47 |
| Figure 2.5: DLC-1 binds OMA-1 <i>in vitro</i> | 50 |
| Figure 2.6: Model of DLC-1 involvement in different modes of post-transcriptional RNA regulation | 51 |
| Table 2.1: Nematode strains used in this study | 28 |
| Table 2.2: DLC-1 predominantly associates with protein-coding mRNAs | 38 |
| Table 2.3: DLC-1-associated mRNAs are enriched in oogenesis-related transcripts | 40 |
| Table 2.4: DLC-1-associated mRNAs are shared with several germline RBPs | 44 |
| Chapter 3 | |
| Figure 3.1: Schematic of <i>C. elegans</i> germlines | 57 |
| Figure 3.2: Representative images of workflow for germline PLA quantification | 63 |
| Figure 3.3: Representative images of germlines following co-immunostaining or PLA | 65 |
| Table 3.1: Summary of PLA results | 67 |

Chapter 4

| | |
|---|-----|
| Figure 4.1: P Granule asymmetry in 1-cell embryos | 76 |
| Figure 4.2: Motif scans identify <i>C. elegans</i> LC8-interacting proteins | 88 |
| Figure 4.3: Proximity ligation detects formation of DLC-1/PGL complexes in the germline | 91 |
| Figure 4.4: DLC-1 is co-expressed with PGL proteins throughout early embryogenesis | 96 |
| Figure 4.5: Proximity ligation assay detects formation of DLC-1/PGL complexes in early embryos | 99 |
| Figure 4.6: DLC-1/PGL complexes are enriched within P granules | 102 |
| Figure 4.7: <i>dlc-1</i> is required for PGL-1 and PGL-3 assembly into embryonic P granules | 108 |
| Figure 4.8: <i>dlc-1</i> is required for embryonic P granule integrity | 111 |
| Table 4.1: Nematode strains used in this study | 82 |
| Table 4.2: Antibodies used in this study for immunostaining | 83 |
| Table 4.3: LC8 interaction sites used for MEME analysis | 86 |

Abbreviations

| Acronym | Definition |
|----------------|---|
| BiFC | Bimolecular Fluorescence Complementation |
| CLIP-seq | Cross-linking Immunoprecipitation coupled with high throughput Sequencing |
| DLC-1 | Dynein Light Chain 1 |
| FP | Fluorescent Protein |
| FRET | Förster Resonance Energy Transfer |
| IDR | Intrinsically Disordered Region |
| IP | Immunoprecipitation |
| LLPS | Liquid-Liquid Phase Separation |
| mRNA | Messenger RNA |
| NG | Neuronal Granule |
| PB | Processing Body |
| PLA | Proximity Ligation Assay |
| PPI | Protein-Protein Interaction |
| PTM | Post-Translational Modification |
| PTR | Post-Transcriptional Regulation |
| RBD | RNA Binding Domain |
| RBP | RNA Binding Protein |
| RIC | RNA Interactome Capture |
| RIP-seq | RNA Immunoprecipitation coupled with high throughput Sequencing |
| RNAi | RNA Interference |
| SG | Stress Granule |
| SLiM | Short Linear Motif |
| SPC | Stem and Progenitor Cell |
| UTR | Untranslated Region |

Chapter 1

Introduction

An Elaborate Regulatory Network for Regulating Simple Messages

1.1: Post-Transcriptional Control of Gene Expression

Regulation of gene expression is a fundamental process that gives rise to different cell types, controls cell function, and ensures that genes are properly expressed during development. In order for a variety of cell types to be made from the same DNA blueprint, several regulatory steps dictate when and where genes are expressed. These regulatory mechanisms include those that govern RNA metabolism, starting with the initiation of transcription through to its decay after translation. RNA binding proteins (**RBP**s) directly interact with RNAs and are involved in post-transcriptional regulation (**PTR**) of RNA metabolism. There are several connected post-transcriptional steps that modify and prepare RNA for translation, including: splicing, capping, polyadenylation, and transport [1]. Following these processing steps, RBPs further regulate the storage and translation of mRNAs, which affects cell function [2,3]. Many RBPs coordinately work together to promote PTR in assemblies that include multiple proteins, and their target mRNAs. Mutations that compromise the function of RBPs can lead to cancer and neurodegenerative diseases [4-6]. Therefore, studies of RBP function in PTR illuminate broader biological processes and how deregulation results in disease. This chapter will describe approaches that are used to characterize RBPs and their target mRNAs, as well as the properties that allow RBPs to assemble into complexes associated with PTR. *C. elegans*, the model organism used in this dissertation research, will also be introduced

and how it can be applied to studies that examine RBP function and assembly. Finally, dynein light chain 1 (DLC-1), initially described as a subunit of the dynein motor complex, will be discussed as an emerging cofactor for RBPs, which is the focus of the research in this dissertation.

1.1.1: Protein-RNA Interactions

RBPs typically interact with the 5' or 3' untranslated regions (**UTRs**) of their target mRNAs [7-11]. Through these interactions with UTRs, RBPs exert post-transcriptional control over their target mRNAs [12]. Conventional RBP-RNA interactions are facilitated either by structured domains in the RBP called RNA-binding domains (**RBDs**), or by disordered RNA-binding regions [13,14]. Many RBPs are recognized based on the presence of a characterized RBD in the protein sequence and some RBPs contain multiple RBDs [15,16]. Amino acid residues of RBDs facilitate molecular interactions with RNA nucleotides allowing RBPs to interact with their target mRNAs [15]. RBP activity and mRNA binding capability is subject to regulation by cofactor binding, which can modulate RBP function [13,17]. For example, several DEAD-box family RNA helicases are known to associate with cofactors that promote their function or specificity for target mRNAs [18,19]. Many RBP-associated cofactors remain to be identified and the extent to which RBPs depend on cofactors also remains to be determined. Nevertheless, the findings to date suggest that cofactors are critical for RBPs to function as post-transcriptional regulators.

To identify what target mRNAs are associated with an RBP of interest, many studies have used protein-centric approaches such as RNA immunoprecipitation and

sequencing (**RIP-seq**) or cross-linking immunoprecipitation and sequencing (**CLIP-seq**) [20]. These approaches are informative for discovery of transcripts that are targeted by a single RBP and provide insight into what biological processes are regulated by the RBP. Sequencing data derived from CLIP-seq experiments can provide information on the binding elements that are recognized by RBPs. For example, PUF family RNA binding proteins, which contain the conserved Pumilio RBD, are extensively studied in several model systems, including *C. elegans*, *S. cerevisiae*, *D. melanogaster*, and humans. A study using CLIP-seq examined target mRNAs of *C. elegans* PUF proteins FBF-1 and FBF-2, which typically interact with target mRNAs in the 3' UTR, and found that target mRNAs contained a UGU triplet in the recognition site [11]. The core UGU interaction motif is conserved among target mRNAs of PUF family RBPs in other model organisms as well [21], suggesting that conserved RBDs can interact with similar recognition elements. This could prove to be useful for prediction of target mRNAs for RBPs that have not yet been documented or vice versa. As target mRNAs continue to be characterized for more and more RBPs, the power to predict potential protein-RNA interactions by comparison of homologous RBDs will improve.

1.1.2: Biochemical and Computational Approaches to Identify RBPs

As the number of documented RBPs continues to grow, the demand for broader identification of RBPs in a model system is increasing. While much of what is known about protein-RNA interactions has been based predominantly on protein-centric studies that look at RBPs individually, this approach is insufficient for broader identification of RBPs. As an alternative, *in silico* prediction software using databases of annotated RBDs

that scan and compare against proteomes can identify putative RBPs. This approach has expanded the landscape of what proteins binds RNAs in different model systems [22,23]. A caveat of this approach is that detection of additional RBPs is limited to comparisons made against characterized RBDs and may exclude RBPs with unknown or intrinsically disordered RBDs. As knowledge of protein sequences for novel RBDs become more available, algorithms that incorporate these RBDs continue to improve their sensitivity to predict RBPs [24,25]. These *in silico* approaches are useful as tools for prediction, however they may not accurately represent all instances of RBPs in a model system.

RNA-centric approaches have recently emerged as an alternate approach to broaden identification of RBPs on a larger scale. RNA interactome capture (**RIC**) uses mass spectrometry to identify RBPs in complex with polyadenylated mRNAs that are captured in a pulldown with oligo(dT)-coupled beads [26,27]. These studies have found that many proteins in complex with RNAs do not contain canonical RBDs [13,28,29], suggesting that the types of protein-RNA interactions are much broader than was previously known. Some RIC studies have found that proteins that were not previously known to interact with RNA, such as metabolic enzymes, have the capacity to bind RNAs [29-31]. To identify the specific peptide sequences in novel RBPs that interact with mRNAs, modified RIC approaches include additional steps that fragment crosslinked protein-RNA complexes by proteolysis to allow isolation of peptides in contact with RNA [32]. Following RNase treatment, these isolated peptides that interacted with mRNAs can be identified by mass spectrometry. RIC studies indicate that intrinsically disordered regions (**IDRs**) of proteins, which lack a stable structural conformation in isolation, also interact with RNA [13,14,33-35]. Taken together, these studies continue to

expand our understanding of what determinants define protein-RNA interactions as well as what is the scope of proteins that are involved in PTR.

1.1.3: Assembly of RNA Granules and Their Role in PTR

Coordination of cellular processes and signaling pathways in eukaryotes often involves compartmentalization of proteins into membrane-bound organelles. RNA regulation follows a similar principle of compartmentalization, where RBPs and RNA are sequestered into biomolecular condensates that are known as RNA granules. These condensates appear as foci in eukaryotic cells but are in fact membraneless organelles [36-38]. Previous research on *C. elegans* P granules, a type of RNA granule, has provided insight into how these condensates can form in the cell. The physical nature of P granules was revealed by several key observations, where P granules: had a spherical morphology, fused with one another upon contact, and exchanged contents with the cytoplasm [39]. These findings led to the proposal that P granules exist as dynamic, liquid droplets that form through phase transitions. This provided a foundation for current models that suggest RNA granule assembly occurs by way of a process called liquid-liquid phase separation (**LLPS**), where proteins are concentrated into a condensate that appears as a granule or a droplet in the cell [37,38,40,41]. LLPS occurs when proteins in a bulk, diffuse phase de-mix, resulting in the formation of a condensed, proteinaceous liquid phase that appears as a droplet and is suspended within the bulk phase, similar to de-mixing of oil and water [42]. This process causes certain proteins to become enriched in these liquid droplets while excluding others, thereby organizing proteins for coordinated function in a pathway [40]. Protein-protein interactions are important for LLPS, as they

can help nucleate the assembly of the core that promotes condensation of additional proteins into the liquid phase. LLPS-mediated RNA granule assembly is made possible by an array of types of protein-protein or protein-RNA interactions as described below.

At the molecular level, formation of RNA granules results from specific properties of granule-associated proteins that promote LLPS. RNA granule-associated proteins that possess oligomerization domains can locally concentrate proteins to promote LLPS and form a condensate [43,44]. IDRs, which are domains found in many RBPs, are also drivers of LLPS-mediated RNA granule assembly [41,45-47]. Disordered domains can interact with similar regions in other proteins that promote assembly and recruitment of additional proteins to RNA granules [45,48-50]. Short linear motifs (SLiMs) are often found in IDRs and serve as docking sites for other proteins that can promote LLPS-mediated RNA granule assembly [48]. Beyond protein-protein interactions, RNA can influence assembly of these condensates. RNA-RNA interactions may form scaffolds or seeds that recruit RBPs [51] and RNA also has the capacity to phase separate on its own without proteins [52,53], which is thought to help stabilize formation of RNA granules under certain conditions. Cofactors of RNA granule-associated proteins, including RBPs, can contribute to RNA granule assembly as well. Inclusion of cofactors can modulate LLPS-mediated assembly of RNA granule components and maintain stability of the condensates [54]. The variety of cofactors involved in this process and how they might contribute to RNA granule assembly is not yet known; however, research presented in this dissertation suggests that RBP cofactors may be integral to RNA granule assembly (see chapter 4). Through the array of different protein-protein, protein-RNA, or even RNA-RNA interactions described above, LLPS-mediated condensation and formation of

RNA granules is made possible. Studies in a number of model systems have documented multiple subtypes of RNA granules, which are differentiated based on their constituent proteins and mRNAs. These include stress granules, processing bodies, neuronal granules, and germ granules, each of which are briefly described next.

Cells adapt to stresses such as oxidation or heat by globally silencing translation through formation of stress granules (**SGs**) [55]. These granules contain stalled preinitiation complexes and RBPs, as well as proteins that nucleate SG assembly in the presence of stress. Translational arrest in SGs results from polysome disassembly and aggregation of RBPs with their target mRNAs [36,56]. Once a stress is removed and the cell recovers, SGs dissociate and translation can resume, suggesting that these types of RNA granules are only short-lived and temporarily store mRNAs in a translationally inactive state.

Processing bodies (**PBs**) are another type of RNA granule that share some components with SGs, such as the eIF4e translation initiation factor and several RBPs [56,57]. PBs are present under normal conditions in the cell, as opposed to SGs, which form under stressed conditions [58]. PBs contain mRNA decay machinery such as decapping enzymes and deadenylases [59,60], suggesting that PBs might be involved in mRNA degradation. However, recent evidence suggests that PBs may also function like SGs to stabilize mRNAs during stress [61]. Studies have identified interactions between PBs and SGs [62,63], suggesting that certain components such as mRNAs or proteins could be shuttled between the granules to facilitate either storage or decay of mRNAs.

Neuronal RNA granules (**NGs**), are transported by motor proteins that move along the cytoskeletal network to deliver NGs to different compartments of the neuron

[64,65]. Formation and transport of NGs to neuronal processes are implicated in remodeling the proteome in neuronal subcompartments like axons or dendrites [66,67]. RBPs localized to NGs target mRNAs to ensure their transport to specific regions of the neuron for local translation [65,68]. As a result, localized synthesis of proteins can create functional domains to promote localization of receptors in dendrites or ion channels in terminal regions of axons.

Germ granules are a type of RNA granule found in germ cells and they contribute to a wide range of germ cell functions including retaining totipotency of the germ cell, preventing aberrant differentiation of germ cells into somatic cells, and facilitating germ cell survival that is needed to transmit genetic information to the next generation. Germ granules are found in all animals; however, their distributions across developmental stages vary. *C. elegans* or *Drosophila* germ granules are present throughout development and are maternally loaded into progeny, while in other animals such as mammals, formation of germ granules is induced *de novo* in germ cells during embryo development [69,70]. Germ granules are required for germ cell function and fertility, but are not involved in specifying germ cells [69]. Germ granules contain RBPs that target and prevent translation of mRNAs encoding factors associated with reprogramming to a somatic cell-like fate [70,71]. Like NGs, germ granules store mRNAs that become translationally active in response to specific cues such as developmental stage [72,73].

Taken together, different subtypes of RNA granules facilitate post-transcriptional regulation through approaches involving transport, storage, or degradation of mRNAs. Findings that define how one subtype assembles or disassembles may prove to be

informative for other subtypes. Since RNA granules are important for regulating mRNA expression, mutations in proteins that are constituents of any of these granule subtypes can have detrimental effects on the function of a cell or animal development. Defects in RNA granule assembly are implicated in protein aggregation-related diseases, such as those associated with neurodegeneration, including amyotrophic lateral sclerosis [74] and Alzheimer's disease [75]. In addition, loss-of-function mutations in core germ granule components of male mammals affects sperm development and leads to defects in fertility [76]. This suggests that RNA granules play important roles in numerous pathways and necessitates further study to understand how they form and what functions they serve under both normal and diseased states.

1.2: Using *C. elegans* as a Model Organism to Study RBPs and PTR

The nematode *Caenorhabditis elegans* has been used as a model organism for biological studies for nearly 50 years. Many aspects of this nematode make it appealing for research, including a short developmental timeline from embryo to adult (~3 days), completely sequenced genome, and a hermaphrodite life cycle, with every individual capable of producing nearly 300 offspring within several days [77]. There is also a male sex of *C. elegans*, which can mate with hermaphrodites and allow exchange of genetic material to create worms with different genetic backgrounds. The nematode possesses a simple body plan that is comprised of: a gut, gonad, muscles, nervous system, and a transparent cuticle that allows observation of internal organs in an intact animal. More than 30% of human genes are orthologous to *C. elegans*, making it an ideal model organism for studying human diseases [78]. With the advent of CRISPR/Cas9 genome

editing in the recent decade, *C. elegans* genes can be mutated to alter and study their function or to include a fluorescent protein tag for the purpose of studying protein localization. In addition to genome editing, RNA interference (**RNAi**) is another facile tool that is used to study the function of genes, which is easily accomplished by directly feeding the nematode double-stranded RNA to knockdown a gene. As a result, RNAi is advantageous for experiments that involve screening many genes. These aspects and many others make *C. elegans* ideal to use as a model organism to study many fundamental biological processes, including PTR.

1.2.1: mRNA Regulatory Pathways that Govern Germ Cell Development

Among the several internal organs of the nematode, the gonad (also referred to as the **germline**) makes up roughly one third to one half the volume of the nematode [79]. The germline is formed by two U-shaped arms connecting to the uterus, from which hundreds of progeny are produced (marked in orange in the adult stage, Figure 1.1A). The organization of the germline resembles an assembly line, where stem cells undergo a differentiation program as they progress through the germline to produce gametes. The distal tip region of the germline contains a pool of self-renewing, mitotically dividing cells, which is referred to here as the germline stem and progenitor cell (**SPC**) zone (SPC zone; Figure 1.1B). These cells have features in common with stem cells found in other animals, such as self-renewal, differentiation, and multipotency [80], making *C. elegans* an ideal model system for studying stem cells and how their development is regulated. The distal tip region is capped by a somatic niche cell, which activates NOTCH signaling in SPCs to promote stem cell fate and maintenance and prevent expression of meiotic

entry proteins in the SPC zone [80,81]. As germ cells exit the SPC zone and enter the transition zone, they undergo a switch from mitotic to meiotic developmental program (Figure 1.1B). This transition and other stages of germ cell development are under control of a coordinated PTR network that ensures germ cells develop properly.

In the *C. elegans* germline, RBPs integrate into a post-transcriptional regulatory network that controls germ cell development [82,83]. In the SPC zone, a number of RBPs such as FBF-1, FBF-2, and PUF-8 regulate expression of their target mRNAs to promote maintenance of stem cells [84,85]. Identification of mRNAs that are targeted by these RBPs has provided insight into how the RBPs regulate this process [11,86]. FBF target mRNAs include cell cycle regulators, suggesting that FBFs regulate these genes to control maintenance of stem cells. Interestingly, FBFs also regulate mRNAs that encode other RBPs, such as *gld-1* and *gld-3* [87,88], which are important for promoting meiosis in germ cells that exit the SPC zone. As a result, FBF function is bipartite: 1) promote stem cell maintenance in the SPC zone and 2) prevent expression of factors associated with differentiation, such as GLD-1 and GLD-3. In contrast, the pachytene region of the germline requires RBPs that promote meiosis and differentiation and prevent mitosis and self-renewal. These include 3 GLD proteins and NOS-3, which form two pathways that promote meiosis and prevent mitosis [81,83]. Interestingly, in *gld-1* mutant germlines, germ cells that enter the pachytene revert back to mitotic divisions, resulting in formation of a tumor [89]. This emphasizes the importance of GLD-1 in regulating mRNA expression to prevent reentry into mitosis. Following meiosis, additional mRNA regulation is necessary for pathways controlling differentiation of meiotic cells into gametes.

A *C. elegans* hermaphrodite produces both male and female gametes from the same germline, which requires sequential activity of distinct regulatory pathways to ensure that the fates of the cells are properly specified. Spermatogenesis occurs during the L4 stage of nematode development (L4 stage; Figure 1.1A) and the RBP FOG-1 is required for differentiation of meiotic germ cells into sperm [90,91]. FOG-1 interacts with another sperm fate regulator, FOG-3 [92], which forms a multimer that binds mRNAs [93]. Identification of target mRNAs for both FOG-3 multimers and FOG-1 show that most are related to oogenesis, suggesting that both FOGs repress the oogenic program [92,93]. This is in agreement with the phenotypes of *fog-1* and/or *fog-3* mutant nematodes, where germ cells only differentiate into oocytes [91,94]. Like the spermatogenic program, the oogenic program also has its own distinct regulators.

During the adult stage of nematode development, the germlines switch from spermatogenesis to oogenesis (Adult stage; Figure 1.1A). RNP-8 is an RBP that forms a complex with GLD-2 to promote specification of oocyte fate and the stability of mRNAs associated with oogenesis [95,96]. Oocyte maturation is promoted by the RBPs OMA-1 and OMA-2 [97,98], which are also required for early embryonic development [99]. The RBP LIN-41 interacts and works antagonistically with OMAs to regulate expression of mRNAs that promote oocyte maturation [100,101]. Some RBPs that are important for the early stages of embryogenesis are expressed in the oocytes, such as the MEX and MEG proteins [102-104]. In particular, MEG-3 and its paralog MEG-4 are RBPs that are critical for promoting asymmetry of germ granules in early embryos [35,105].

Taken together, the *C. elegans* germline uses an elaborate post-transcriptional regulatory network to control germ cell development. Germline RBPs coordinately work

together to regulate different stages of development, forming regulatory units, also known as regulons [106,107]. These regulons govern critical steps in germ cell development such as: whether to continue proliferation or initiate meiosis, or whether to become a sperm or an oocyte. Through this regulatory network, RBPs facilitate a stereotypical program of development that has made the germline a useful resource for studying PTR. Beyond germline, RBPs are also involved in germ granule assembly in embryos, which also follow a stereotyped pattern of development.

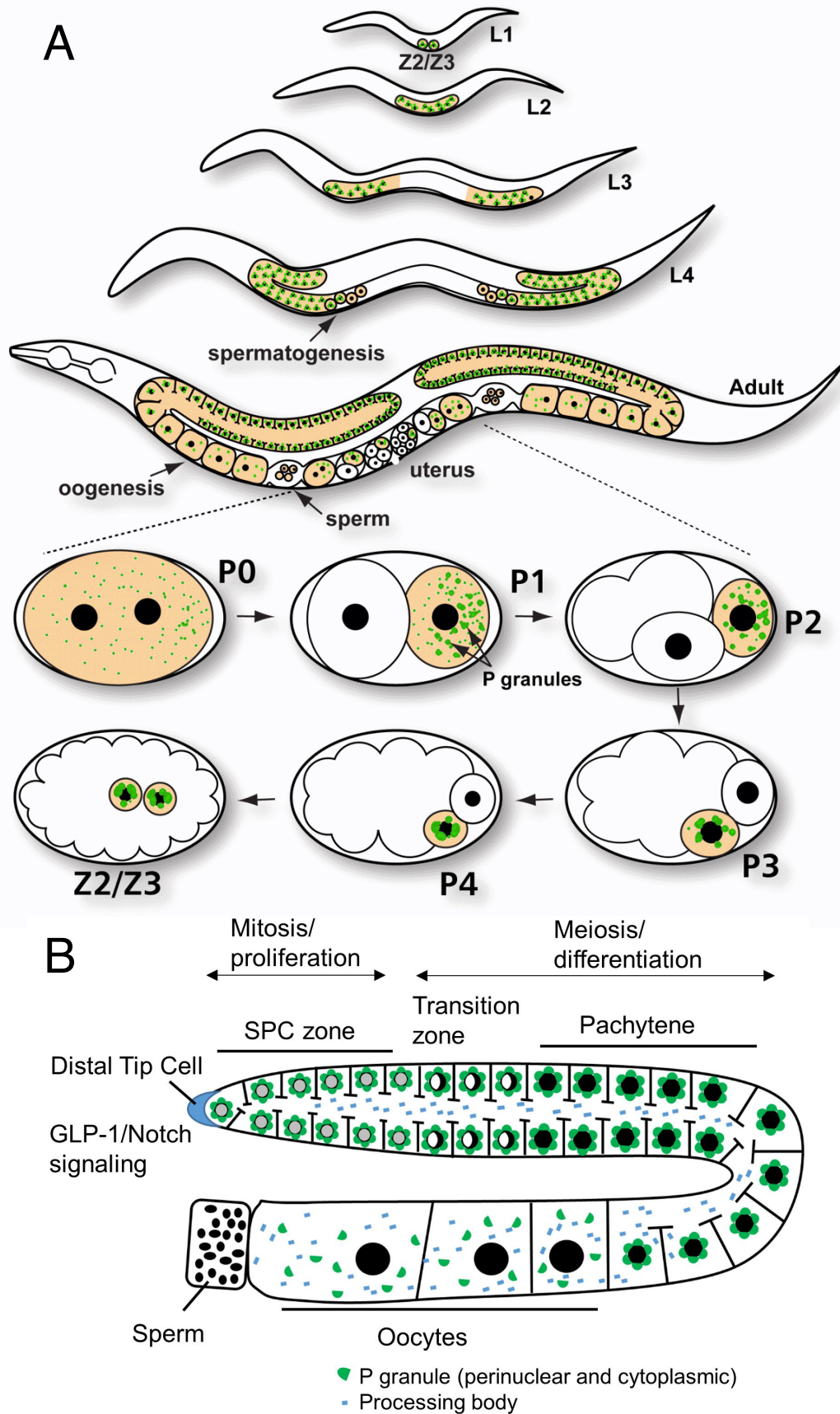


Figure 1.1: *C. elegans* Germline Development

- A) A schematic showing the development of the hermaphroditic germline. The germline is shaded in orange and P granules (i.e. germ granules, a subtype of RNA granules) are shown in green. As nematodes progress through larval stages L1-L3, the germline continues to proliferate and grow. During the L3 stage, some proliferating germ cells transition to meiotic divisions and initiate a differentiation program to produce sperm at the L4 stage. Adult stage germlines switch to oogenesis to produce oocytes that are self-fertilized by the previously made sperm. A more detailed view of the germline is provided below in panel B.
- During embryo development, the germ cell is recognized by asymmetric segregation of P granules into posterior region of the zygote. At the 2-cell stage, P granules are enriched in the P cell that serves as the germline precursor during further embryo development. This cell will asymmetrically divide 4 times during embryo development (stages P2-P4), as P granules continue to condense and become perinuclear. At approximately the 100-cell stage, the P4 cell symmetrically divides once to produce the Z2/Z3 cells, thereby establishing the primordial germ cells (PGCs) that remain quiescent until the L1 stage. L1-4 denotes larval stages. Figure is from [108].
- B) Detailed schematic of the adult, hermaphroditic germline. The distal tip cell activates GLP-1/Notch signaling in the germline to promote proliferation of cells in the stem and progenitor cell (SPC) zone. Progenitor cells that enter the transition zone switch to meiotic development and initiate a differentiation

program in preparation for becoming gametes (oocytes). P granules are shown in green and P bodies are in blue. Figure is adapted from [82].

1.2.2: Germ Granules in *C. elegans* Development

C. elegans germ cells contain germ granules, also known as P granules, which are present throughout the lifetime of the worm in the germline and embryos (Figure 1.1A) [109] and are required for fertility. In the germline, simultaneous depletion of multiple core P granule components leads to sterile worms with germ cells that express somatic-cell associated proteins and undergo defective oogenesis [71,110]. P granules protect germ cells by post-transcriptionally repressing expression of mRNAs that would drive them to differentiate into a somatic cell [70,71]. While P granules prevent abnormal differentiation of germ cells, they are not required for specification of germ cells during embryogenesis. Loss of components that promote P granule assembly or the disruption of P granule localization in early embryos still results in fertile and viable adult worms [103,111]. This suggests that P granules are not the main determinants needed to specify the germline in embryos, but are more important for PTR in the germline. Despite P granules being dispensable for germ cell specification in the embryo, their mechanism of assembly continues to be of interest during this stage of development as it provides insight into the mechanisms of cellular asymmetry.

Embryonic *C. elegans* P granules are a useful model system to study RNA granule assembly as the principles of their assembly and function may be similar to germ granules or even other types of RNA granules present in other animals. There are more than 40 known P granule proteins [108] and some of these proteins are homologous to

those found in other animals, such as the DEAD-box RNA helicases [112]. Conservation of germ granule components suggests that the mechanisms that drive germ granule assembly may also be conserved [113]. This supports the importance of understanding the principles of RNA granule assembly in model systems that can be applied to other animals. Identification of proteins involved in stepwise assembly of P granules (see introduction of chapter 4) or types of protein interactions that promote LLPS (as described in section 1.1.3) has provided insight into the determinants of RNA granule assembly. Research presented in chapter 4 highlights the importance of an RBP cofactor DLC-1 in promoting P granule assembly during the early stages of embryogenesis. DLC-1 was previously identified as a subunit of the dynein motor complex and as such, the remainder of this introduction chapter will describe the origin of DLC-1 and its homologs and how they came to be characterized as protein complex assembly cofactors.

1.3: Dynein Motor Complex

Molecular motors that move along cytoskeletal networks in eukaryotic cells are important for executing a number of different processes. Transport of proteins, vesicles, and organelles, as well as segregation of chromosomes in eukaryotic cells is facilitated by type 1 cytoplasmic dynein motor complexes [114,115]. In addition, type 2 cytoplasmic dynein is associated with intraflagellar transport of cargo that is important for formation and maintenance of cilia and flagella [116,117]. The axonemal class of dynein is involved in generation of force in flagella or cilia, which are required for motility [116,118]. Minus-end directed movement of the dynein motors along microtubules is

powered by ATP hydrolysis [116,119]. For clarity, only cytoplasmic dynein will continue to be discussed within the scope of this dissertation.

In addition to the functions described above, dynein motor complexes are also associated with RNA granules. The dynein motor localizes to and affects formation of stress granules in various cell types, including neurons and fibroblasts [120,121]. Through RNAi experiments, these reports demonstrated that knockdown of different subunits of the dynein motor impaired assembly of stress granules. As an alternate approach, additional studies have shown that destabilization of microtubules by nocodazole also prevents formation of stress granules [122,123]. In contrast, destabilization of microtubules induced formation of processing bodies [124,125], suggesting that dynein plays a dynamic role in promoting or impeding formation of different RNA granules. In zebrafish germ cells, dynein controls the size and distribution of germ granules [126]. This was based on observation that inhibition of dynein function led to fewer, but larger germ granules in the germ cell and also results in a significant reduction in the number of germ cells. These studies show that dynein contributes to the regulation of multiple types of RNA granules. Dynein motor complexes are comprised of multiple components that are crucial for motor function and will be briefly introduced below.

As a whole, the dynein motor is a multi-protein complex that is over 1 megadalton in size [127]. Heavy, intermediate, and light chain subunits of the dynein motor are defined based on their mass and mobility in SDS-PAGE gels [128]. Heavy chain subunits of the motor complex form dimers and bind ATP that powers their movement along microtubules [114,116,127]. An additional complex called dynactin

associates with the dynein motor as a cofactor, which promotes cargo binding as well as the movement of the dynein motor complex along microtubules [129,130]. The heavy chains contain long N-terminal tail domains that are recognized by the intermediate and light chains that promote assembly of the motor complex and docking of cargo [116,127]. These associated subunits also assemble as dimers on the motor complex and have important roles in maintaining the integrity of the motor complex dimers [116]. Absence of a light chain subunit results in defective function of the motor complex, where it aggregates, has reduced velocity and processivity, or becomes immobilized, as demonstrated in yeast [131]. Further, *in vitro* reconstitution of human dynein complexes found that the heavy chains aggregate without the presence of associated subunits, however inclusion of the intermediate and light chains promotes the assembly of the complex [132]. While these subunits are critical to the assembly, function, and recruitment of cargo, some serve additional functions beyond and independent of the dynein motor, making them important contributors to other cell functions.

1.4: Dynein Light Chain in Protein Complex Assembly and mRNA Regulation

1.4.1: Dynein Light Chains in Protein Complex Assembly

Dynein motor complexes contain three different classes of light chains known as: TCTEX, Roadblock, and LC8 [116,128]. Among these, the LC8 class of light chains are of particular interest as these subunits serve additional roles beyond the dynein motor, including post-transcriptional regulation (discussed below in section 1.4.2). LC8 family light chains were initially described as a subunit of the axonemal dynein motors present in single-celled algae [133], however they are also associated with cytoplasmic dynein

motor complexes [134,135]. Comparative analysis of LC8 genes shows that they are highly conserved across eukaryotes [118], and knockdown or knockout of LC8 is lethal in model systems such as *C. elegans* [136], *D. melanogaster* [137], and mouse [138]. This suggests that LC8 plays an essential role in these model organisms, however it may accomplish this through different mechanisms.

LC8 proteins have a wide array of protein interaction partners besides the dynein intermediate chain subunits [139]. These observations led to the initial proposal that LC8 functions as a cargo adapter for the dynein motor complex [140,141]. However, some LC8 partner proteins are not associated with the dynein motor [139,142]; these include but are not limited to: the pro-apoptotic factor Bim [143], the transcription factor of LC8 itself, ASCIZ [144], and Nup159 nucleoporin [145]. In addition, observation of cytosolic LC8 that is not bound to the dynein motor supports LC8's function independent of motor complex [146,147]. As a result, these observations led LC8 to be characterized as a motor-independent hub protein that is essential for a variety of different pathways, such as transcriptional regulation, tumor suppression, and apoptosis [139,142,148]. Research on the molecular interactions between LC8 and its binding partners has provided insight into how LC8 can serve a hub-like role. LC8 proteins assemble as homodimers that form 2 symmetrical binding grooves where binding partners interact [149]. With these 2 binding sites, LC8 can promote homo- or hetero-dimerization of its interaction partners and facilitate changes in their structural conformation or function [139,150]. For example, the interaction partner Swallow, contains disordered regions that form alpha helices upon binding to LC8 [151,152]. Through these types of interactions, LC8 can function as a bivalent scaffold that recruits additional proteins to form larger complexes

[139,150]. To better understand LC8's role as a hub, identification of interaction sequences that LC8 recognizes has been important for the field.

Studies of LC8 binding sites in a variety of proteins revealed that they are short, linear motifs (SLiMs), similar to other SLiMs in that they often confer binding between LC8 and different disordered proteins (recall SLiMs from section 1.1.3) [139,142,153]. Additionally, many LC8 interacting proteins and individual binding sites were identified by high throughput approaches including pepscanning [154,155], yeast-two hybrid [156], and phage display [146,157]. Together, these studies generated a consensus interaction motif that represents how often residues are observed at a specific position. In general, LC8 interaction sequences are at least 8 amino acids long and contain a conserved Threonine-Glutamine-Threonine (TQT) triplet [139,158,159], also known as the TQT motif anchor [160]. LC8 interaction sequences do diverge from the TQT motif and may contain residues such as Glutamine-Valine-Aspartate (QVD) [139,154], suggesting that the LC8 interaction interface has some plasticity for a variety of different binding sequences. Interestingly, the residues in LC8 that confer plastic binding with different interaction sequences are actually well conserved across animals [146]. Together, conservation of LC8 and the large volume of documented LC8 interaction sequences have enabled prediction of additional interaction partners through *in silico* analysis of different model system proteomes [157,161] (also see chapter 4). As a result, these approaches have expanded the interactome of LC8 and provided insight into other potential pathways that are regulated by LC8. Since LC8 interacts with many proteins and promotes their function, it is likely an important component for a variety of pathways

in the cell. In particular, the research presented in this dissertation is focused on LC8's role in post-transcriptional regulation, through interaction with RBPs.

1.4.2: Dynein Light Chain in mRNA Regulation

LC8 can contribute to PTR either through supporting dynein motor function or in a dynein-independent fashion. Transport of mRNAs by the dynein motor has been observed in different model systems [162] and LC8 may contribute to this process by promoting motor function [131]. LC8 has also been proposed to link cargoes such as RBPs with their target mRNAs to the dynein motor complex for transport. This is suggested based on observations where LC8 interacts with RBPs that are transported by the dynein motor. One example is the male mouse germ cell-expressed protein Dazl, which is a member of the DAZ family RBPs that are important for fertility [163]. Dazl binds with LC8, which leads to transport of Dazl and its associated mRNAs by the dynein motor in the cell [164]. However, recent mounting evidence suggests that LC8 functions with RBPs independent of the motor.

The dynein motor-independent role of LC8 is supported by findings that highlight LC8's incompatibility with its proposed role as a cargo adapter. When LC8 dimers associate with dynein-motor subunits, both binding sites are occupied by the interaction with dimeric dynein intermediate chains [165,166]. As a result, cargo is unable to be linked to the dynein motor via LC8 and suggests that only the cytoplasmic, dynein-free LC8 is able to interact with its partners [147,167]. This argues against LC8's cargo adapter function suggesting that LC8 supports interactions between RBPs and the dynein motor through a different mechanism. If LC8 does not link cargoes such as RBPs to the

dynein motor, then the question becomes: what is the role of LC8 in post-transcriptional mRNA regulation in the cell? Studies on the *Drosophila* RBP Egalitarian and its associated protein Bicaudal-D may provide insight into alternate functions of LC8. Both Egalitarian and Bicaudal-D function together to link mRNA to the dynein motor so that it is transported in oocytes and embryos [168]. LC8 interacts with Egalitarian [169], which in turn promotes Egalitarian dimerization and RNA binding [170]. This allows Egalitarian to then bind to Bicaudal-D that also interacts with dynactin, thereby promoting association of Egalitarian with the dynein motor [170]. This suggests that LC8 serves as a cofactor to promote dimerization and/or function of its diverse network of interacting partners, including those associated with the dynein motor.

Previous research in the Voronina lab has concluded that LC8 functions as a cofactor for RBPs that facilitate post-transcriptional regulation of development in the *C. elegans* germline. Dynein light chain 1 (**DLC-1**) is the representative homolog of the LC8 protein family in *C. elegans*. DLC-1 was previously found to directly interact with and promote the function and localization of the stem cell maintenance RBP FBF-2 [171]. By genetic interaction, *dlc-1* is important for FBF-2 function and promotes FBF-2 activity independent of the dynein motor. Additionally, the RBP GLD-1, which is important for transition of germ cells to meiosis, also was found to directly interact with DLC-1 [172]. Like FBF-2, GLD-1 requires DLC-1 as a cofactor for its function as a post-transcriptional regulator in the germline. These findings led to the proposal that DLC-1 has an alternate function as a germline RBP cofactor independent of the dynein motor. Both FBF-2 and GLD-1 function as translational repressors of their target mRNAs and loss of *dlc-1* results in de-repression of target mRNAs for both RBPs. Since FBF-2 and

GLD-1 serve opposing roles in the germline, it is possible that DLC-1's function is not limited to a single regulatory circuit, and DLC-1 may facilitate other germline mRNA regulatory pathways. The prevalence of DLC-1's role as a germline RBP cofactor remains unknown and raises additional questions about how it may facilitate germline mRNA regulation. In this study, **we hypothesized that DLC-1 interacts with many RBPs and promotes their mRNA regulatory role in *C. elegans* germline development.** The research in this dissertation aims to address several major questions about DLC-1 as an RBP cofactor. 1) What mRNAs are associated with DLC-1/RBP complexes? 2) Do these associated mRNAs depend on DLC-1 for regulation of their expression? 3) What are the RBPs beyond FBF-2 and GLD-1 that associate with and require DLC-1 for their function?

Chapter 2

***C. elegans* DLC-1 Associates with Ribonucleoprotein Complexes to Promote mRNA**

Regulation

(The following chapter is a modified version of the manuscript that was published in FEBS Letters 2018. <https://febs.onlinelibrary.wiley.com/doi/full/10.1002/1873-3468.13259>)

Abstract

Ribonucleoprotein complexes, which contain mRNAs and their regulator proteins, carry out post-transcriptional control of gene expression. The function of many RNA-binding proteins depends on their association with cofactors. Here we use a genomic approach to identify transcripts associated with DLC-1, a protein previously identified as a cofactor of two unrelated RNA-binding proteins that act in the *C. elegans* germline. Among the 2732 potential DLC-1 targets, most are germline mRNAs associated with oogenesis. Removal of DLC-1 affects expression of its targets expressed in the oocytes, *meg-1* and *meg-3*. We propose that DLC-1 acts as a cofactor for multiple ribonucleoprotein complexes, including the ones regulating gene expression during oogenesis.

Introduction

Post-transcriptional mRNA regulation is crucial for gene expression control [1]. RNA-binding proteins (RBPs) carry out this regulation by forming complexes with messenger RNAs (mRNAs), and each RBP associates with multiple mRNA species. The mRNAs associated with a specific RBP are thought to be coordinately regulated to govern a specific biological function and form a “post-transcriptional RNA operon” [106,107,173]. The development of the *Caenorhabditis elegans* germline is a prime example of a process extensively regulated at the post-transcriptional level [174]. *C. elegans* germ cells follow a defined developmental pathway aimed at the production of gametes [175]. Stem cell proliferation and self-renewal takes place at the distal region of the gonad supported by activation of GLP-1/Notch signaling [81]. At the post-transcriptional level, stem and progenitor cell proliferation is supported by PUF-domain RBPs FBF-1, FBF-2, and PUF-8 [84,85,176,177]. As germ cells exit the proliferative zone, they enter meiosis. This switch from proliferation to differentiation is mediated by the activities of diverse post-transcriptional regulators including a KH/STAR domain RBP GLD-1 and cytoplasmic poly(A) polymerase GLD-2 [88,178,179].

After completion of the pachytene stage of meiosis, the germ cells undergo sex-specific differentiation to produce mature gametes. Formation of oocytes in the hermaphrodite germline depends on the activity of GLD-2 in complex with the RRM-motif RBP RNP-8 [95,96] and the translational repressor TRIM-NHL RNA-binding protein LIN-41 [100,101,180]. During differentiation, the oocytes accumulate a number of proteins required for embryogenesis. One such protein family is a set of MEG intrinsically

disordered proteins regulating RNA/protein condensate formation in embryos [102,103,181]. Finally, oocyte maturation requires the activity of redundant TIS11 zinc-finger RBPs OMA-1 and OMA-2 [98]. High-throughput approaches have characterized the targets of many RNA regulators mentioned above including FBF-1 and FBF-2 [11], PUF-8 [86], GLD-1 [182,183], RNP-8 and GLD-2 [96], LIN-41 [100], and OMA-1 [184].

One widespread mechanism regulating the activity of RNA-binding proteins is their association with co-regulators or cofactors. Previous research in our lab found that the activities of two *C. elegans* germline RBPs, FBF-2 and GLD-1, are promoted by association with a small protein, DLC-1 ([171,172]). DLC-1 is an LC8-family protein that was originally identified as a component of the dynein motor complex [134,135]. Recent studies suggested that in addition to the dynein motor complex, LC8 proteins contribute to a large number of protein complexes, and function as general cofactors facilitating numerous cellular functions [139]. Supporting this model, we found that the cooperation between DLC-1 and both FBF-2 and GLD-1 is independent of the dynein motor activity. FBF-2 and GLD-1 are dissimilar proteins with opposing biological functions. The fact that DLC-1 cooperates with both, as well as the widespread expression of DLC-1, led us to hypothesize that DLC-1 may facilitate the function of additional RNA-binding proteins.

Here, we performed immunoprecipitation followed by RNA sequencing to determine the transcripts found in association with DLC-1. We found a large number of functionally

diverse transcripts associated with DLC-1, supporting broad input by DLC-1 in post-transcriptional regulation. Although DLC-1 might bind RNA directly [185,186], we expect that the majority of transcripts were recovered through indirect association of DLC-1 with RNA-binding proteins. A large number of DLC-1-associated transcripts contribute to oogenesis, a process disrupted in *dlc-1* mutants. We report that two oocyte genes, *meg-1* and *meg-3*, depend on DLC-1 for regulation of their expression in the germline and maturing oocytes, which suggests that DLC-1 contributes to regulation of gene expression at this developmental stage.

Materials and Methods

Nematode Strains and Culture

C. elegans strains (Table 2.1) were cultured as per standard protocols [187] at 20°C or 24°C (if expressing GFP-tagged genes). The *3xFLAG::dlc-1(mntSi13); dlc-1(tm3153)* rescued strain UMT290 was generated by first crossing UMT281 with *him-8(tm611)* and then with *dlc-1(tm3153)/qC1 III*. The UMT376 strain expressing both *3xFLAG::DLC-1* and *OMA-1::GFP* was generated by crossing UMT281 and TX189.

Table 2.1

Nematode strains used in this study

| Genotype | Description | Strain | Reference |
|--|---|--------|------------|
| Transgene | | | |
| <i>mntSi13[pME4.1] II;</i> <i>unc-119(ed3)III</i> | <i>dlc-1 prom::3xFLAG::dlc-1::dlc-1 3'UTR</i> | UMT281 | [171] |
| <i>unc-119(ed3) III; tel1</i> | <i>oma-1 prom::oma-1::GFP</i> | TX189 | [99] |
| <i>mntSi13[pME4.1] II;</i> <i>unc-119(ed3) III; tel1</i> <i>[pRL475]</i> | <i>dlc-1 prom::3xFLAG::dlc-1::dlc-1 3'UTR;</i> <i>oma-1 prom::oma-1::GFP</i> | UMT376 | This study |
| Mutant strains + Transgene | | | |
| <i>mntSi13 [pME4.1] II;</i> <i>dlc-1(tm3153)III</i> | <i>dlc-1 prom::3xFLAG::dlc-1::dlc-1 3'UTR</i> | UMT290 | This study |

| Mutant strains | | | |
|-------------------------------------|-----------------------------|--------|-------|
| <i>meg-1(tn1722)</i> | GFP::<3xFLAG::MEG-1 | DG4213 | [100] |
| <i>meg-3(ax3054)</i> | MEG-3::meGFP | JH3503 | [35] |
| <i>meg-3(ax3051); meg-4(ax2080)</i> | MEG-3::OLLAS; MEG-4::3xFLAG | JH3374 | [35] |
| <i>dlc-1(tm3153)/qC1 III</i> | | UMT222 | [171] |

RNA Interference Assays

RNAi was performed by feeding synchronized L1 larvae with HT115(DE3) *E. coli* transformed with the relevant plasmids for 3 days at 24°C as described before [188]. The identity of all plasmids used for RNAi was confirmed by sequencing.

Immunostaining and Imaging

The fixation and immunostaining procedure has been previously described in [171]. Prior to application of primary anti-FLAG antibody, dissected gonads were pre-blocked with PBS/0.1%BSA/0.1%Tween-20/10% normal goat serum (PBS-T/NGS) for 1 hour at room temp. Descriptions of the antibodies and relevant dilutions are listed in Supplemental Table 1 (available online with article). Gonads were incubated in primary antibody solution overnight at 4°C followed by 3 washes with PBS-T and then with secondary antibody for 2 hours at room temperature and washed 3 times with PBS-T. Coverslips were mounted to immunostained gonads with Vectashield with DAPI (Vector Labs). Epifluorescence images were captured using a Leica DFC3000G camera attached to a Leica DM5500B microscope using LAS-X software (Leica). Confocal images were obtained using a Zeiss LSM 880 confocal microscope. Image processing including assembly of full-length germlines from several fields of view was performed in Adobe Photoshop CS3.

Immunoprecipitation

Immunoprecipitation of 3xFLAG::DLC-1 was performed with a protocol adapted from [189] using mouse anti-FLAG antibody (Sigma) or mouse non-specific IgGs as controls, see supplemental file S1 (available online with article) for details. RNA was extracted from the eluents and input samples suspended in TRIzol using the Direct-zol RNA MiniPrep kit (ZymoResearch) and quantified by Qubit 3.0 fluorometer RNA HS assay kit (ThermoFisher). Immunoprecipitated RNA derived from anti-FLAG pulldowns averaged 8 ng/ μ L across five replicates, while IgG-associated RNA was undetectable by Qubit. Immunoprecipitation of 3xFLAG::DLC-1 from the UMT376 strain followed the same procedure, except the RNA extraction procedure was omitted.

GST Pulldowns

Full-length proteins were amplified from Bristol N2 cDNA and cloned into pDEST17 (Thermo Fisher Scientific) to generate 6xHis-tagged proteins. GST-tagged full length DLC-1 has been previously described [171]. All constructs were sequenced and transformed into *E. coli* strain BL21(DE3) for expression. Expression of 6xHis-tagged proteins was induced with 0.1 mM IPTG at 15°C for 16-18 hrs. Expression of GST-tagged DLC-1 was induced with 1 mM IPTG at 37°C for 4 hrs. The GST pulldown assay was performed as described in [171].

Western Blots

Western blots were used to evaluate nematode gene expression, immunoprecipitation of 3xFLAG::DLC-1, and to determine the outcome of GST::DLC-1 pulldowns, as previously described [171]. Detailed information for the antibodies is in Supplemental Table 1 (available online with article). Blots were developed using Luminata Western

HRP reagent (EMD Millipore) and imaged using ChemiDoc MP Imaging System (Bio-Rad).

RNA Sequencing and Bioinformatics

Library preparation and sequencing of the total and immunoprecipitated RNA was performed at the Washington State University Spokane Genomics Core. Total RNA was oligo-dT primed to generate the input libraries while immunoprecipitated RNA was processed without enrichment. Total RNA and IP RNA (5 replicates each) libraries were pooled together to run on two Illumina HiSeq2500 lanes for a total of 439.61 million reads with a length of 100bp. Reads were almost equally distributed among these samples, 93.4% reads have a quality score higher than Q30. RNA-seq data is deposited in NCBI Gene Expression Omnibus database (GSE 115281).

Details of RNA-seq data analysis are in Supplemental File S1 (available online with article). Briefly, sequenced reads were trimmed with Trim Galore! [190] to remove Illumina adapter sequences (v 0.4.2) and filtered for rRNA sequences using Bowtie2 (2.3.0) [191]. Reads that did not map to the rRNA sequences were then applied to the workflow adapted from a previous report [100]. The reads were mapped to WBcel235/ce11 genome using RNA Star (v 2.5.2b-0) [192]. Normalization and enrichment calculations for the RIP experiments were performed using DESeq2 (version 1.12.3) [193]. Genes were considered enriched when they had a $\log_2\text{foldchange} > 1$ and $P_{adj} < 0.01$. Genes that did not correspond to the annotated features of the current reference genome were removed from the list of enriched genes. The finalized list of 2732 genes enriched in the 3xFLAG::DLC-1 RIP is reported in File S2 (available online with article).

For 3'UTR motif analysis, all available 3'UTRs for the genes enriched in the 3xFLAG::DLC-1 RIP were obtained through Wormbase (<http://parasite.wormbase.org/biomart/martview/>) and analyzed using Discriminative Regular Expression Motif Analysis (DREME) tool available on MEMESuite.org [194]. A library of 3' UTRs for all other genes not enriched in 3xFLAG::DLC-1 RIP was used as a control to evaluate the number of motif occurrences using the Find Individual Motif Occurrences (FIMO) tool available on MEMESuite.org [195].

Results

RIPseq of FLAG::DLC-1 from the intact animal

Using a single-copy insertion technique, we generated a transgene encoding 3x-FLAG tagged DLC-1 under the control of its endogenous promoter and 3'UTR [171]. This transgene was used to complement the *dlc-1(tm3153)* deletion, which renders the mutant animals sterile (at 24°C) or causes maternal-effect embryonic lethality (at 15°C). The 3xFLAG::DLC-1 transgene largely rescued *dlc-1* deletion hermaphrodite fertility and embryonic viability at 24°C (99% embryonic viability, $N=797$; 100% fertility, $N=794$). We concluded that the transgenic 3xFLAG-tagged DLC-1 is fully functional *in vivo*. 3xFLAG-tagged DLC-1 was expressed throughout the germline, from the distal stem cells and progenitors to the oocytes [171], consistent with the previously reported endogenous expression pattern [196]. To test whether 3xFLAG::DLC-1 was also expressed in somatic tissues, we disrupted germline tissue formation in 3xFLAG::DLC-1 animal by double RNAi against *sygl-1* and *lst-1* [197]. Loss of germ cells was confirmed by a decrease in the levels of germline-specific protein FBF-1 (Figure 2.1A). Western

blotting detected expression of 3xFLAG::DLC-1 in sterile worms following double *sygl-1/lst-1(RNAi)*, suggesting that 3xFLAG::DLC-1 is also abundant in somatic tissues (Figure 2.1A), consistent with a previous report [198].

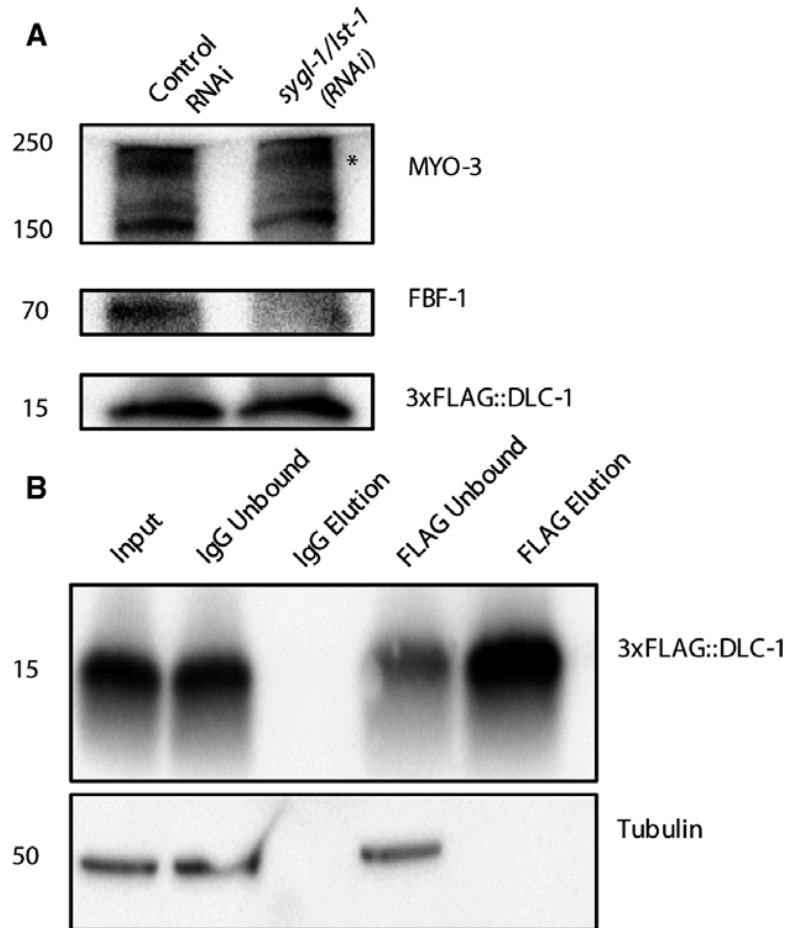


Figure 2.1: Expression and immunopurification of 3xFLAG::DLC-1

A) Western blot of 3xFLAG::DLC-1 worms treated with control RNAi or *sygl-1/lst-1(RNAi)* that prevents germ cell proliferation. Sterility was visually confirmed in *sygl-1/lst-1(RNAi)* treatment. 50 worms per treatment were collected and boiled in 2x loading buffer for 30 min before loading onto gel. Loss of germline tissue is followed through decreased abundance of FBF-1 protein. 3xFLAG::DLC-1 does not decrease in the background of *sygl-1/lst-1(RNAi)*. Somatic myosin MYO-3 is

used as loading control. Asterisk denotes the 210 kD myosin A heavy chain.

Molecular weight of the protein bands is denoted by the numbers on the left side of western blot images.

- B) 3xFLAG::DLC-1 is specifically immunoprecipitated with anti-FLAG antibody (FLAG Elution), but not in the IgG control. The anti-FLAG immunoprecipitation reduces the amount of tagged protein in the lysate (FLAG Unbound), demonstrating an efficient IP. Tubulin is not recovered in either the IgG control or FLAG eluents.

We expect that the transgenic 3xFLAG::DLC-1 is able to enter all relevant protein complexes, including complexes with RNA-binding proteins, and allow for isolation of target mRNAs. For 3xFLAG::DLC-1 immunoprecipitation, we used the rescued strain where the transgene is the sole source of DLC-1. We immunoprecipitated 3xFLAG::DLC-1 from replicate lysates of young adult nematodes (24 hrs post-L4 stage; Figure 2.1B). The immunoprecipitation of 3xFLAG::DLC-1 was specific, and not observed in the control with non-specific IgGs. The anti-FLAG antibodies were also selective as no immunoprecipitation of tubulin was observed (Figure 2.1B). In agreement with our hypothesis, we detected RNA in the 3xFLAG::DLC-1 immunoprecipitate (108-432 ng/300 mg input tissue), but not in the non-specific IgG immunoprecipitate.

Total RNA associated with DLC-1-containing RNPs was purified and sequenced in five independent biological replicates. In parallel, we sequenced the mRNAs in five replicates of the corresponding input lysates after enriching them with oligo(dT) selection. We did

not sequence the material isolated with non-immune IgG since an undetectable amount of isolated RNA was expected to result in amplification artifacts during sequencing library preparation. We mapped the sequencing reads from all replicates to the WBcel235/ce11 version of the *C. elegans* genome and excluded the reads mapping to the ribosomal RNA genes from further analysis. We used principal component analysis (PCA) to evaluate the variability of our replicates. The PCA analysis indicated that the 3xFLAG::DLC-1 IP replicates tightly clustered together (Figure 2.2A) suggesting their similarity and reproducibility. The input samples were clearly segregated from the immunoprecipitated mRNAs (Figure 2.2A). We observed only a weak correlation between average fragment abundance of transcripts in 3xFLAG::DLC-1 IP and in the input RNAseq ($R^2 \sim 0.4$) suggesting that the procedure didn't simply return the most abundant mRNAs in the samples (Figure 2.2B).

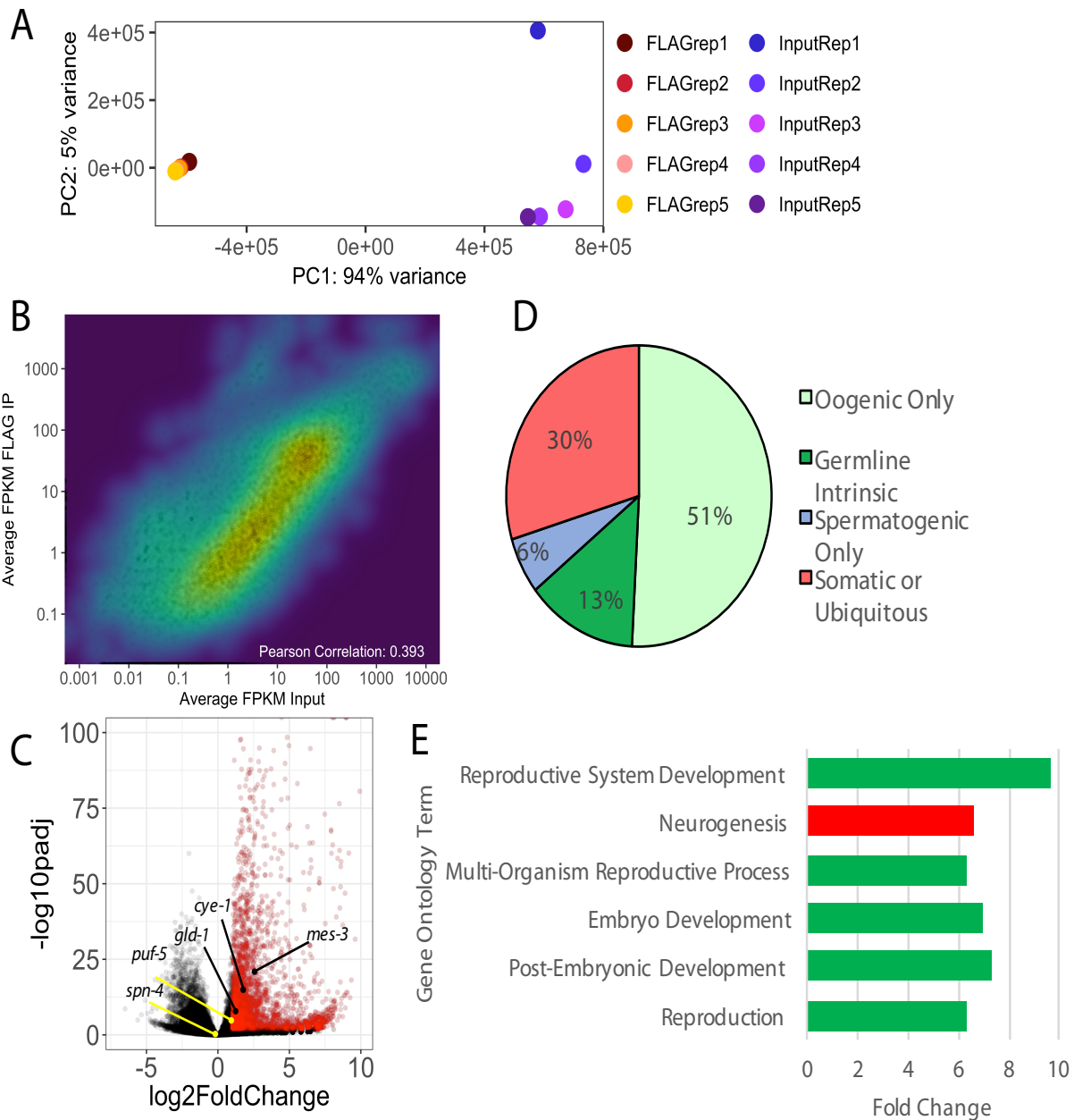


Figure 2.2: Identification and characterization of DLC-1-associated RNAs

- A) Principal component analysis of five 3xFLAG::DLC-1 replicate RNA immunoprecipitations (RIPs; FLAGrep1-5) compared against five inputs (InputRep1-5). PC, Principal Component. PC1 explains 94% of variance, and PC2 explains 5% of variance.

- B) RNA-seq enrichment heatmap showing the distribution of average RIP FPKM versus average Input FPKM. Overall, the correlation is low ($R^2=0.393$).
- C) Volcano plot of 3xFLAG::DLC-1 RIPseq. Inverse of the adjusted statistical significance ($-\log_{10}(P_{adj})$; y-axis) is plotted against the average fold change (anti-FLAG/Input) for five samples (x-axis). Points have been colored by enrichment, red are enriched in 3xFLAG::DLC-1 RIP ($P_{adj} < 0.01$ and $\log_2\text{FoldChange} > 1$; 2732 genes; File S2 (available with article online)). The FBF-2 or GLD-1 target mRNAs *cye-1*, *gld-1*, and *mes-3* are enriched in 3xFLAG::DLC-1 RIP. The GLD-1 target mRNAs *puf-5* and *spn-4* were not enriched in the RIP.
- D) DLC-1-associated mRNAs are enriched for genes in the oogenic transcriptome. Comparison of DLC-1-associated genes against genes associated with a specific spermatogenic or oogenic program as defined in [92]. Genes termed “Somatic or Ubiquitous” did not fall under the other 3 specified categories.
- E) Gene ontology analysis reveals that DLC-1 associated genes are involved in reproduction, development, and neurogenesis. The categories associated with germline expression (reproduction, development) are colored green, while neurogenesis associated with somatic expression is colored red. Analysis was performed using the Gene Enrichment Analysis (GEA) tool available on <https://wormbase.org/tools/enrichment/tea/tea.cgi> [199]. Fold change is expressed as the ratio of the enriched genes observed for the category over the number of genes expected to be recovered.

To identify transcripts enriched in the DLC-1 immunoprecipitations, we used DESeq2 to calculate log₂ fold change [193] of the RNAs in the DLC-1 eluates relative to their abundance in the oligo(dT)-enriched inputs. While RNAs in DLC-1-containing RNPs appeared enriched several fold, the majority of RNAs in the lysate were moderately depleted compared to the IP sample (Figure 2.2C). We identified 2732 RNAs exhibiting a statistically significant (adjusted $P < 0.01$) enrichment of two-fold or greater in the DLC-1 immunoprecipitation (highlighted in red in Figure 2.2C; Supplemental File S2 (available online with article)). This number of transcripts is ~2.3-fold greater than typically recovered by isolation of a single RBP. These transcripts included 2206 protein-coding mRNAs, 346 long non-coding RNAs (lincRNAs, ncRNAs, antisense RNAs), and 87 small non-coding RNAs including snoRNAs and snRNAs (Table 2.2). We concluded that DLC-1 predominantly associates with mRNA-containing RNPs, and the non-coding RNAs might appear enriched in DLC-1 IP since the RNAs were not oligo(dT) selected for library preparation.

Table 2.2

DLC-1 predominantly associates with protein-coding mRNAs

| Biotype* | # of Enriched Genes with Biotype | % of Enriched Genes |
|-----------------|---|----------------------------|
| mRNA | 2206 | 81% |
| long noncoding | 346 | 13% |
| short noncoding | 87 | 3% |
| pseudogene | 86 | 3% |

Biotype analysis of DLC-1 associated genes based on assigned biotype from *C. elegans* genome annotation WS236 performed with Wormbase Parasite. “mRNA” represents “protein coding” category. Long noncoding is comprised of lincRNA, antisense, ncRNA. Short noncoding includes snRNA and snoRNA. * 7 DLC-1-associated RNAs have no biotype annotation.

The mRNAs in DLC-1-containing complexes included *mes-3*, *cye-1*, and *gld-1* (previously-characterized targets of FBF-2 and GLD-1 that depend on DLC-1 for their regulation [171,172]), but not *puf-5* or *spn-4* (GLD-1 targets that were not affected by *dlc-1* loss; Figure 2.2C). We conclude that the mRNAs identified in the DLC-1-containing RNPs (DLC-1-associated mRNAs) are likely relevant to DLC-1 biological activity.

Many DLC-1-associated transcripts (1756 of 2732 transcripts; Table 2.3) belong to the general oogenic mRNA program as defined in [92]. This overlap was statistically significant by the hypergeometric distribution test ($P < 1E^{-90}$). DLC-1-associated mRNAs were depleted of spermatogenesis transcripts, reflecting preparation of IP samples from young adult (oogenic) hermaphrodites (Table 2.3). We also compared overlap of our transcripts with a different dataset of transcripts that increase in abundance over twofold in the oogenic germlines as compared to spermatogenesis [200] and similarly recovered a significant overlap (321 of 2732; $P < 1E^{-53}$; Table 2.3). Based on analysis of overlap with the two distinct datasets, a large number of DLC-1-associated mRNAs are related to oogenesis. Despite the enrichment of germline transcripts, a sizeable fraction of somatic

or ubiquitous mRNAs were also present (828 of 2732; Figure 2.2D) in agreement with DLC-1 expression in somatic tissues. Analysis of the DLC-1 targets by Gene Ontology functional annotation clustering [199] identified the expected enrichment of transcripts associated with development and reproduction (Figure 2.2E). Enriched transcripts were also related to neurogenesis (Figure 2.2E), a process similarly associated with extensive post-transcriptional regulation and RNA transport [201-203]. We concluded that despite broad expression of 3xFLAG::DLC-1, it enters into mRNP complexes predominantly in the germline and neuronal tissues.

Table 2.3

DLC-1-associated mRNAs are enriched in oogenesis-related transcripts

| Transcriptome | # of Overlapped Genes | % Overlap | Representation Factor | P value |
|-----------------------------------|------------------------------|------------------|------------------------------|----------------|
| Oogenic Transcriptome [92] | 1756 | 19% | 1.4 | 6.82E-91 |
| Spermatogenic Transcriptome [92] | 533 | 8% | 0.6 | 3.23E-63 |
| Enriched in Oogenesis [200] | 321 | 32% | 2.4 | 5.3E-54 |
| Enriched in Spermatogenesis [200] | 115 | 13% | 1 | 0.403 |

DLC-1-associated mRNAs were compared against oogenic or spermatogenic transcriptomes. Representation factor and significance of overlap was evaluated by hypergeometric distribution test using the gene list comparison tool available at nemates.org/MA/progs/overlap_stats.html. Representation factor above 1.0 indicates more overlap than expected between independent groups, and below 1.0 indicates less overlap than expected.

Binding motifs in the 3'UTRs of mRNAs isolated with DLC-1

To test whether the mRNAs isolated with DLC-1 contain RBP binding motifs, we searched for sequences enriched in the 3'UTRs of this gene set. Using DREME [194], we identified the enriched motifs in the 3'UTR set compared to shuffled sequences (Figure 2.3A-C; Supplemental File S3 (available with online article)). Based on previously discovered DLC-1 association with FBF-2, we expected to recover motifs consistent with the presence of FBF targets. Indeed, within the ten most significant recovered motifs, we found two motifs similar to those recognized by PUF family RNA-binding proteins that includes FBF-2 (Figure 2.3B, C; [11,204]). The top-scoring motif is a low-affinity OMA-1 binding site (UA[a/u]-rich repeats, Figure 2.3A; [97]); the remaining high ranking motifs were not among the previously characterized targets of *C. elegans* RBPs. Since the DREME analysis estimates motif enrichment in comparison to shuffled 3'UTR sequences, it might return motifs that are highly represented across *C. elegans* 3'UTRs. To evaluate this possibility, we compared the prevalence of the motifs uncovered in the 3'UTRs of RIPseq mRNA set to their frequency across the 3'UTRs of the transcripts not associated with DLC-1. We find that all motifs were significantly enriched in the DLC-1-associated 3'UTR set with *P* values calculated by chi-square test smaller than 10^{-4} (Figure 2.3D).

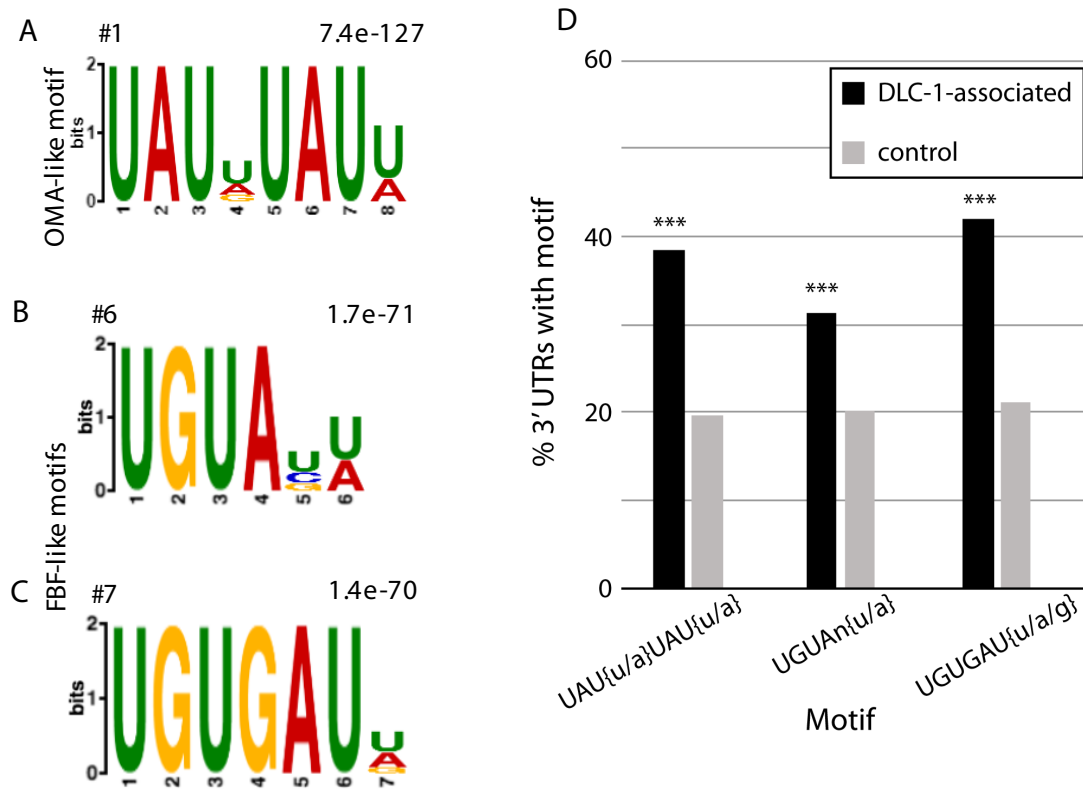


Figure 2.3: 3'UTR motifs in mRNAs associated with DLC-1

A-C) Motifs identified by DREME [194] analysis of the annotated 3' UTRs of the DLC-1 associated mRNAs; WebLogo, rank and *P*-value (Fisher's Exact test) are shown.

A) Top overrepresented motif similar to OMA-1-binding element [97].

B,C) Short motifs similar to the FBF-binding element (UGUNNNAU, [204]) were recovered from the top 10 most enriched motifs. The top 20 most represented motifs in the 3xFLAG::DLC-1 RIP are reported in File S3 (available online with article).

D) Motifs in A-C are significantly enriched in the DLC-1 associated 3'UTRs compared to the control set of *C. elegans* 3'UTRs. Motifs in A-C were used as

input for FIMO [195] to scan DLC-1 associated UTRs or all other *C. elegans* 3'UTRs (at P value < 0.001). The graph plots percentage of genes containing a specific motif as the ratio of observed motif occurrences (with a $P < 0.001$) against the size of the input library for enriched in 3xFLAG::DLC-1 RIP (black) or control 3'UTRs (grey). Differences in motif prevalence between sets of 3'UTRs were evaluated by chi-square test; *** $P < 0.0001$.

Identification of candidate DLC-1-containing RNPs through overlap in mRNAs

If DLC-1 is an integral component of regulatory RNPs, we expect to recover a significant overlap between mRNAs recovered in the DLC-1 IP and the documented targets of regulatory RNA-binding proteins. Initially, we compared DLC-1-associated mRNAs to those recovered in complex with FBF-2 [11] and GLD-1 [183]. We found that the set of DLC-1-associated mRNAs significantly overlapped with both FBF-2 targets (412 overlapped genes; hypergeometric distribution $P < 10^{-60}$) and GLD-1 targets (44 overlapped genes; hypergeometric distribution $P < 10^{-3}$; Table 2.4) in agreement with the known molecular and genetic interaction of DLC-1 with these RBPs ([171,172]). We concluded that overlap comparison has the potential to identify the mRNAs regulated with involvement of DLC-1.

We then compared the mRNAs isolated with DLC-1 to the previously published targets of several germline RNA-binding proteins including FBF-1 [11], GLD-2 [96], RNP-8 [96], LIN-41 [100], OMA-1 [184], FOG-3 and FOG-1 [92], and PUF-8 [86]. We observed significant (hypergeometric distribution $P < 0.05$) overlap of DLC-1-associated

mRNAs with the targets of FBF-1 ($P < 10^{-59}$), GLD-2 ($P < 10^{-7}$), LIN-41 ($P < 0.01$), and OMA-1 ($P = 0.02$; Table 2.4). The significant overlap with FBF-1 targets was expected since the targets of FBF-1 and FBF-2 are highly similar [11].

Table 2.4

DLC-1-associated mRNAs are shared with several germline RBPs

| RBP Transcriptome | # of Overlapped Genes | % of RBP targets in overlap | Representation Factor | P value |
|--------------------------|------------------------------|------------------------------------|------------------------------|----------------|
| FBF-2 [11] | 412 | 30% | 2.2 | 5E-61 |
| FBF-1 [11] | 547 | 26% | 1.9 | 1.23E-60 |
| GLD-2 [96] | 119 | 22% | 1.6 | 7.48E-08 |
| GLD-1 [183]* | 44 | 23% | 1.7 | 2.9E-04 |
| LIN-41 [100] | 188 | 17% | 1.2 | 0.001 |
| OMA-1 [184] | 173 | 16% | 1.2 | 0.02 |
| RNP-8 [96] | 129 | 15% | 1.1 | 0.194 |
| FOG-3 [92] | 94 | 13% | 1 | 0.328 |
| FOG-1 [92] | 6 | 7% | 0.5 | 0.062 |
| PUF-8 [86] | 6 | 4% | 0.3 | 2.5E-05 |

The 2732 RNAs enriched in DLC-1 RIP were compared for overlap with known RBP mRNA targets. # of overlapped genes is the number of DLC-1 associated RNAs that overlap with the mRNA targets for a specified RBP. Representation and *P* values were derived as in Table 2.3. * Similar overlap was observed using alternate GLD-1 target mRNA datasets from T. Schedl, personal communication, 19% overlap, $P = 7.47E-07$ and from [182], 16% overlap, $P = 0.009$.

DLC-1 contributes to several mechanisms of germline translational control

As we hypothesized that DLC-1 has the potential to contribute to the regulatory activity of multiple germline RNA-binding proteins, we sought to test if DLC-1 might affect the expression of its other associated mRNA targets, beyond the previously identified targets of FBF-2 and GLD-1. We focused on a set of MEG proteins that are only expressed in the oocytes and early embryos. We chose *meg-3* since its regulation has not been previously studied, and used *meg-1* and *meg-4* for comparison and contrast.

Endogenously tagged GFP::FLAG::MEG-1, MEG-3::meGFP, and MEG-4::FLAG are expressed in the -1 to -3 oocytes in the wild type background [100,103]. Despite similar protein expression patterns and related function, mRNAs encoding the MEG proteins might be differentially regulated as they have been recovered in association with distinct RNA-binding proteins. *meg-1* mRNA was found in complexes with GLD-1, GLD-2, LIN-41, RNP-8, and FBF-1 [11,96,100] and its expression is regulated by LIN-41, OMA-1, and OMA-2 [100]. *meg-3* mRNA has not been identified in complex with germline RBPs so far, and *meg-4* mRNA was recovered with GLD-2 and RNP-8 [96]. All three *meg* mRNAs are among the DLC-1-associated transcripts.

Following depletion of DLC-1 by RNAi, we assessed the expression of MEG proteins in the resulting sterile germlines. Similar to *dlc-1(tm3153)* mutant, *dlc-1(RNAi)* at 24°C resulted in initiation of oocyte differentiation followed by deterioration of gametes and formation of an “oocyte mass” at the proximal end of the gonad. The expression of GFP::FLAG::MEG-1 was lost in 52% of *dlc-1(RNAi)* sterile germlines (Figure 2.4A,C; *n* = 39), suggesting that DLC-1 contributes to the activation of GFP::FLAG::MEG-1

expression. A decrease in GFP::FLAG::MEG-1 expression was also observed by western blot (Figure 2.4B). By contrast, in *dlc-1(RNAi)* background expression of MEG-3::meGFP was expanded in the proximal region of the gonad and extended into the late pachytene region in 51% of germlines (Figure 2.4D,E; $n = 49$). Finally, the expression of MEG-4::FLAG was not affected by *dlc-1(RNAi)* (Figure 2.4F,G; $n = 35$), although western blot suggested that MEG-4::FLAG post-translational modifications were altered compared to the control (Figure 2.4G). We conclude that DLC-1 might contribute to the function of the proteins activating MEG-1 expression as well as translational repressors of MEG-3.

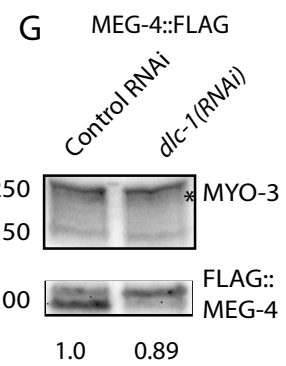
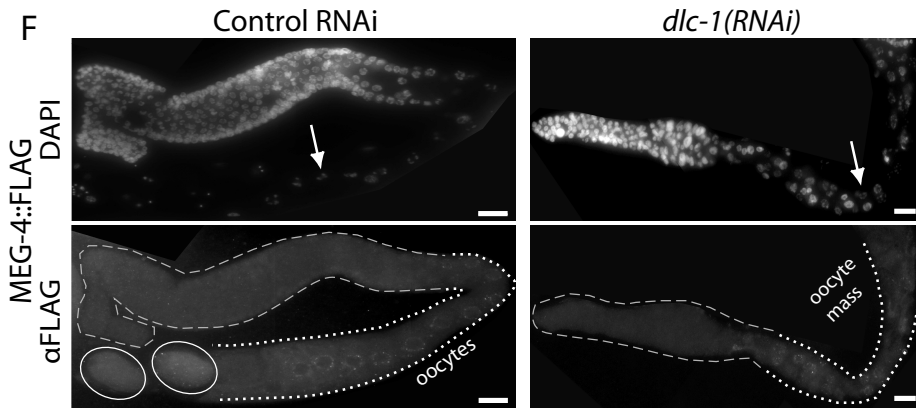
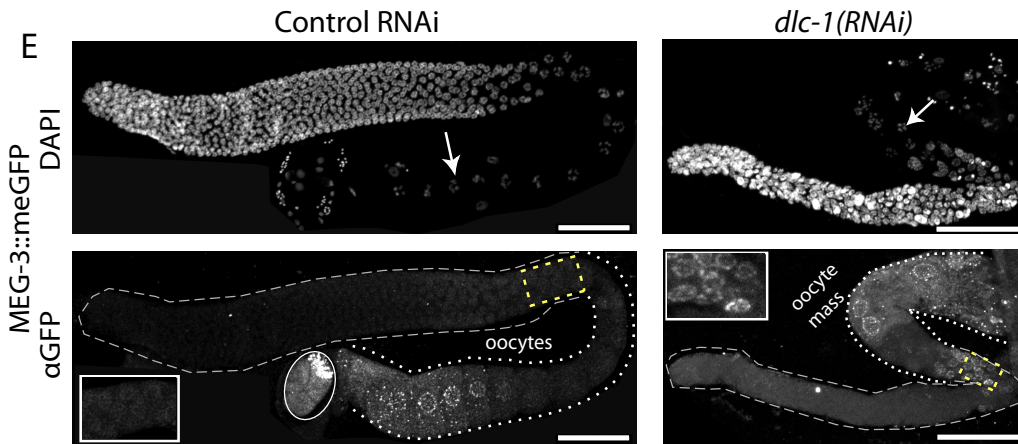
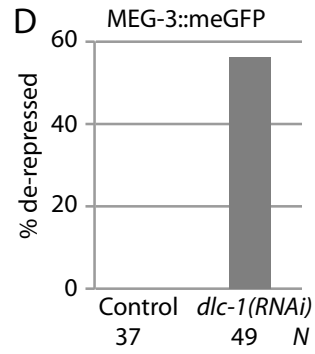
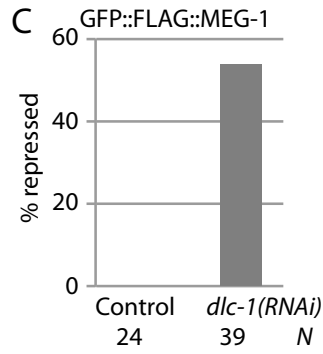
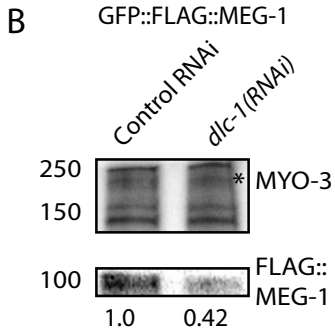
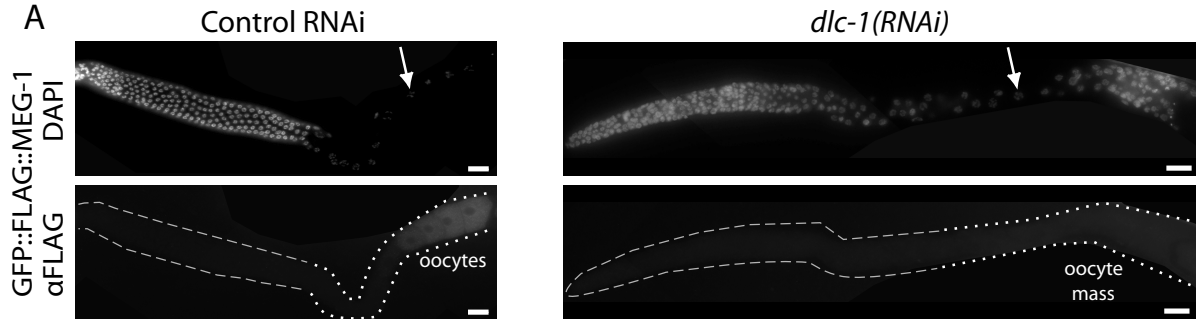


Figure 2.4: DLC-1 promotes expression control of its targets

A, E-F) The expression of CRISPR-tagged GFP:: $3\times$ FLAG::MEG-1, MEG-3::meGFP, or MEG-4:: $3\times$ FLAG was evaluated in dissected, fixed, and immunostained gonads of worms treated with control or *dlc-1(RNAi)*. DNA was stained by DAPI; arrows point to nuclei in diplotene characteristic of the oocytes. In the immunostained panels, gonads are outlined with dashed lines, while the oocytes (control treatment) or oocyte masses following *dlc-1(RNAi)* are identified with dotted lines. Enlarged regions in the insets of MEG-3::meGFP germlines are marked by yellow dashed boxes. Ovals in MEG-3::meGFP and MEG-4::FLAG control panels outline embryos. Images in panels A and F were obtained using an epifluorescent microscope, while images in panel E were obtained using a confocal microscope. Scale bars: 50 μ M.

B, G) Representative Western blots of GFP:: $3\times$ FLAG::MEG-1 (B) and MEG-4:: $3\times$ FLAG (G) adult worms treated with *dlc-1(RNAi)* or control RNAi (MEG-1, 50 worms/lane; MEG-4, 100 worms/lane). Sterility was visually confirmed in *dlc-1(RNAi)* treatment. Band density was quantified using Bio-Rad Image Lab v5.1 software from the Bio-Rad ChemiDoc MP. The intensity of FLAG-tagged transgene band was normalized to the intensity of somatic myosin MYO-3 for loading control and then scaled to 1 in control RNAi (reported below the anti-FLAG Western blot for each protein). GFP:: $3\times$ FLAG::MEG-1 is depleted after *dlc-1(RNAi)* treatment, while MEG-4:: $3\times$ FLAG levels are largely unchanged following the same RNAi treatment. Molecular weight of the protein bands is denoted by

the numbers on the left side of Western blot images. Asterisk marks the 210 kD myosin A heavy chain.

C, D) Bar plots showing the percentage of germlines exhibiting abnormal repression or expression of GFP::FLAG::MEG-1 or MEG-3::meGFP respectively after control or *dlc-1(RNAi)*. *N*, number of germlines scored (below the bars). Expression of MEG-4::FLAG did not change following *dlc-1(RNAi)*, *N* = 35. Effectiveness of *dlc-1(RNAi)* was confirmed as 100% of treated nematodes became sterile.

DLC-1 interacts with OMA-1 *in vitro*

DLC-1 might facilitate activation of MEG-1 expression by interacting with its regulators. Activation of MEG-1 expression in the oocyte requires the activities of OMA-1, OMA-2, and GLD-2 [100], and the overlaps between the mRNAs in complex with DLC-1 and GLD-2 and OMA-1 targets were significant. Based on these results, we tested OMA-1, OMA-2, and GLD-2 for direct interaction with DLC-1. GST pulldown assays performed with bacterially-expressed proteins indicated that DLC-1 could directly interact with OMA-1, but not with GLD-2 or OMA-2 (Figure 2.5A). Selective interaction of DLC-1 with OMA-1, but not OMA-2 was surprising since OMA-1 and OMA-2 are highly similar (64% identity in the coding sequences) and largely functionally redundant [98]. The absence of detectable interactions between DLC-1 and GLD-2 or OMA-2 *in vitro* might result from the lack of other cofactors or post-translational modifications that may facilitate DLC-1 binding or indicate that the interactions are indirect. To explore DLC-1/OMA-1 interaction *in vivo*, we performed FLAG::DLC-1 immunoprecipitation from a strain that was also expressing GFP-tagged OMA-1. We find that OMA-1 did not co-

immunoprecipitate with FLAG::DLC-1 (Figure 2.5B) suggesting that the protein interaction might be unstable, occurs only in a subset of OMA-1 RNP complexes, or is an artifact of an *in vitro* experiment. A transient interaction of DLC-1 with OMA-1 provides one possible mechanism for DLC-1 input in RNA regulation during oogenesis.

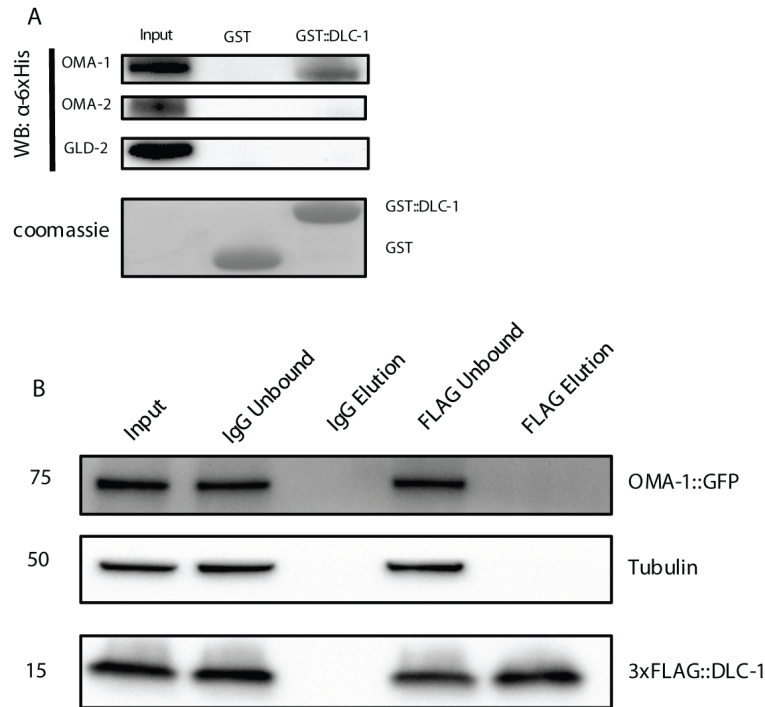


Figure 2.5: DLC-1 binds OMA-1 *in vitro*

- A) Full length 6x-His-tagged OMA-1, OMA-2, and GLD-2 (detected by Western blotting) were tested for binding to GST-tagged DLC-1 (Coomassie). GST alone was used as a control.
- B) 3xFLAG::DLC-1 is specifically immunoprecipitated from 3xFLAG::DLC-1; OMA-1::GFP worms with anti-FLAG antibody (FLAG Elution), but not in the IgG control. Tubulin is not recovered in either the IgG control or FLAG eluents. OMA-1::GFP is not recovered in the FLAG::DLC-1 eluents.

Discussion

In this study, we report that the LC8 family protein DLC-1 enters multiple RNP complexes that collectively contain thousands of mRNAs. Our findings identify new requirements for DLC-1 in the control of both translational activation and repression during oocyte differentiation (Figure 2.6).

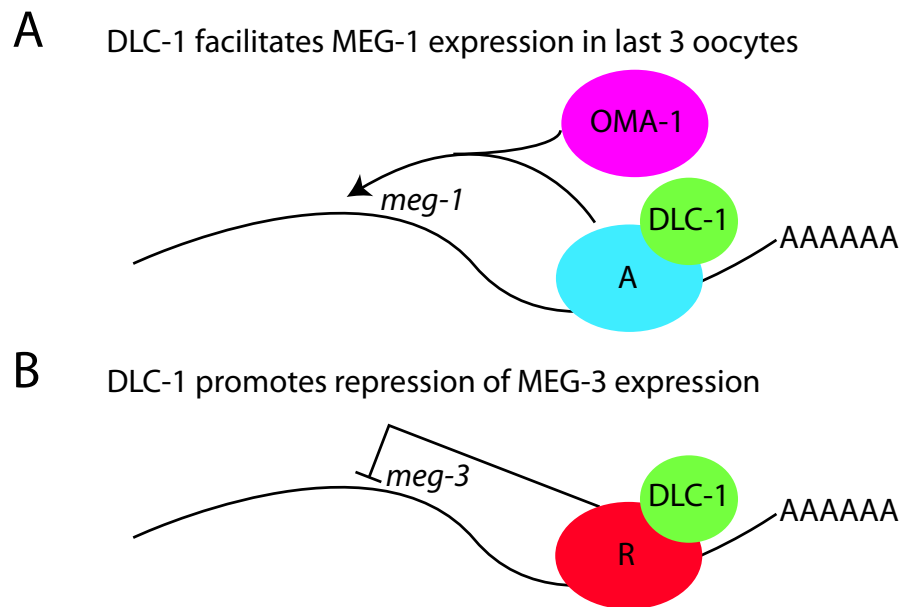


Figure 2.6: Model of DLC-1 involvement in different modes of post-transcriptional RNA regulation

- A) A subset of DLC-1-associated transcripts including *meg-1* requires DLC-1 for their activation in the oocytes. DLC-1 associates with these transcripts through the activator proteins, “A” in the schematic. Both GLD-2 and OMA-1/2 contribute to *meg-1* activation [100], and DLC-1 may play a role in the transient recruitment of OMA-1 required for this process.

B) Other DLC-1-associated transcripts such as *meg-3* require DLC-1 for their repression. These mRNA targets that also include *gld-1*, *cye-1* and *mes-3* are derepressed upon inactivation of DLC-1. DLC-1 associates with these transcripts through translational repressors, denoted “R”. DLC-1 is required for function of these translational repressors including FBF-2, GLD-1, and likely others. The model does not indicate the actual location of proteins on the transcript nor does it represent all components of regulatory RNP complexes.

We find that DLC-1 is incorporated in multiple RNP complexes expanding upon our previous results of DLC-1’s role in RNA regulation by two *C. elegans* RBPs, FBF-2 and GLD-1 ([171,172]). The number of DLC-1-associated transcripts (2732) is greater than the typical number recovered with single RBPs, which is 1000-2000. This may suggest that DLC-1 acts as a cofactor for many RNP complexes. The mRNAs associated with DLC-1 are related to development and reproduction as well as neurogenesis, reflecting previously reported sites of DLC-1 expression and function. DLC-1 and other dynein motor components are required for the function of *C. elegans* ciliated neurons [205], but a role for DLC-1 in neuronal post-transcriptional gene expression control has not been previously reported. Many DLC-1-associated mRNAs belong to the oogenic transcriptome, which is consistent with DLC-1 expression in germlines undergoing oogenesis in young adult nematodes used for sample preparation and with disruption of oogenesis observed in *dlc-1* mutant.

Among the recovered mRNAs are previously identified transcripts that require DLC-1 for regulation of their expression in the germline ([171,172]). In addition, we identified new DLC-1 contributions to translational repression at the end of meiotic pachytene and translational activation in the oocytes (Figure 2.6). Loss of DLC-1 causes derepression of MEG-3 in pachytene cells. Since the regulators that affect MEG-3 expression are unknown, we hypothesize that DLC-1 might contribute to the function of additional translational repressors beyond FBF-2 and GLD-1. By contrast, oocyte expression of MEG-1 was lost after *dlc-1* knockdown. Activation of MEG-1 expression in the oocytes requires the activities of GLD-2 and OMA-1/OMA-2 [100]. We found direct interaction of DLC-1 with OMA-1 using an *in vitro* system, which might be relevant to activation of MEG-1 expression. However, we were unable to detect co-immunoprecipitation of OMA-1 with DLC-1 *in vivo*, thus the interaction might be transient or only reflect a small subset of OMA-1 regulatory RNP complexes. Alternatively, there is a possibility that the interaction is absent *in vivo*. Expression of MEG-4, another member of MEG protein family, was not affected by the depletion of DLC-1, although MEG-4 post-translational modifications were altered in the sterile *dlc-1(RNAi)* germlines. Further studies are needed to determine whether this differential protein modification is due to disrupted oogenesis or is caused specifically by the absence of DLC-1.

We scanned the 3'UTRs of *meg-1*, *meg-3*, and *meg-4* for the presence of motifs enriched in DLC-1-associated mRNAs and found that each 3'UTR contained several instances of the enriched motif shown in Figure 2.3B, while *meg-1* and *meg-4* 3'UTRs additionally contained the motif shown in Figure 2.3C. Therefore, simple presence or absence of these

enriched motifs is unlikely to account for differential contribution of DLC-1 to the regulation of *meg* transcripts. Future experiments will test the importance of these motifs for regulation of *meg-1* and *meg-3* expression. Diverse contributions of DLC-1 to post-transcriptional control are enabled by its incorporation in a variety of regulatory complexes (Figure 2.6). Binding to DLC-1 causes structural changes and/or facilitates higher-order complex assembly of its partner proteins [139,206], likely relevant to DLC-1 function in RNP complexes. Future work will determine DLC-1's contribution to OMA-1 function as well as identify other components of DLC-1-containing RNP complexes.

Chapter 3

In Situ Detection of Ribonucleoprotein Complex Assembly in the *C. elegans*

Germline using Proximity Ligation Assay

(The following chapter is a modified version of the manuscript that was published in JoVE 2020. <https://www.jove.com/video/60982/in-situ-detection-ribonucleoprotein-complex-assembly-c-elegans>)

Abstract

Understanding when and where protein-protein interactions (PPIs) occur is critical to understanding protein function in the cell and how broader processes such as development are affected. The *Caenorhabditis elegans* germline is a great model system for studying PPIs that are related to the regulation of stem cells, meiosis, and development. There are a variety of well-developed techniques that allow proteins of interest to be tagged for recognition by standard antibodies, making this system advantageous for proximity ligation assay (PLA) reactions. As a result, the PLA is able to show where PPIs occur in a spatial and temporal manner in germlines more effectively than alternative approaches. Described here is a protocol for the application and quantification of this technology to probe PPIs in the *C. elegans* germline.

Introduction

Over 80% of proteins are estimated to have interactions with other molecules [207], which emphasizes how important PPIs are to the execution of specific biological functions in the cell [208]. Some proteins function as hubs facilitating assembly of larger complexes that are necessary for cell survival [207]. These hubs mediate multiple PPIs and help organize proteins into a network that facilitates specific functions in a cell [209]. Formation of protein complexes is also affected by biological context, such as the presence or absence of specific interacting partners [210], cell signaling events, and developmental stage of a cell.

C. elegans is commonly used as a model organism for a variety of studies, including development. The simple anatomy of this animal is comprised of several organs, including the gonad, gut, and transparent cuticle, which facilitates the analysis of worm development. The germline residing in the gonad is a great tool to study how germline stem cells mature into gametes [175] that develop into embryos and eventually the next generation of progeny. The distal tip region of the germline contains a pool of self-renewing stem cells (Figure 3.1). As stem cells leave the niche, they progress into the meiotic pachytene and eventually develop into oocytes in the young adult stage (Figure 3.1). This program of development in the germline is tightly regulated through different mechanisms, including a post-transcriptional regulatory network facilitated by RNA-binding proteins (RBPs) [174]. PPIs are important for this regulatory activity, as RBPs associate with other cofactors to exert their functions.

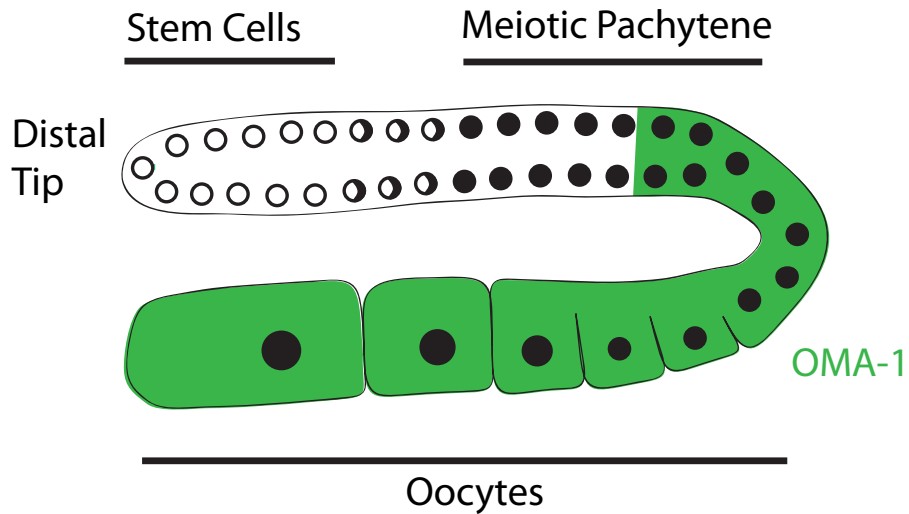


Figure 3.1: Schematic of *C. elegans* germline

The distal tip region contains the stem cell pool, which is followed by meiotic pachytene, where cells have switched from mitosis to meiosis. Cells that exit the meiotic pachytene develop into oocytes, with the most mature oocyte at the proximal end. The region shaded in green, which spans from the late meiotic pachytene through all the oocytes, represents the OMA-1 pattern of expression.

There are several approaches that can be used to probe for PPIs in the worm, but each has unique limitations. *In vivo* immunoprecipitation (IP) can be used to isolate protein-protein complexes from whole worm extracts; however, this approach does not indicate where the PPI occurs in the worm. In addition, protein complexes that are transient and only form during a specific stage of development or in a limited number of cells can be difficult to recover by co-immunoprecipitation. Finally, IP experiments need to address the concerns of protein complex reassembly after lysis and non-specific retention of proteins on the affinity matrix.

Alternative approaches for *in situ* detection of PPIs are co-immunostaining, Förster resonance energy transfer (FRET), and bimolecular fluorescence complementation (BiFC). Co-immunostaining relies on simultaneous detection of two proteins of interest in fixed worm tissue and measurement of the extent of signal colocalization. Use of super-resolution microscopy, which offers greater detail than standard microscopy [211], helps to more stringently test protein colocalization beyond the diffraction-limited barrier of 200–300 nm [212]. However, co-immunostaining using both conventional and super-resolution microscopy works best for proteins with well-defined localization patterns. By contrast, it becomes much less informative for diffusely distributed interacting partners. Measuring for co-localization of signals based on overlap does not provide accurate information about whether the proteins are in complex with each other [213,214].

Furthermore, co-immunoprecipitation and co-immunostaining of protein-protein complexes are not quantitative, making it challenging to determine if such interactions are significant. FRET and BiFC are both fluorescent-based techniques. FRET relies on tagging proteins of interest with fluorescent proteins (FPs) that have spectral overlap at which energy from one FP (donor) is transferred to another FP (acceptor) [215]. This nonradiative transfer of energy results in fluorescence of the acceptor FP that can be detected at its respective wavelength of emission. BiFC is based on reconstitution of a fluorescent protein *in vivo*. It entails splitting GFP into two complementary fragments, such as helices 1–10 and helix 11 [216], which are then fused to two proteins of interest. If these two proteins interact, the complementary fragments of GFP become close enough

in proximity to fold and assemble, reconstituting the GFP fluorophore. Reconstituted GFP is then directly observed as fluorescence and indicates where a PPI has occurred.

As such, both FRET and BiFC depend on large fluorescent tags that can disrupt the function of the tagged protein. In addition, FRET and BiFC require abundant and comparable expression of the tagged proteins to obtain accurate data. FRET may not be suitable for experiments where one partner is in excess of the other, which can lead to high background [217]. Overexpression in BiFC experiments should also be avoided, as this can induce nonspecific assembly [218] that results in increased background. Both techniques require optimization of expression and imaging conditions of the tagged proteins, which may prolong the time required to complete experiments.

The proximity ligation assay (PLA) is an alternative approach that can address the limitations of the techniques mentioned above. PLA takes advantage of primary antibodies that recognize the proteins of interest (or their tags). These primary antibodies are then bound by secondary antibodies containing oligonucleotide probes that can hybridize with one another when within a 40 nm (or shorter) distance [219]. The resulting hybridized DNA is amplified through a PCR reaction, which is detected by probes that complement the DNA. This results in foci that are visualized by a microscope. This technology can detect PPIs *in situ* in complex tissues (i.e., the worm gonad), which is organized as an assembly line containing cells at various stages of development and differentiation. With PLA, PPIs can be directly visualized in a fixed worm gonad, which is advantageous for investigating whether PPIs occur during a specific stage of

development. PLA offers greater resolution of PPIs as opposed to co-localization-based assays, which is ideal for making precise measurements. If used, super-resolution microscopy has the potential to provide finer detail about the location of PLA foci within a cell. Another advantage is that the foci resulting from PLA reactions can be counted by an ImageJ-based analysis workflow, making this technique quantitative.

The LC8 family of dynein light chains was first described as a subunit of the dynein motor complex [135] and hypothesized to serve as a cargo adapter. Since its initial discovery, LC8 has been found in multiple protein complexes in addition to the dynein motor complex [139,156,157,161]. Scanning for protein sequences that contain the LC8 interaction motif [139] suggests that LC8 may have many interactions with a wide array of different proteins [139,146,150,156,157,161]. As a result, LC8 family proteins are now considered hubs that help promote the assembly of larger protein complexes [139,146], such as assemblies of intrinsically disordered proteins [150].

One *C. elegans* LC8-family protein, dynein light chain-1 (DLC-1), is widely expressed across many tissues and not enriched in specific subcellular structures [171,196].

Consequently, identification of biologically relevant *in vivo* partners of DLC-1 in *C. elegans* is challenging for a number of reasons: 1) co-immunoprecipitation does not indicate the tissue source where the interaction occurs; 2) limited expression of particular partners or transient interactions may hinder the ability to detect an interaction by co-immunoprecipitation; and 3) diffuse distribution of DLC-1 leads to non-specific overlap

with potential partner proteins by co-immunostaining. Based on these challenges, PLA is an ideal approach for testing *in vivo* interactions with DLC-1.

It has been previously reported that DLC-1 directly interacts with and serves as a cofactor for the RNA-binding proteins (RBPs) FBF-2 [171] and GLD-1 [172]. Our work supports the model of DLC-1 serving as a hub protein and suggests that DLC-1 facilitates an interaction network that spans beyond dynein [139,146]. Using a GST pulldown assay, a new DLC-1-interacting RBP named OMA-1 has been identified [220]. OMA-1 is important for oocyte growth and meiotic maturation [98] and functions in conjunction with a number of translational repressors and activators [184]. While FBF-2 and GLD-1 are expressed in the stem cells and meiotic pachytene regions, respectively, OMA-1 is diffusely expressed in the germline from the meiotic pachytene through the oocytes [98] (Figure 3.1). This suggests that DLC-1 forms complexes with RBPs in different regions of the gonad. It has also been found that the direct interaction between DLC-1 and OMA-1 observed *in vitro* is not recovered by an *in vivo* IP. The PLA has been successfully used as an alternate approach to further study this interaction in the *C. elegans* germline, and results suggest that PLA can be used to probe many other PPIs in the worm.

Materials and Methods

*The protocol with extensive details describing materials, step by step sample preparation, and image analysis is provided with the article online.

NOTE: This protocol uses *C. elegans* strains in which potential interacting partners are both tagged. It is strongly recommended that a negative control strain be used, in which one tagged protein is not expected to interact with another tagged candidate interaction partner. Here, GFP alone was used as a negative control to assess background, as DLC-1 is not expected to interact with GFP in the worm. GFP-tagged OMA-1 was used as the experimental strain, as preliminary data suggest an interaction with DLC-1. Nematode strains co-expressing control and test proteins with 3xFLAG-tagged DLC-1 are referred to in this text as 3xFLAG::DLC-1; GFP and 3xFLAG::DLC-1; OMA-1::GFP (strains available upon request; more information in Table of Materials (available online with article)), respectively. Here, the 3xFLAG and GFP tags are used; however, other tags may be substituted as long as their antibodies are compatible with the PLA kit reagents.

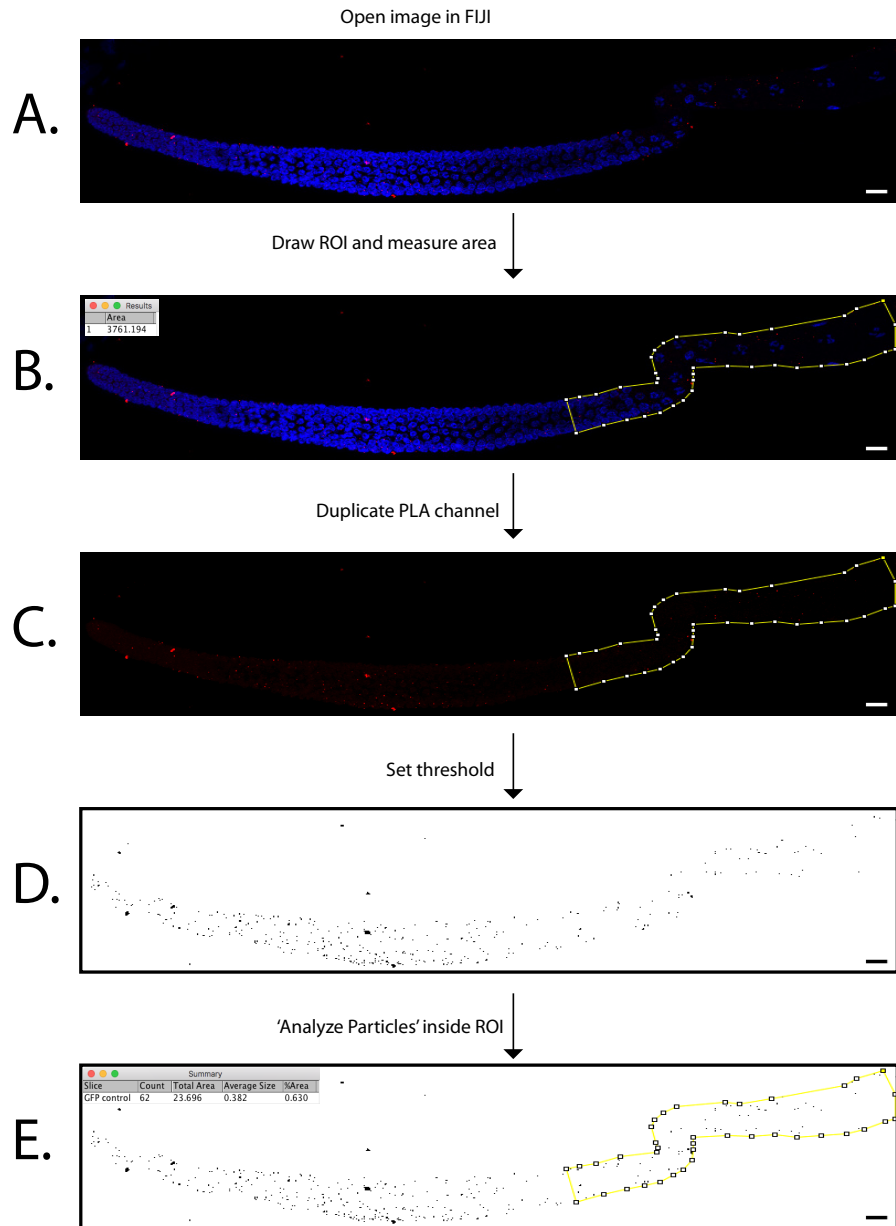


Figure 3.2: Representative images of workflow for germline PLA quantification

The germline used in this figure is a representative 3xFLAG::DLC-1; GFP germline from Figure 3.3C. Images are snapshots from FIJI/Image J: Plugins | Utilities | Capture Image. Scale bars = 10 μ M.

A) Image of merged PLA and DAPI channels opened in FIJI/ImageJ.

- B) The polygon tool in FIJI is used to outline and define the region of interest (ROI) in the germline (yellow line with white boxes) that is quantified, and the area of the ROI (μM^2) is measured (inset of B).
- C) A single image of the PLA channel is obtained by duplicating or splitting the original image in (A, B).
- D) The threshold is carefully set to distinctly highlight all PLA foci in the PLA image. The same threshold must be applied to all experimental and control images that will be analyzed together.
- E) With the ROI selected in the threshold image, the Analyze Particles function will return a table of results that includes the total count of foci included inside the ROI (inset of E).

Representative Results

Co-immunostaining of both 3xFLAG::DLC-1; GFP and 3xFLAG::DLC-1; OMA-1::GFP germlines with FLAG and GFP antibodies revealed their patterns of expression in the germline (Figure 3.3Aii-iii, 3-3Bii-iii). While GFP was expressed throughout the germline (Figure 3.3Aiii), OMA-1::GFP expression was restricted to the late pachytene and oocytes (Figure 3.3Biii) [98]. FLAG immunostaining shows that 3xFLAG::DLC-1 was expressed throughout the germline in both strains (Figure 3.3Aii, 3.3Bii). By co-immunostaining, the overlap between 3xFLAG::DLC-1 and OMA-1::GFP is indistinguishable from that between 3xFLAG::DLC-1 and GFP (negative control).

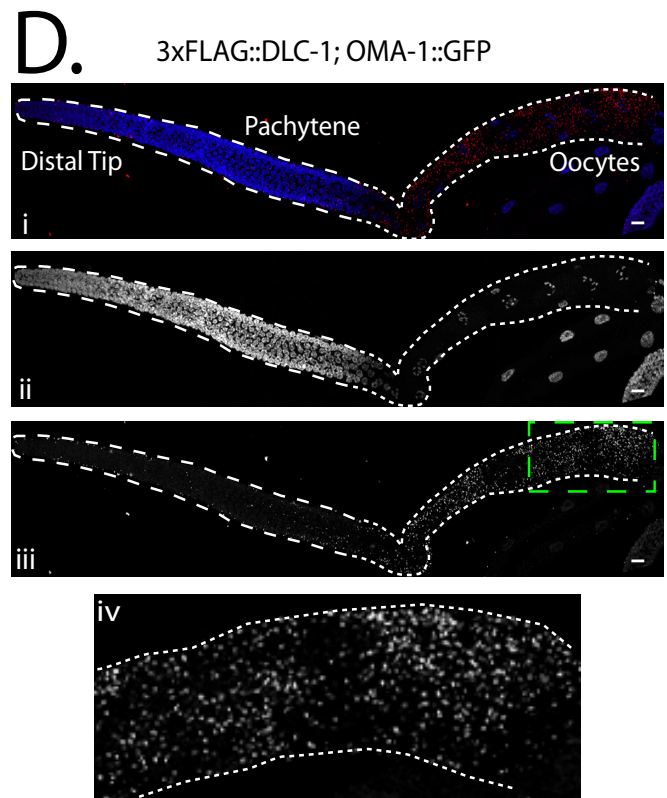
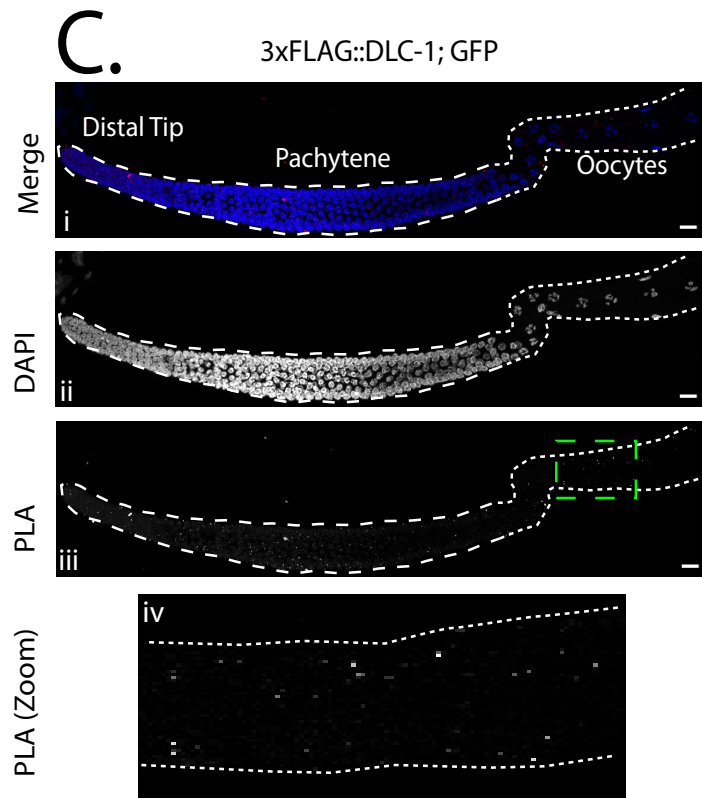
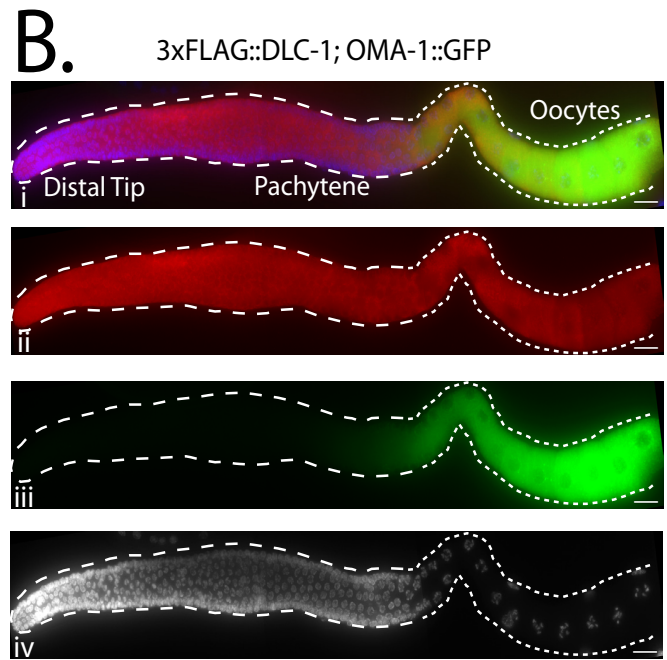
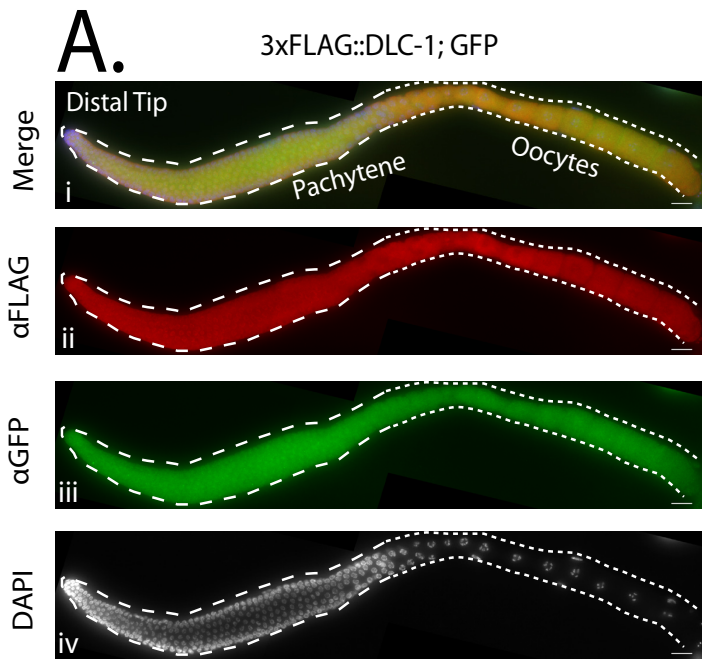


Figure 3.3: Representative images of germlines following co-immunostaining or PLA

A, B) The expression patterns of tagged proteins in 3xFLAG::DLC-1; GFP (Ai-iv) and 3xFLAG::DLC-1; OMA-1::GFP (Bi-iv) were evaluated in dissected, fixed, and immunostained gonads. Anti-FLAG antibody was used at a 1:1000 dilution, while anti-GFP antibody was used at a 1:200 dilution, which is optimal for immunofluorescence images. DNA was stained by DAPI, and the individual channel is shown in grayscale for better contrast (Aiv, Biv). In each image, the stem cells and meiotic pachytene are outlined with dashed lines, while the oocytes are outlined with dotted lines. Images were acquired with an epifluorescent microscope. Scale bars = 10 μ M.

C,D) PLA in extruded 3xFLAG::DLC-1; GFP (C) and 3xFLAG::DLC-1; OMA-1::GFP (D) gonads. Anti-FLAG antibody was used at a 1:1000 dilution, while anti-GFP antibody was used at a 1:4000 dilution. DNA was stained by DAPI, and both the individual DAPI (Cii, Dii) and PLA channels (Ciii, iv, Diii, iv) are shown in grayscale for better contrast. The green, dashed box (Ciii, Diii) denotes the location of the zoomed-in PLA images (Civ, Div). In each image, the stem cells and meiotic pachytene are outlined with dashed lines, while the oocytes are outlined with dotted lines. Images were acquired with a confocal microscope. Scale bars = 10 μ M. (A, B, C, D) were all assembled with image processing software (see Table of Materials).

Since these experiments tested for interactions between DLC-1 and OMA-1, the region of interest for PLA quantification in the germline encompassed the late pachytene through the oocytes in all germlines examined (Figure 3.2B), as this is the region of OMA-1 expression (Figure 3.1, Figure 3.3Biii). 3xFLAG::DLC-1; OMA-1::GFP germlines appeared to have a greater quantity of PLA foci within this region compared to the 3xFLAG::DLC-1; GFP germlines (Figure 3.3Ciii-iv, 3.3Diii-iv). Quantification of PLA revealed that the number of PLA foci present in 3xFLAG::DLC-1; OMA-1::GFP germlines was significantly greater than 3xFLAG::DLC-1; GFP (Figure 3.3Ciii-iv, 3.3Diii-iv; Table 3.1). Further, even with 10x higher dilution of GFP and FLAG antibodies, the difference between the control and experimental PLA was still significantly different; however, the overall density and average size of foci were reduced (Table 3.1).

Table 3.1: Summary of PLA results

| Antibody Dilution | Strain Tested | <i>N</i> | Average PLA Density (foci/ μM^2) $\times 10^{-2}$ | T test | Average Size of PLA Foci (μM^2) | T test |
|--|------------------------------|----------|---|----------------------|--|-----------|
| αFLAG (1:1000), αGFP (1:4000) | 3xFLAG::DLC-1; GFP | 11 | 4 \pm 1 | $P=1.917\text{E-}05$ | 0.5 \pm 0.1 | $P=0.057$ |
| | 3xFLAG::DLC-1; OMA-1::GFP | 11 | 9 \pm 3 | | 2 \pm 2 | |
| αFLAG (1:10,000), αGFP (1:40,000) | 3xFLAG::DLC-1; GFP | 13 | 3 \pm 2 | $P=3.395\text{E-}04$ | 0.5 \pm 0.1 | $P=0.019$ |
| | 3xFLAG::DLC-1; OMA-1::GFP | 12 | 8 \pm 3 | | 0.7 \pm 0.2 | |

Table reporting a summary of PLA quantification at two dilutions of primary antibody. The differences in average PLA density or average size of PLA foci for OMA-1::GFP between both antibody titrations were not significant (p-value not shown). The same comparison was also applied to GFP, which also resulted in no

significant difference (p-value not shown). The N values denote the number of germlines observed for analysis of PLA density and average foci size. The p-values were determined using a two-tailed/equal variance t -test.

Discussion

When studying PPIs in the *C. elegans* germline, the higher resolution offered by PLA compared to co-immunostaining allows visualization and quantification of locations where interactions occur in the germline. It was previously reported that DLC-1 directly interacts with OMA-1 using an *in vitro* GST pulldown assay [220]; however, this interaction was not recovered by an *in vivo* pulldown. The fluorescent co-immunostaining of 3xFLAG::DLC-1; OMA-1::GFP germlines shows an overlap in the expression patterns for DLC-1 and OMA-1; however, there is no indication of where their interactions occur in the germline, and the overlap itself is not greater than that between 3xFLAG::DLC-1 and GFP that is not fused to any protein (negative control). Using *in situ* PLA, it was found that DLC-1 does interact with OMA-1 in the germline, which suggests that PLA may be more sensitive for detection of PPIs compared to other approaches. Through this approach we continue to expand upon the emerging role of DLC-1 as an RBP cofactor. This work demonstrates the capability of PLA to detect PPIs in the germline and establishes a reference for future users exploring the interactions between proteins of their own interest.

PLA offers users the ability to test for PPIs with comparable sensitivity without the drawbacks associated with other techniques such as FRET and BiFC. Biologically

relevant levels of protein expression may not be optimal for FRET and BiFC. Also, the function of potential interaction partners may be affected by the large tags used in both approaches. Furthermore, FRET assays require a specialized microscopy set-up that may not be readily available. PLA may also be a cost-effective approach to study PPIs compared to other techniques. Users only need to obtain PLA reagents and access to a confocal microscope for imaging in addition to the reagents needed for immunostaining. Image analysis is performed using the open-source program FIJI/ImageJ, which is available to any user at no cost. Users that have no experience with FRET or BiFC may find PLA to be a suitable alternative. The protocol presented here only contains several additional steps beyond a typical immunostaining procedure, making this technique virtually accessible to any user with immunostaining experience.

Extrusion of the gonad by dissection is important for PLA to work successfully. Tissues that are retained inside of the worm cuticle are not labeled by PLA using this protocol. It has been further found that extruded embryos are effectively labeled by this PLA protocol. This suggests that other tissues that are released during dissection, such as the gut, are also likely to be compatible with PLA. It has been found that PLA produces robust signals on gonad as well as embryo samples prepared with two fixation protocols that are often used for immunostaining. This suggests that additional fixation procedures used in the field may be compatible with PLA but will need to be individually evaluated by the user.

Determining the optimal dilution of primary antibodies is critical for successful PLA. It is best to start with the dilution that has been optimized for immunofluorescence. This is typically achieved by titrating the primary antibody in an immunofluorescence experiment to find the optimal dilution where there is low background and a high, specific signal. Once the optimal dilutions for immunofluorescence have been established, these same dilutions can be tested in a PLA assay that compares the signal produced by a pair of potential interactors to the signal produced by a control pair of non-interacting proteins.

In the case in which abundant signal is observed in the control sample, further dilution of primary antibodies is required. It has been found that the optimal primary antibody dilutions for PLA are at least the same or even more dilute than what is used for immunofluorescence. For example, immunofluorescence images in Figure 3.3A, B are representative of a 1:1000 dilution of anti-FLAG and a 1:200 dilution of anti-GFP. However, the antibody dilutions in PLA images in Figure 3.3C, D were 1:1000 of anti-FLAG and 1:4000 of anti-GFP. The dilution of anti-GFP antibody used in PLA is greater than what was used for immunofluorescence, suggesting that PLA is much more sensitive. It was found that diluting antibodies 10-fold further resulted in a reduction of PLA density as well as the size of DLC-1/OMA-1 foci (Table 3.1). Despite this reduction, the difference in PLA density between the negative control and DLC-1/OMA-1 was still significantly different. This suggests that PLA is still very sensitive with higher dilutions of primary antibody; however, the prevalence of detectable interactions will be underestimated.

By contrast, too low of an antibody dilution might have two kinds of detrimental consequences. First, it may produce significant background signal in the negative control. Second, PLA foci produced by the interacting partner proteins might merge and overlap, making them difficult to resolve in a max projection image. This leads to an underestimation of PLA foci number and density during image analysis. PLA signal is a balance of detecting spurious proximity between non-interacting partners and detecting every instance of real PPIs that occur in the sample. As a result, incorporation of a negative control where two proteins do not interact is essential for determining the level of background in PLA experiments. Omission of a primary antibody in a PLA experiment has been used as a negative control in other reports [213,214]; however, this approach cannot account for nonspecific interactions or nonspecific antibody binding that may impact the result in the experimental PLA. GFP was used here as a negative control, since no direct interaction between DLC-1 and GFP was expected. It was found that the negative control did have some background signal. This further supports the importance of a negative control for a PLA assay when evaluating the experimental data.

Once PLA-optimized dilutions are established, these dilutions can be used to test across an array of different worm strains that contain different pairs of interaction partners tagged with the same affinity tags. It is important to use the same pair of primary antibodies to ensure a fair comparison of resulting PLA signals, as variation in antibody affinity can affect the outcome of a PLA experiment. Another report on PLA suggests optimizing dilution of the PLA secondary antibodies [214]; however, this is not

recommended. Higher dilutions of secondary antibodies may reduce the efficacy of the other downstream PLA steps that depend on recognition of PLUS and MINUS probes that are conjugated to the secondary antibodies.

Chapter 4

P Granule Components Interact with and Require DLC-1 for their Subcellular Localization

Abstract

Germ granules are cytoplasmic assemblies of RNA binding proteins (RBPs) that execute post-transcriptional regulation to ensure germ cells remain totipotent and maintain their identity from generation to generation. Compartmentalization of proteins and RNAs into germ granules is critical for their function in germ cells. Localization and formation of *Caenorhabditis elegans* germ granules, also known as P granules, in zygotes depends on ordered assembly of several core proteins *in vivo*. Here we investigate the role of the RBP cofactor and hub protein, DLC-1, as an additional determinant of P granule assembly. We find that DLC-1 directly interacts with several core P granule proteins, predominantly during embryogenesis. Additionally, we show that loss of *dlc-1* disrupts assembly of multiple P granule components, regardless of whether or not DLC-1 directly interacts with these proteins. Our findings highlight the importance of the RBP cofactor DLC-1 for P granule assembly.

Introduction

Membraneless organelles, such as RNA granules, are linked to regulatory pathways in the cell and are also implicated in diseases [40,45]. These condensates sequester different proteins and RNAs in the cell to carry out specific functions. Protein constituents of RNA granules have different types of domains that promote protein-protein interactions and can contribute to granule assembly (see section 1.1.3). The molecular interactions of RNA granule constituents are under intense investigation to elucidate the principles behind RNA granule assembly. Using P granules in *C. elegans* 1-cell stage embryo as a model system for RNA granule assembly, the field has begun to reveal the factors that drive this process.

In *C. elegans*, localization and assembly of P granules are most dynamic in zygotes, prior to the first cell division. During this time, P granules transition from a uniform distribution throughout the zygote to localization in the posterior region, leading to an asymmetric distribution of P granules (Figure 4.1A). This results in segregation of P granules into the cell designated for the germline lineage (see orange cells in P0-P1 embryos in Figure 1.1A). Previous studies proposed conflicting mechanisms explaining dynamic P granule localization. Initial analysis suggested directed cytoplasmic flow of granules to the posterior region [221,222]. A later study found that the fluxes of P granule components in the anterior and posterior regions of a 1-cell stage embryo were similar, suggesting that cytoplasmic flow is not involved [39]. By contrast, the asymmetry is established through regulated dissolution and condensation of P granule components in the anterior and posterior, respectively [39]. In turn, P granule condensation in the

posterior was postulated to proceed by liquid-liquid phase separation (LLPS; described in 1.1.3) [39], giving rise to the cell lineage that will become the germline.

Current models explaining selective LLPS of P granules in the posterior describe sequential asymmetric segregation of cytoplasmic RBPs (Figure 4.1A). First, RBPs MEX-5 and MEX-6 form a cytoplasmic gradient during the first cell division as a consequence of localized phosphorylation and dephosphorylation. Phosphorylation of MEX-5/6 by the posteriorly-localized PAR-1 kinase increases their diffusivity in the posterior of the zygote [104,223,224]. By contrast, dephosphorylation of MEX-5/6 proteins by phosphatases in the anterior results in their slower diffusivity, leading to an anterior-rich concentration gradient of MEX-5/6 proteins (Figure 4.1A)[104,224]. The cytoplasmic gradient of MEX-5/6 proteins in turn controls the segregation of several other RBPs by promoting their redistribution from the anterior to the posterior [225]. This mechanism ensures posterior localization of paralogous RBPs MEG-3 and MEG-4 [35,226], as depletion of *mex-5/6* by RNAi result in MEGs becoming dispersed throughout the embryo (Figure 4.1B)[35]. In the anterior region, MEX-5/6 proteins bind and sequester mRNAs, reducing availability of RNA for MEG-3/4 [35]. This in turn inhibits MEG-3/4's ability to phase separate [35]. By contrast, MEG-3/4 still interact with mRNAs in the posterior, where the MEX-5/6 concentration is low. This allows the MEG proteins to concentrate and phase-separate in the posterior where they nucleate assembly of P granules [35]. Phase separation of MEG-3 involves both interactions mediated by IDRs and binding to mRNAs [34,35]. Posterior-localized MEG proteins promote localization of other P granule components to this region, including PGL-1 and its paralog PGL-3 (Figure 4.1A)[103,105]. In *meg-3/meg-4* mutant embryos, PGLs are

scattered throughout the embryo and fail to enrich in the germ cell during later stages of development (Figure 4.1C) [103]. On the contrary, mutation or depletion of both *pgl-1* and *pgl-3* does not disrupt posterior localization of MEGs (Figure 4.1D)[35,103]. This suggests that MEG proteins are important for establishing PGL asymmetry perhaps through facilitating P granule assembly in the posterior.

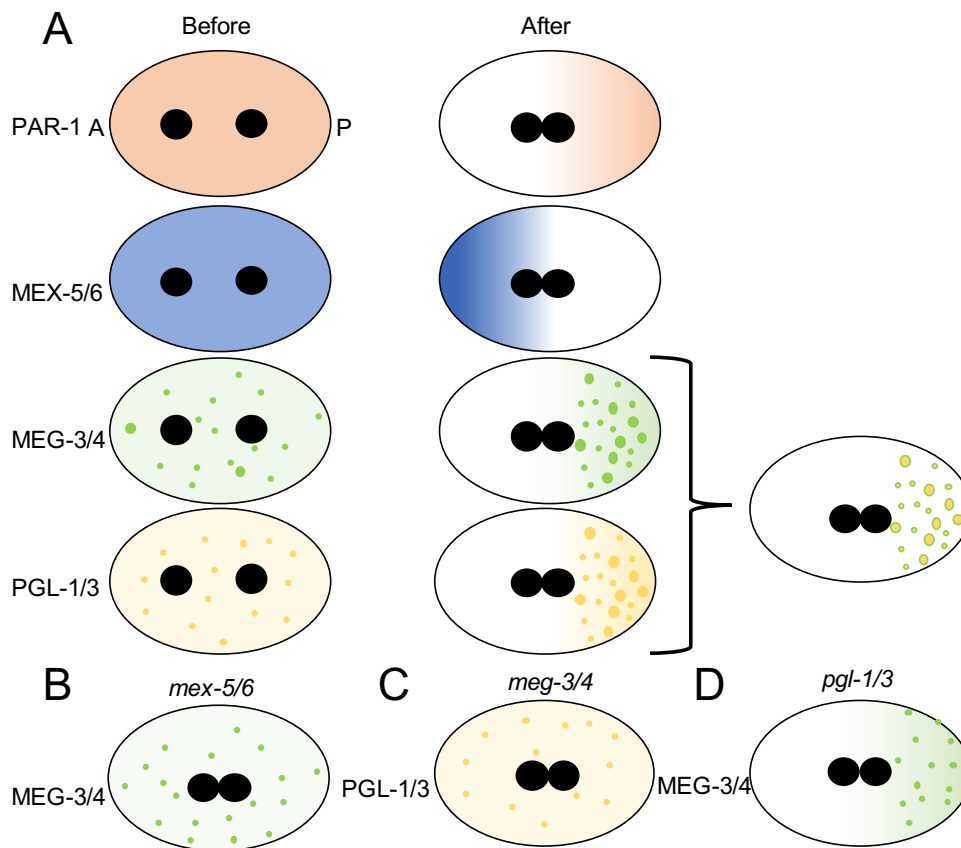


Figure 4.1: P granule asymmetry in 1-cell embryos

A) Schematic showing distribution of different proteins involved in P granule asymmetry before (pronuclear formation) and after (when pronuclei meet) polarization has occurred. Shaded regions denote presence of diffuse protein, while puncta represent formation of P granules. The bracket points to an embryo showing that MEG and PGL proteins condense together, where MEGs form a

shell around a core of PGL proteins [103,105]. 'A' and 'P' labels denote the orientation of the anterior and posterior regions, respectively, of all embryos in schematic.

B-D) Distribution of proteins when polarization occurs in embryos mutant or knocked down by RNAi for: B) *mex-5/6* [35]; C) *meg-3/4* [35,103]; D) *pgl-1/3* [35,103] (noted above each embryo).

Additional proteins required for P granule assembly include the GLH family of RNA helicases. GLH-1 and its paralog GLH-4, which are also P granule constituents, are critical for PGLs to assemble with P granules. Upstream of GLH-1 is DEPS-1, which promotes GLH-1 protein expression and subsequent assembly of P granules [227]. *glh-1* mutant worms exhibit sterility at high temperatures (26°C) and PGL-1 does not localize to P granules in germlines and embryos [228]. Further, a double mutant of *glh-1* and its paralog, *glh-4*, enhances sterility and has a similar effect on PGL-1 localization to P granules in the germline [229,230]. In addition, co-depletion of *glh-1* and *glh-4* by RNAi results in loss of PGL-3 localization to embryonic P granules [231]. These findings support the role of GLHs in functioning upstream of PGL proteins to promote their localization to P granules. Like *glh-1* mutants, *pgl-1* null single mutants exhibit sterility at high temperature [228], while *pgl-3* null single mutants show no significant sterility at any temperature (16°, 20°, or 26°C) [232]. *pgl-1; pgl-3* double mutants exhibit significant sterility at all temperatures, suggesting that PGL-3 functions redundantly with PGL-1 to promote fertility. In *pgl-1; pgl-3* mutants, GLH-1 shows no defect in localization to germline P granules [232], however knockdown of *pgl-1* and *pgl-3* by RNAi revealed

that GLH-1 protein requires PGLs to localize to embryonic P granules [231]. In addition, this knockdown also led to a reduction in localization of other proteins to P granules, such as: IFE-1 [233], MEX-3 [231], and POS-1 [231], suggesting that PGLs are important for recruiting other P granule components. Assembly of these P granule components is important for overall function of P granules in both the germline and embryos. Simultaneous depletion of both *pgl-1/3* and *glh-1/4* genes by RNAi has detrimental effects on the germline, where absence of assembled P granules causes germ cells to differentiate into somatic cells [71]. Together, these genetic approaches highlight GLH and PGL proteins as core components that are important for both P granule assembly and fertility. These studies point to a pathway of embryonic P granule assembly, where MEGs assemble with and promote localization of PGLs (and likely GLHs) to the posterior, which leads to recruitment of additional proteins to P granules.

Beyond the core P granule components, genetic approaches identified additional genes that are required for formation of P granules [234,235]. Many of these genes are involved in diverse cellular processes such as: cell cycle regulation, protein degradation, RNA splicing, and nuclear-cytoplasmic transport. These findings suggest that P granule localization and assembly are not based only on core constituents, but are also influenced by other genes and cellular processes. To this point, cofactors could also have a role in P granule assembly as they affect localization and function of RBPs in the cell. We previously identified a light chain subunit of the dynein motor complex, dynein light chain 1 (DLC-1), as a cofactor for the germline RBPs FBF-2 [171] and GLD-1 [172]. These findings demonstrated that DLC-1 promoted the function of these RBPs and the localization of FBF-2 to P granules. Through RIP-seq, we found that DLC-1 associates

with more than 2700 mRNAs, suggesting that DLC-1 is a cofactor for many RBPs [220]. DLC-1 is member of the LC8 family proteins that serve as hubs to promote assembly of larger protein complexes (see section 1.4 of Introduction), suggesting that DLC-1 could be in complex with many RBPs. As a result, we hypothesized that DLC-1 interacts with multiple RBPs and affects their subcellular localization. In this report, we use an *in silico* interaction motif scanning approach to predict what other RBPs interact with DLC-1. We find that DLC-1 directly interacts with several P granule component RBPs and is important for their localization in embryos. Our findings suggest that DLC-1 is integral for P granule assembly and highlights the importance of cofactors in promoting subcellular localization of RBPs.

Materials and Methods

Nematode Strains and Culture

C. elegans strains (Table 4.1) were cultured as described in Chapter 2. The *3xFLAG::dlc-1(mntSi13); gfp::pgl-3(mntIs9)* strain (UMT420) was generated by crossing UMT282 males with JH2469. The *3xFLAG::dlc-1(mntSi13); pgl-1::gfp(ax3122)* strain (UMT432) was generated by crossing UMT282 males with JH3269. The *meg-3::ollas (ax3051); meg-4::3xFLAG; dlc-1(tm315)//hT2* strain (UMT398) was generated by crossing UMT351 males with JH3374.

Bioinformatics

Biochemically verified LC8 binding sites (Table 4.3) were analyzed by the motif discovery tool Multiple EM for Motif Elicitation (MEME) [236] to generate consensus motifs. The best represented consensus motif was then used by the Find Individual Motif

Occurrences (FIMO) [195] program to scan the *C. elegans* proteome (Ensembl Release 96, WBcel235). Proteins that contained at least one instance of the motif and met the threshold for a significant match of $P < 0.0001$ were sorted to the output. To identify RBPs, the output was compared against comprehensive lists of *C. elegans* RBPs [22,26] and is represented in Figure 4.2D and Supplemental Table 1.

***In vitro* pulldowns**

Cloning and bacterial overexpression of proteins was performed as described in Chapter 2. Additionally, full length MEG-3, MEG-4, and DAZ-1 were each cloned into the pMALc2 vector to generate Maltose Binding Protein (MBP)-tagged proteins to improve solubility. Expression of MBP tagged proteins followed the similar protocol as described in Chapter 2 for 6xHis-tagged proteins.

RNAi

The procedure for RNAi is described in Chapter 2, with the exception of incubation temperature for growing synchronized L1 nematodes, which were grown at 20°C. This temperature was still permissible for GFP::*PGL-3* expression and also ensured that *dlc-1* (*RNAi*) worms were able to produce embryos.

Western Blotting

The protocol for Western blotting of *in vitro* pulldowns is described in Chapter 2. Additionally, anti-Maltose Binding Protein antibody (DSHB-MBP-3D7) [237] was used at 1:800 to determine the outcome of pulldowns using MBP-tagged proteins.

Nematode Dissection, Immunostaining, and Imaging

The procedure for dissection, immunostaining, and imaging of germlines is described in Chapter 2. Immunostaining of embryos followed the same procedure as for germlines;

however, worms were dissected in half at the vulva to release embryos. The primary and secondary antibodies and their dilution factors used for immunostaining 3xFLAG::DLC-1, GFP-tagged proteins, and endogenous P granule proteins are described in Table 4.2. Colocalization analysis was performed in FIJI/ImageJ using the Just Another Colocalization Plugin (JACoP) program [238].

Proximity Ligation Assay, Imaging, and Quantification

The protocol for proximity ligation assay of germlines and embryos is described in Chapter 3 and antibody dilutions are reported in Table 4.2. All PLA-treated germlines and embryos were imaged using a Zeiss 880 confocal microscope and their PLA densities were quantified using the FIJI/Image-based workflow described in Chapter 3. To quantify the PLA density, the germlines were split into three standardized regions of interest (ROIs) corresponding to distinct developmental stages for all strains analyzed (see Figure 4.3Div, Eiv, Fiv). Zone 1 encompassed the distal tip region through the early pachytene. Zone 2 is comprised of the proximal half of the pachytene, where the mid-pachytene region was defined as starting at the 16th cell row back from the last cell row of the pachytene before individual oocytes are observed, based on the pattern of expression for GFP::PGL-3 in the germline. Finally, zone 3 encompassed all oocytes. To measure PLA density in embryos, the ellipse tool in FIJI/ImageJ was used to encompass the whole embryo to define the ROI. The anti-PGL-1 antibody was used to co-immunostain for PGL-1 to mark P granules in the germ cell during embryo PLA experiments, using the same dilution as with the immunostaining of embryos. The antibody was incorporated into the primary antibody solution along with the anti-FLAG and anti-GFP antibodies and incubated for the same time and temperature (overnight, 4°C). When the PLA probes

were added to the sample the next day, the anti-Mouse IgM Alexa 633 was also included in the mix using the same dilution as with the immunostaining of embryos and incubated at the same time and temperature (1hr, 37°C). For quantification of relative area of PLA at P granules, a single focal plane where the PGL-1 immunostain signal is best visible was chosen. An ROI that encompassed the germ cell and P granules was drawn using the ellipse tool. This germ cell ROI was duplicated and placed on a somatic cell (ideally on a cell on the opposite side of the embryo) containing PLA foci, to ensure that the same area of measurement is used. The image was then subjected to the same particle threshold as was used to quantify whole embryo PLA. Quantification of relative area of PLA within each ROI was obtained using the same workflow described in Chapter 3. For embryos where PLA was only observed at the P granule but not in the somatic cell, the relative area for the somatic cell was substituted with the minimum value observed among somatic cells in the dataset.

Table 4.1: Nematode strains used in this study

| Genotype | Description | Strain | Reference |
|---|---|---------|------------|
| Transgene | | | |
| <i>unc-119(ed3); mntIs9 [pEV6.02]</i> | <i>pie-1 prom::lap::pgl-3::pgl-3 3'UTR + unc-119 (+)</i> | JH 2469 | This study |
| <i>mntSi13[pME4.1]; him-8(tm611) IV; unc-199 (ed3)</i> | <i>dlc-1 prom::3xFLAG::dlc-1::dlc-1 3' UTR</i> | UMT 282 | [171] |
| <i>mntSi13[pME4.1] II; mntSi21 (pXW6.22; ceGFP); unc-119(ed3) III</i> | <i>dlc-1 prom::3xFLAG::dlc-1::dlc-1 3' UTR; gld-1 prom::ceGFP::jbf-1 3' UTR + unc-119 (+)</i> | UMT 422 | [239] |
| <i>mntSi13[pME4.1] II; unc-119 (ed3) III; mntIs9 [pEV 6.02]</i> | <i>dlc-1 prom::3xFLAG::dlc-1::dlc-1 3' UTR; pie-1 prom::lap::pgl-3::pgl-3 3'UTR + unc-119 (+)</i> | UMT 420 | This study |
| <i>mntSi13[pME4.1] II; unc-119 (ed3) III;</i> | <i>dlc-1 prom::3xFLAG::dlc-1::dlc-1 3' UTR; pgl-1 prom</i> | UMT 432 | This study |

| | | | |
|---|---|---------|------------|
| <i>pgl-1(ax3122[pgl-1::gfp]) IV</i> | <i>::pgl-1::GFP::pgl-1 3'UTR+unc-119(+)</i> | | |
| Mutant Strains | | | |
| <i>meg-3(ax3051); meg-4(ax2080)</i> | MEG-3::OLLAS; MEG-4::3xFLAG | JH 3374 | [35] |
| <i>dlc-1(tm3153)/hT2 (III); him-8(tm611) IV</i> | | UMT 351 | [172] |
| <i>dlc-1(tm3153)/hT2 [bli-4(e937) let-?(q782) qIs48] (III); meg-3(ax3051); meg-4 (ax2080) X</i> | MEG-3::OLLAS; MEG-4::3xFLAG | UMT 398 | This Study |
| <i>pgl-1(ax3122[pgl-1::gfp]) IV</i> | <i>pgl-1 prom ::pgl-1::GFP::pgl-1 3'UTR</i> | JH 3269 | [105] |

Table 4.2: Antibodies used in this study for immunostaining

| Primary Antibody | Host | Manufacturer | Dilution | Secondary Antibody | Host | Manufacturer | Dilution |
|--|--------|-------------------|----------|---------------------------|--------|----------------|----------|
| Antibodies used to immunostain embryos and germlines to demonstrate DLC-1 and PGL-1/3 patterns of expression | | | | | | | |
| Anti-FLAG | Mouse | Sigma-Aldrich | 1:1000 | Anti-Mouse IgG Alexa 594 | Goat | Jackson Immuno | 1:200 |
| Anti-GFP | Rabbit | Life technologies | 1:200 | Anti-Rabbit IgG Alexa 488 | Goat | Jackson Immuno | 1:200 |
| Antibodies used for PLA | | | | | | | |
| Anti-FLAG | Mouse | Sigma-Aldrich | 1:1000 | Anti-Mouse MINUS | Donkey | Sigma-Aldrich | 1:5 |
| Anti-GFP | Rabbit | Life technologies | 1:4000 | Anti-Rabbit PLUS | Donkey | Sigma-Aldrich | 1:5 |
| Antibodies used for immunostaining wild type or <i>dlc-1</i> mutant embryos | | | | | | | |
| Anti-OLLAS | Rat | Novus Bio | 1:200 | Anti-Rat IgG Alexa 594 | Goat | Jackson Immuno | 1:200 |
| Anti-FLAG | Mouse | Sigma-Aldrich | 1:1000 | Anti-Mouse IgG1 Alexa 488 | Goat | Jackson Immuno | 1:700 |

| | | | | | | | |
|--|--------|-------------------|-------|---------------------------|------|----------------|-------|
| Anti-PGL-1 (K76) | Mouse | DSHB | 1:125 | Anti-Mouse IgM Alexa 633 | Goat | Thermo-Fisher | 1:200 |
| Antibodies used for immunostaining embryos treated by control or <i>dlc-1</i> RNAi | | | | | | | |
| Anti-PGL-1 (K76) | Mouse | DSHB | 1:125 | Anti-Mouse IgM Alexa 594 | Goat | Jackson Immuno | 1:200 |
| Anti-GFP | Rabbit | Life technologies | 1:200 | Anti-Rabbit IgG Alexa 488 | Goat | Jackson Immuno | 1:200 |

Results

In Silico and *In Vitro* Identification of RBPs that Bind DLC-1

Given the high number of DLC-1-associated mRNAs that were identified using RIP-seq (Chapter 2), we hypothesized that DLC-1 interacts with multiple RBPs. In order to predict what these other RBPs might be, a bioinformatic scan was used to identify RBPs that contained the LC8 interaction motif. Using previously published LC8-interacting peptides [139] together with DLC-1 interaction sites on the RBPs FBF-2 [171] and GLD-1 [172] confirmed in our lab (Table 4.3), we used the bioinformatic MEME tool [194] to create an interaction motif that represents all of these determined and verified LC8 interaction sequences. This interaction motif contains the conserved ‘TQT’ residues and resembles the canonical LC8 interaction motif [139] (referred to as Motif A; Figure 4.2A). This motif best represents the peptides containing ‘TQT’ residues present in more than half of input sequences, but does not represent the peptides without the ‘TQT’ residues. In an effort to better represent the diversity of LC8-interacting sequences, we generated additional motifs by varying the peptides used as input for MEME. Two

selections of divergent interaction sequences sourced from different model organisms in the initial dataset were used as input for the MEME tool to generate more diverse binding motifs (Motifs B and C, Figure 4.2B-C). The DLC-1 interaction sites on the RBPs FBF-2 [171] and GLD-1 [172] were included in a group of input sequences that generated motif B, the ‘DRSSQT’ motif (Figure 4.2B). Alternatively, the low-complexity and serine-rich FBF-2 interaction sites were replaced with sequences containing the representative ‘QVD’ residues reported in [154] to avoid creating a degenerate motif that recovers non-specific, false-positive interactors. This selection of input sequences produced motif C, the ‘PASSAY’ motif (Figure 4.2C). Together, motifs B and C share less resemblance with the overrepresented ‘TQT’ residues in motif A and reflect greater diversity of LC8 interaction sites. Motifs A-C were then used to scan the *C. elegans* proteome to identify proteins that contained at least one instance of one of these interaction motifs. To identify RBPs, the output from these proteome scans was compared against comprehensive lists of *C. elegans* RBPs [22,26]. Together, scans with each of the three motifs yielded a total of 108 RBPs predicted to interact with DLC-1 by a single motif scan and an additional 18 RBPs that were identified by more than one motif scan (Figure 4.2D; Supplemental Table 1). Motif scans were able to identify known DLC-1 RBP interactors including GLD-1 [172] (by all three scans) and FBF-2 [171] (by the Motif B scan). Furthermore, several predicted DLC-1 interactors have been previously recovered by high-throughput yeast two-hybrid screens including CEH-100 (Motif A) [240], F26F4.5 (Motif A) [240], SPAT-1 (Motif B) [240], R07B7.2 (Motif B) [240], SAS-7 (Motifs A and B) [240], and PGL-3 (Motif C) [241] (Figure 4.2D). We conclude that motif scans are capable of retrieving DLC-1 interaction partners. Surprisingly, all three motif scans identified

putative RBP interactors that are also components of P granules, which include: GLD-1 [242], PGL-1 [228], PGL-3 [232], GLH-4 [230], MEG-4 [103], GLD-2 [243], and POS-1 [244]. P granules are required for fertility and post-transcriptional mRNA regulation; however, the mechanism of their assembly is not fully understood. The emerging role of DLC-1 as a hub for protein complex assembly in other studies led us to test whether it directly interacts with these RBPs, which could support its role in P granule assembly.

Table 4.3 LC8 interaction sites used for MEME analysis

| Motif A | Motif A Cont. | Motif B | Motif C |
|-------------|---------------|-------------|-------------|
| CITLVKSTQTV | IPVKHNSTQTV | CITLVKSTQTV | CITLVKSTQTV |
| KRMLDAQVQTD | VGMHSGTQTA | VKLVDAESQTL | VKLVDAESQTL |
| LESLDIETQTD | AEMKDTGIQVD | TEVETREIGVG | TEVETREIGVG |
| VTQNTASQTM | SASADFDVQTS | LNAWDNASQAY | LNAWDNASQAY |
| PTTANYGSQTE | DNYAESGIQTD | TPTRDVATSPI | TPTRDVATSPI |
| SPMVAQGTQTP | VETCNFSVQTF | DSISDRHIQTM | DSISDRHIQTM |
| RATAEFSTQTP | KEAVDNLQTE | QPKDDKNTMTD | QPKDDKNTMTD |
| PMSCDKSTQTP | PSQNNIGIQTM | SPISSAYSQTP | SPISSAYSQTP |
| TSQEDKATQTL | ETVVSAAATQTI | IDRSKSYGSSK | RDTGVQVDR |
| PRMLHRSTQTT | TPTRDVATSPI | SSVSVKFSSSG | LSIGIQVDD |
| TLVYTKQTQTT | RSEDKSTQTT | | |
| VVSYSKETQTP | KSTEDKSTQTP | | |
| IVTYTKETQTP | LGVCKYTVQDE | | |
| LVLKDLGIQVD | RATTSQATQTE | | |
| VKLVDAESQTL | TILVSRSTQTG | | |
| PSLVSRGTQTE | LGHFTRSTQTS | | |
| KQTEDKGVQCE | GVQMAKSTQTF | | |
| NRCLSIGIQVD | QDVLRRTVQTR | | |
| SKFQSVGVQVE | SATSAKATQTD | | |
| TEVETREIGVG | SCMQERAIQTD | | |
| DHHQDKQTQTP | TEKVDRSTQDE | | |
| TTIPTKQTQTF | DSISDRHIQTM | | |
| SHRTTKSTQTQ | PKTRNSQTQTD | | |
| SRSKSKSTQTV | SPISSAYSQTP | | |
| VVAYPKRSQTS | IDRSKSYGSSK | | |
| LNAWDNASQAY | SSVSVKFSSSG | | |
| QPKDDKNTMTD | | | |

Table reporting the LC8 interaction peptides used for generating each consensus motif shown in Figure 4.2D.

To determine whether DLC-1 might directly interact with predicted RBP partners, DLC-1 and six putative interacting RBPs were expressed in bacteria and tested for direct interaction using *in vitro* GST pulldowns. Tested RBPs included PGL-1, PGL-3, GLH-4, MEG-4, IFG-1, and DAZ-1. Four of these (PGL-1, PGL-3, GLH-4, MEG-4) directly interacted with DLC-1 (Figure 4.2E). Interaction between DLC-1 and PGL-3 was previously observed in a high-throughput yeast two hybrid screen [241]. DAZ-1 did not directly interact with DLC-1 despite a report that the mouse ortholog of DAZ-1, Dazl, interacted with LC8 [164], and neither did IFG-1. PGL, GLH, and MEG proteins are members of protein families containing several paralogous proteins, so we investigated whether the remaining paralogs not recovered by motif scans were able to interact with DLC-1. MEG-3, a paralog of MEG-4 with 71% identity [103], weakly interacted with DLC-1 compared to MEG-4. By contrast, PGL-2 and GLH-1 did not interact with DLC-1 at all. We conclude that the bioinformatic analysis has successfully enriched DLC-1-interacting proteins within the list of putative interaction candidates.

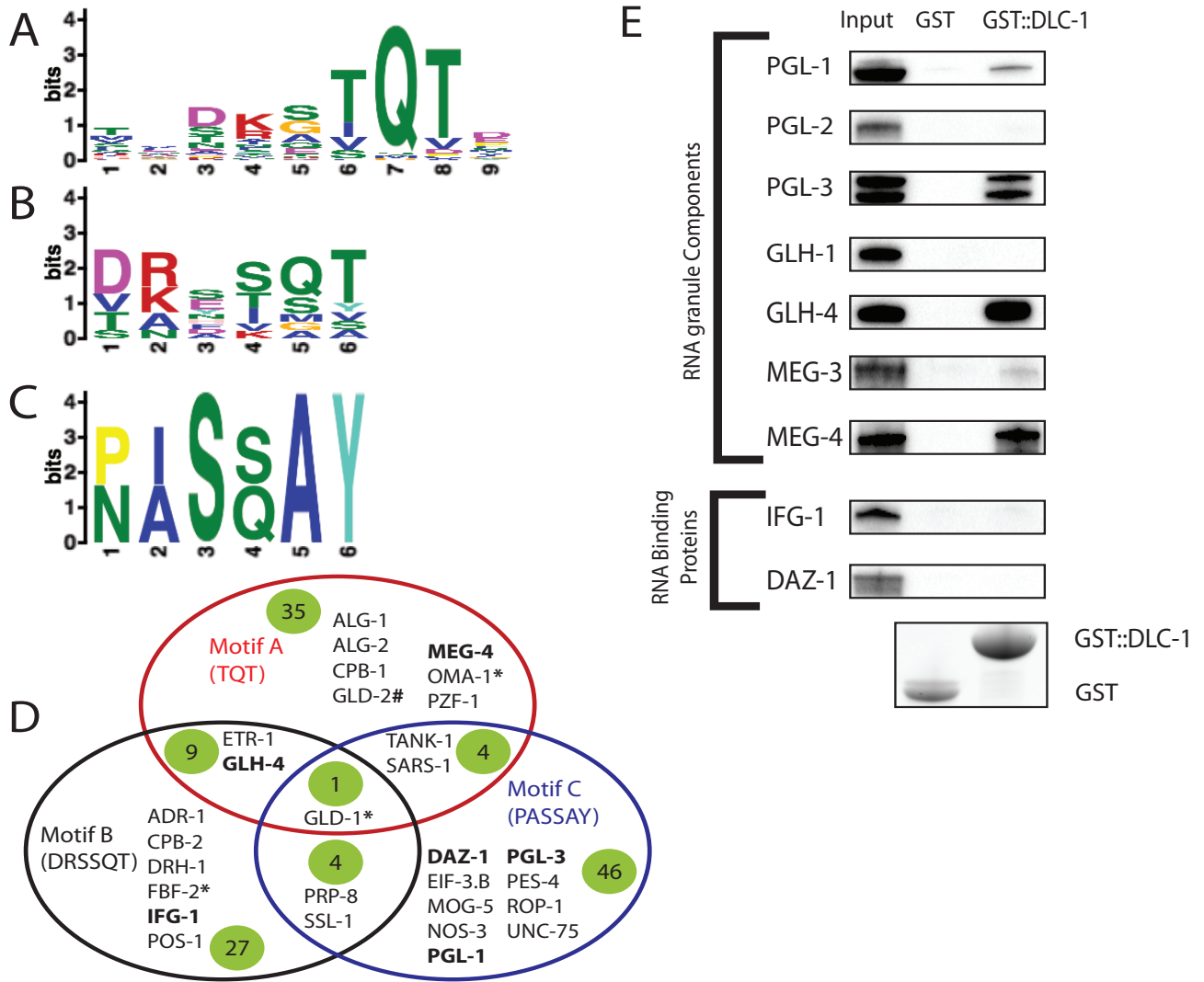


Figure 4.2: Motif scans identify *C. elegans* LC8-interacting proteins

- A) MEME analysis of published LC8 binding sites (Table 4.3) generates the canonical binding motif A similar to one reported in [139].
- B) MEME analysis of less-represented LC8 binding sites that include binding sites from GLD-1 [172] and the FBF-2 [171] (Table 4.3) generates an alternative motif B.

- C) MEME analysis of less-represented LC8 binding sites, GLD-1, and additional atypical LC8 binding sites from [154] (Table 4.3) generates an alternative motif C.
- D) Scanning the *C. elegans* proteome with motifs shown in A-C identifies 126 RBPs as defined by ([26] and [22]). The red, black, and blue circles represent the results from each respective motif scan (A-C). Examples of RBPs found exclusively by each motif scan are presented in each circle. Examples of RBPs found by more than 1 scan are shown in regions where circles overlap. The numbers in green circles represent how many RBPs were identified in each exclusive group or overlap between groups. Bold text indicates RBPs that have been tested for interaction *in vitro* in this report. Both * and # denotes that the protein has been tested for interaction in prior work. * indicates an interaction with DLC-1, while # indicates no interaction with DLC-1.
- E) Representative western blots of *in vitro* GST pulldowns between GST::DLC-1 and RBPs identified by the proteome scan. All RBPs tested were 6xHis-tagged with the exception of MEG-3, MEG-4, and DAZ-1, which were MBP-tagged. PGL-2, GLH-1, and MEG-3 were included for comparison against their paralogs PGL-1, PGL-3, GLH-4, and MEG-4, which were recovered with the motif scan.

DLC-1 is Incorporated into PGL-1-Containing Complexes in the Germline

To test whether DLC-1-RBP interactions identified *in vitro* are observed *in vivo*, we used an *in situ* approach to observe and quantify these interactions. For these experiments, we focused on core P granule components PGL-1 and PGL-3 [231]. We first examined

whether DLC-1 is co-expressed with PGL-1 and PGL-3 in the germline, as overlapping regions of expression may indicate where these proteins interact. Using co-immunostaining, we observed their patterns of expression in 3xFLAG::DLC-1; GFP, 3xFLAG::DLC-1; PGL-1::GFP, and 3xFLAG::DLC-1; GFP::PGL-3 germlines (Figure 4.3A-C). Anti-FLAG immunostaining of germlines expressing 3xFLAG::DLC-1 revealed uniform expression throughout the germline, as also observed in Chapter 3 and previous reports [171,196] (Figure 4.3Aii, Bii, Cii). Anti-GFP immunostaining of GFP control germlines found GFP uniformly distributed throughout the germline, similar to a previous observation made in Chapter 3 (Figure 4.3Aiii). Expression patterns of GFP-tagged PGL-1 and PGL-3 in the germline (Figure 4.3Biii, Ciii) showed both proteins localized to P granules in germ cells and oocytes, however PGL-1 is expressed throughout the germline while PGL-3 expression begins in the mid-pachytene region, as previously observed [232]. Based on these observations, we concluded that both PGL-1 and PGL-3 are co-expressed with DLC-1, suggesting that they could interact in the germline.

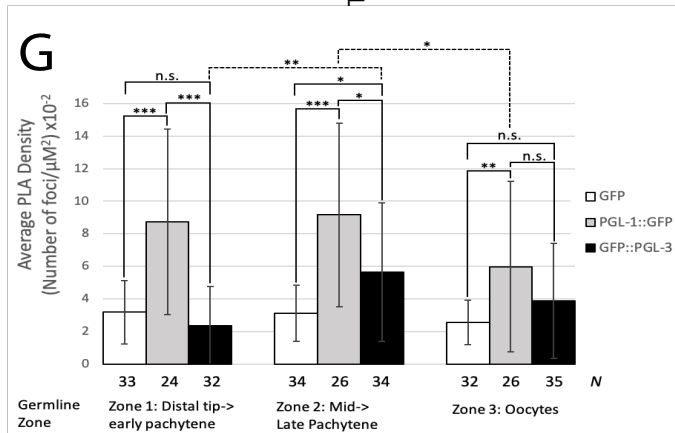
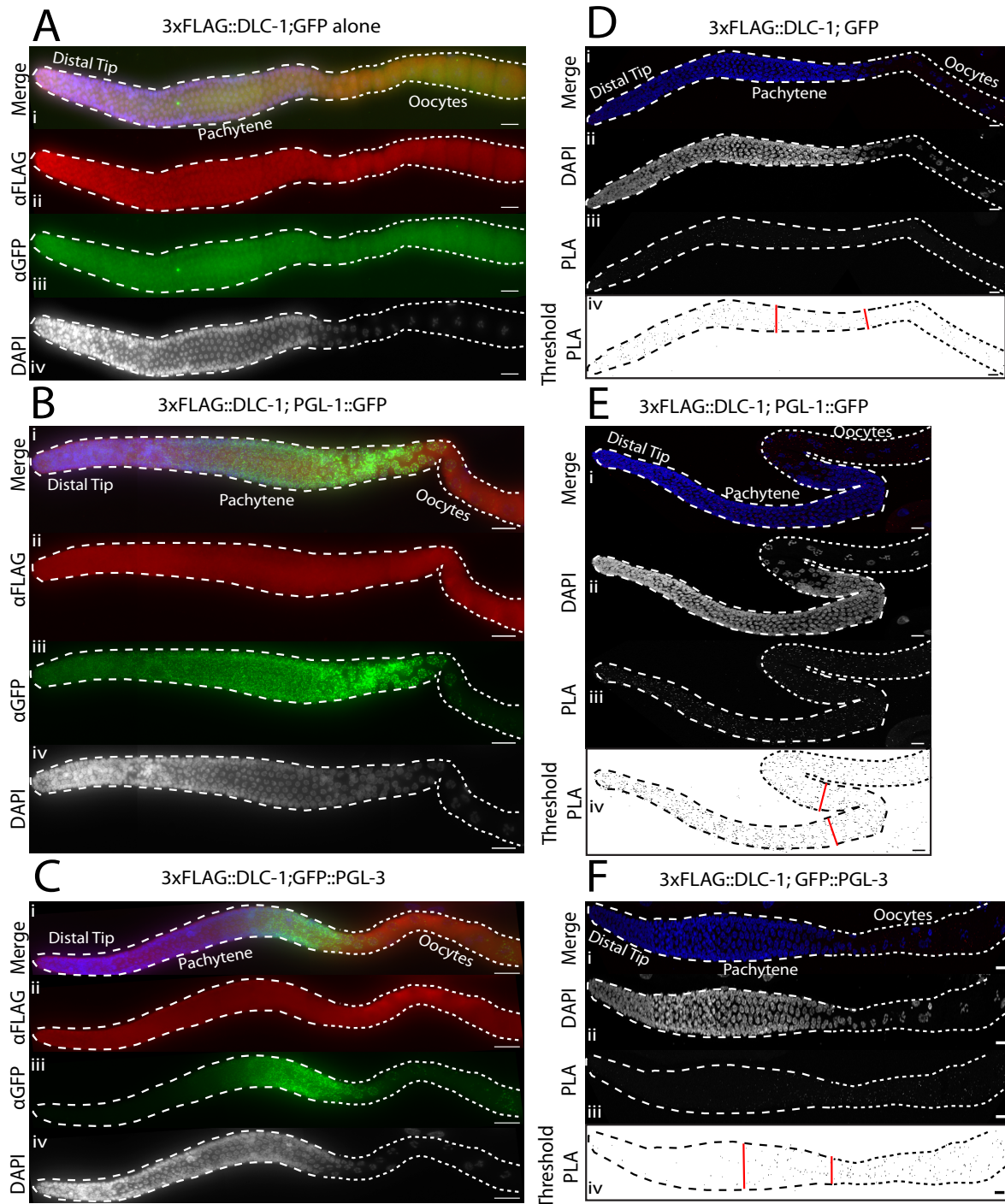


Figure 4.3: Proximity ligation detects formation of DLC-1/PGL complexes in the germline

A-C) The expression patterns of tagged proteins in 3xFLAG::DLC-1; GFP (Ai-iv), 3xFLAG::DLC-1; PGL-1::GFP (Bi-iv), and 3xFLAG::DLC-1; GFP::PGL-3 (Ci-iv) immunostained gonads. 3xFLAG::DLC-1 is in red, GFP or GFP-tagged proteins are in green, and DNA is labeled by DAPI (blue in the merged image and the individual channel in grayscale; Aiv, Biv, Civ). In each image, the stem cells and meiotic pachytene are outlined with dashed lines, while the oocytes are outlined with dotted lines. Images were acquired with an epifluorescent microscope. Scale bars = 10 μ M.

D-F) Representative images of PLA (red) in 3xFLAG::DLC-1; GFP (Di-iv), 3xFLAG::DLC-1; PGL-1::GFP (Ei-iv), and 3xFLAG::DLC-1; GFP::PGL-3 (Fi-iv) extruded germlines. DAPI was used to label DNA (blue) and both the individual DAPI (Dii, Eii, Fii) and PLA channels (Diii, Eiii, Fiii) are shown in grayscale for better contrast. For quantification, the PLA foci in the grayscale PLA channels were subjected to the particle thresholding procedure. PLA foci that met the threshold for each respective germline are shown (Div, Eiv, Fiv). Red lines separate the 3 zones used for quantification below in G. In each image, the stem cells and meiotic pachytene are outlined with dashed lines, while the oocytes are outlined with dotted lines. Images were acquired with a confocal microscope. Scale bars = 10 μ M.

G) The average PLA density (number of PLA foci per μ M²) $\times 10^{-2}$ was measured for germlines co-expressing 3xFLAG::DLC-1 with: GFP (- control), or PGL-1::GFP,

or GFP::PGL-3. For quantification, the germline was segmented into 3 zones (see Materials/Methods) as denoted by the red lines shown in each threshold image (Div, Eiv, Fiv). Zone 1 extends from the distal tip to the first line, while zone 2 is comprised of the pachytene area in between the 2 lines. Zone 3 begins at the second red line and encompasses all oocytes. The number of germlines analyzed (N) for each strain in each zone is shown below the graph. Differences in average PLA density for each protein analyzed in each zone were evaluated by one-way ANOVA followed by t -test with Bonferroni correction post-test. Cross-zone comparisons of PLA density that are significantly different are shown with dashed brackets. Asterisks denote statistical significance (***, $P < 0.0001$; **, $P < 0.001$; *, $P < 0.0167$; n.s.=not significant, $P > 0.0167$). Data is representative of 3 biological replicates and error bars represent standard deviation from the mean.

To visualize and quantify interactions between DLC-1 and PGL-1 or PGL-3 *in vivo*, we implemented an *in situ* proximity ligation assay using the same anti-FLAG and anti-GFP antibodies that were used for immunofluorescence. This assay was used on extruded and fixed germlines (Figure 4.3D-F) to determine whether DLC-1 is incorporated into PGL-1 or PGL-3-containing complexes in the germline. For quantification of PLA, we implemented the workflow described in Chapter 3 and used 3xFLAG::DLC-1; GFP as a negative control, as DLC-1 and GFP are not expected to interact. The PLA density was quantified in 3 different zones in the germline, where zone 1 included the distal tip to early pachytene, zone 2 included mid to late pachytene, and zone 3 included all oocytes (demarcated by red lines in panel iv of Figure 4.3D-F). Among the 3 types of interactions

tested, 3xFLAG::DLC-1; PGL-1::GFP germlines had the highest mean PLA density in zone 1 (Figure 4.3G). In contrast, we found that the PLA density in 3xFLAG::DLC-1; GFP::PGL-3 germlines was less than the background in zone 1, but showed a moderate yet statistically significant increase in PLA density in zone 2 compared to the GFP control (Figure 4.3G). This may be explained by the expression pattern of PGL-3, which starts at the mid-pachytene (Figure 4.3Ciii). Despite the increase in PLA density for PGL-3 at zone 2, PGL-1's PLA density in this zone was still significantly higher compared to PGL-3's, suggesting that DLC-1 predominantly interacts with PGL-1 in this zone. PLA density was also quantified in the oocytes (Zone 3, Figure 4.3G), as P granules start to change their localization during oogenesis and oocyte maturation [245]. While the mean PLA densities for 3xFLAG::DLC-1; PGL-1::GFP were similar in zones 1 and 2, we observed more than a 30% decrease in oocytes of zone 3 (Figure 4.3G). 3xFLAG::DLC-1; GFP::PGL-3 also exhibited a 30% reduction in mean PLA density for this zone compared to zone 2 that resulted in background PLA density. Based on this data, we conclude that DLC-1 preferentially interacts with PGL-1 over PGL-3 in the germline. Further, the reduction of DLC-1/PGL PLA density in the oocytes suggests that continual co-expression of partners does not necessarily suggest maintenance of protein-protein interactions in the germline.

DLC-1 Remains in Complex with PGL-Containing RNPs in Embryos

Both PGL-1 and PGL-3 are expressed in germ cells during every phase of *C. elegans* development with the exception of spermatogenesis [232] and DLC-1 is ubiquitously expressed in both somatic and germ cell cells throughout development [196,220]. To test

whether DLC-1 is in complex with these RBPs during embryo development, we continued to investigate potential interactions between DLC-1 and PGL-1 or PGL-3 in developing embryos using the same *in situ* approach that was used for the germlines. Co-immunostaining of embryos expressing 3xFLAG::DLC-1; GFP, 3xFLAG::DLC-1; PGL-1::GFP, and 3xFLAG::DLC-1; GFP::PGL-3 with anti-FLAG antibody revealed that 3xFLAG::DLC-1 is expressed throughout the embryo in both somatic and germ cells during all stages of development (column ii, Figure 4.4A-L). Interestingly, anti-FLAG immunostaining in embryos beyond 50-cell stage shows that 3xFLAG::DLC-1 is enriched in primordial germ cells (yellow asterisk, Figure 4.4D, H, L), which were identified by the location of PGL-1 or PGL-3 in the embryo. Much like DLC-1, the GFP control is expressed throughout the embryo during all stages of development (column iii, Figure 4.4A-D). Anti-GFP immunostaining of PGL-1 and PGL-3 also recapitulated their specific subcellular localization with P granules throughout during embryo development as previously reported [232](column iii, Figure 4.4E-L). Together, the overlapping patterns of expression of DLC-1 in somatic and germ cells and PGL-1 and PGL-3 in germ cells suggests that DLC-1 could interact with these RBPs in developing embryos.

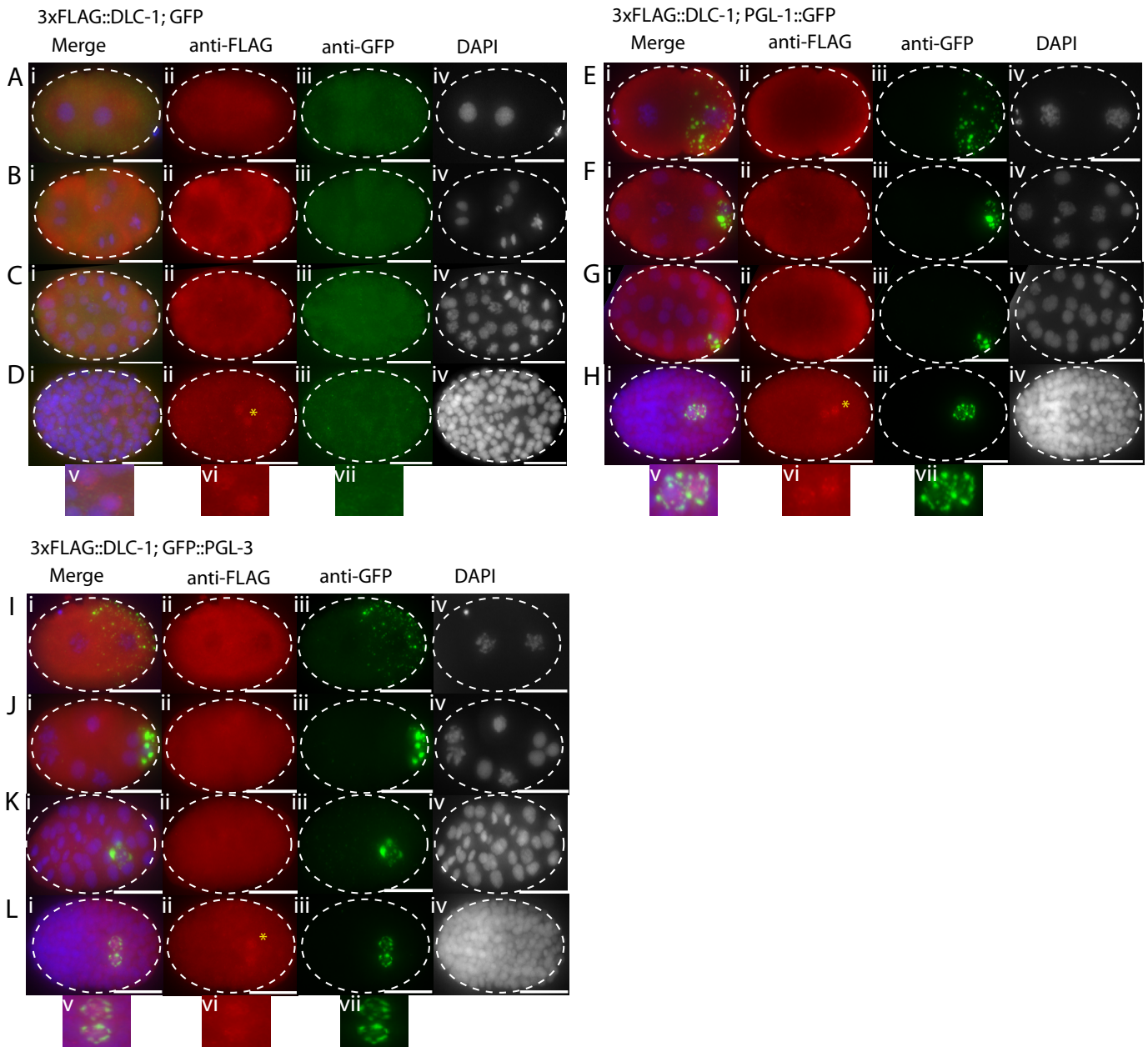


Figure 4.4: DLC-1 is co-expressed with PGL proteins throughout early embryogenesis

A-L) The expression patterns of tagged proteins in 3xFLAG::DLC-1; GFP (A-D), 3xFLAG::DLC-1; PGL-1::GFP (E-H), and 3xFLAG::DLC-1; GFP::PGL-3 (I-L) were evaluated in extruded, fixed, and immunostained embryos. For each strain,

images in rows 1 (A, E, and I) and 2 (B, F, and J) represent early stage embryos, where cytoplasmic P granules segregate to the germ cell. Images in row 3 (C, G, and K) represent embryos where P granules condense and become perinuclear in the germ cell. Row 4 (D, H, and L) contains later stage embryos where PGL proteins are degraded by autophagy in somatic cells, while the germ cell has undergone a symmetric division forming two primordial germ cells with perinuclear P granules. Embryos in this and following Figures are oriented with Anterior to the left. Yellow asterisk denotes enriched DLC-1 signal in germ cells identified by PGL-1 and PGL-3 localization. In rows D, H, and L, insets v-vii are zoomed in images of i-iii showing enrichment of DLC-1 in germ cells. DNA is labeled with DAPI (blue), and the individual channel is shown in grayscale for better contrast (iv for each row). Images were acquired using an epifluorescent microscope. Scale bars = 10 μ M.

Using PLA, we quantified interactions between DLC-1 and PGL-1 or PGL-3 in embryos across several different stages of development binned based on changes in subcellular localization of P granules as shown in Figure 4.4. Overall, the average PLA densities observed in 3xFLAG::DLC-1; PGL-1::GFP and 3xFLAG::DLC-1; GFP::PGL-3 embryos throughout embryo development were significantly higher than the negative control (Figure 4.5P). Interestingly, both PGL-1 and PGL-3 average PLA density values in the embryo were higher than those observed in germlines (Figure 4.3G). This suggests that incorporation of DLC-1 into PGL-1 or PGL-3 RNPs is more prevalent in embryos than in the germlines or oocytes. PGL-1 interacts with DLC-1 most prominently at the 30-49-cell

stages, where P granules have completed their transition to a perinuclear localization in the germ cell (Figure 4.5P). In contrast, PGL-3 interactions with DLC-1 peak at the 16-29-cell stage, when P granules condense and start to become perinuclear in the germ cell. Surprisingly, PLA foci in 3xFLAG::DLC-1; PGL-1::GFP and 3xFLAG::DLC-1; GFP::PGL-3 embryos appeared throughout the embryo, including both somatic and germ cells (Figure 4.5F-O) as opposed to PGL-1 and PGL-3 that are enriched at P granules in the germ cells of the embryo (column iii, Figure 4.4E-L). This suggests that DLC-1 might be a part of PGL-1 and PGL-3 RNP complexes not only in germ cells, but also in somatic cells [246]. As embryos continue to develop beyond the 50-cell stage, the average PLA density for both PGL-1 and PGL-3 decreases, which may result from clearance of PGL-1 and PGL-3 in somatic cells through autophagy [247]. While PLA was observed in both somatic and germ cells of embryos, 3xFLAG::DLC-1; GFP::PGL-3 embryos showed enrichment of PLA around the germ cell in later stage embryos (yellow asterisk, Figure 4.5N-O). In contrast to PGL-3, 3xFLAG::DLC-1; PGL-1::GFP embryos did not show a robust pattern of enrichment (Figure 4.5I-J). This result led us to further investigate the enrichment of PLA at P granules in the germ cell.

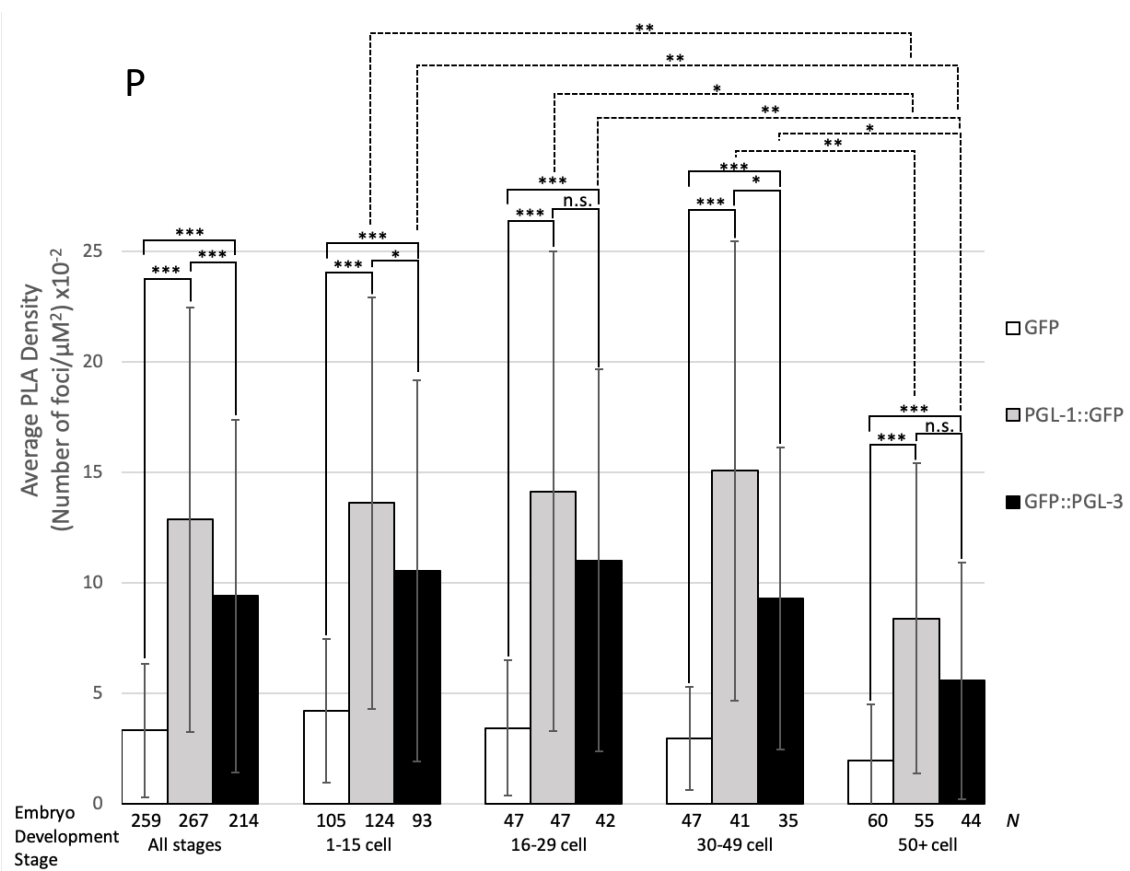
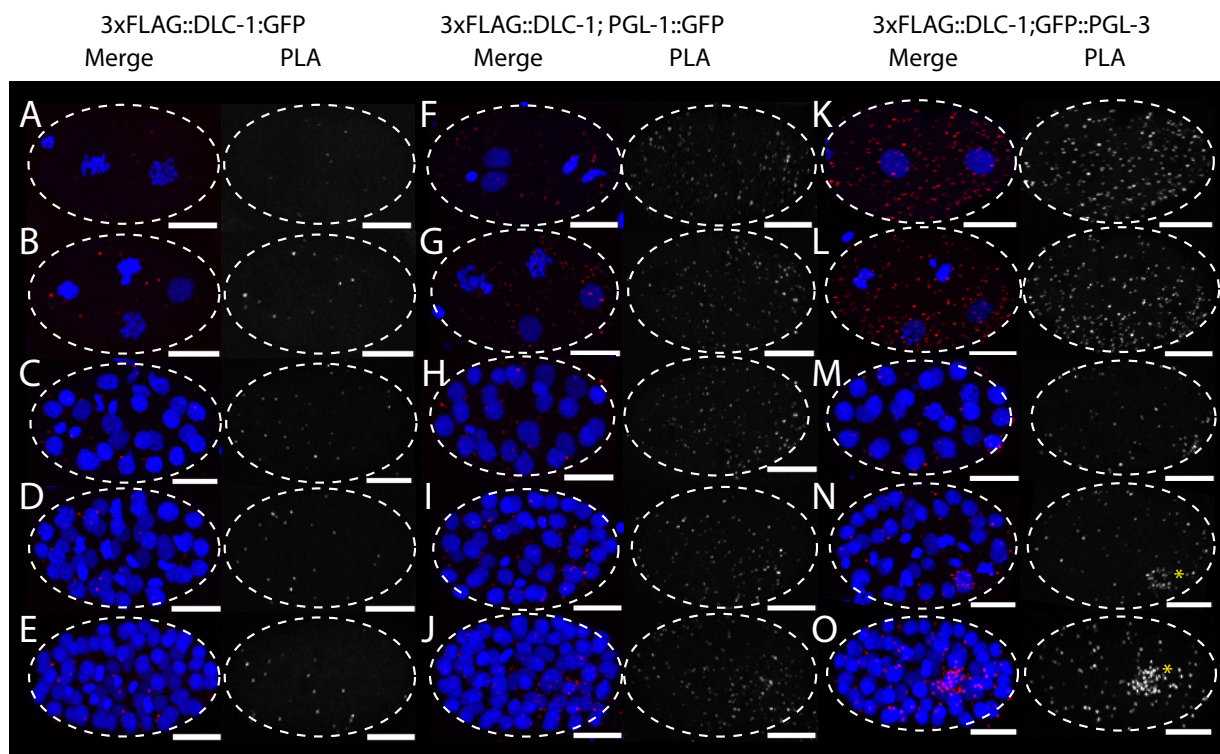


Figure 4.5: Proximity ligation assay detects formation of DLC-1/PGL complexes in early embryos

- A-O) Representative images of PLA (red) in 3xFLAG::DLC-1; GFP (A-E), 3xFLAG::DLC-1; PGL-1::GFP (F-J), and 3xFLAG::DLC-1; GFP::PGL-3 (K-O) extruded embryos. Panels in row 1 (A, F, and K) and row 2 (B, G, and L) represent 2- and 4-cell stage embryos that belong to the 1-15 cell stage group, where cytoplasmic P granules segregate with the germ cell. Panels in row 3 (C, H, and M) represent embryos in the 16-29 cell stage, when P granules condense in the germ cell. Panels in row 4 (D, I, and N) represent embryos at the 30-49 cell stage, when P granules complete their perinuclear localization in the germ cell. Finally, panels in row 5 (E, J, and O) represent embryos at the 50 cell and above stage, when autophagy of PGL proteins takes place in somatic cells. DNA is labeled with DAPI (blue in the merged images). The PLA channels are also shown in grayscale for better contrast. Images were acquired using a confocal microscope. Yellow asterisk denotes PLA signal enriched at germ cells. Scale bars = 10 μ M.
- P) The average PLA density (number of PLA foci per μ M²) $\times 10^{-2}$ was measured within each whole embryo co-expressing 3xFLAG::DLC-1 with: GFP (- control), or PGL-1::GFP, or GFP::PGL-3. The total number of embryos observed (N) for each strain is shown under the bar graphs in the 'All stages' category. These total observations were subsequently binned into different groups based on developmental stage of the embryo and plotted as separate bar graphs (N values indicated under each respective bar). These stages represent different timepoints

in development as in A-O. Differences in average PLA density for each protein pair analyzed at each stage were evaluated by one-way ANOVA followed by *t*-test with Bonferroni correction post-test. Cross-stage comparisons of PLA density that are significantly different are shown with dashed brackets. Asterisks denote statistical significance (***, $P < 0.0001$; **, $P < 0.001$; *, $P < 0.0167$; n.s.=not significant, $P > 0.0167$). Data is representative of 4 biological replicates and error bars represent standard deviation from the mean.

DLC-1/PGL-3 RNPs are Enriched at P Granules

Observing PLA foci at germ cell P granules of 3xFLAG::DLC-1; GFP::PGL-3 embryos (Figure 4.5N-O) led us to hypothesize that PGL-3/DLC-1 complexes are more enriched at P granules than PGL-1/DLC-1 complexes. Using PLA in tandem with a PGL-1 immunostaining to mark P granules in the germ cell (Figure 4.6A-C), we first scored embryos based on whether PLA foci were observed at P granules at all (Figure 4.6D). Both 3xFLAG::DLC-1; GFP::PGL-3 and 3xFLAG::DLC-1; PGL-1::GFP embryos had a significantly high prevalence of PLA at P granules (85% and 65% of all embryos observed, respectively). In contrast, only 55% of 3xFLAG::DLC-1; GFP embryos had PLA at P granules, which was not statistically significant (Figure 4.6D). We conclude that PGL-3/DLC-1 and PGL-1/DLC-1 complexes are often observed at P granules. To evaluate whether the PGL-3/DLC complexes were more restricted to P granules than PGL-1/DLC-1 complexes, we sought to quantitatively compare PLA signal at P granules to that observed in the somatic cells.

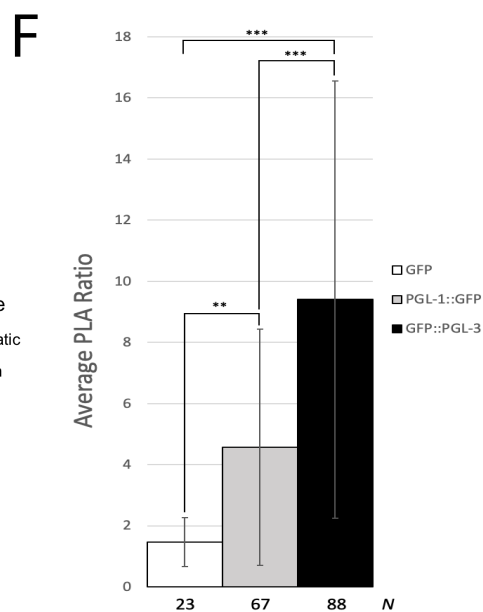
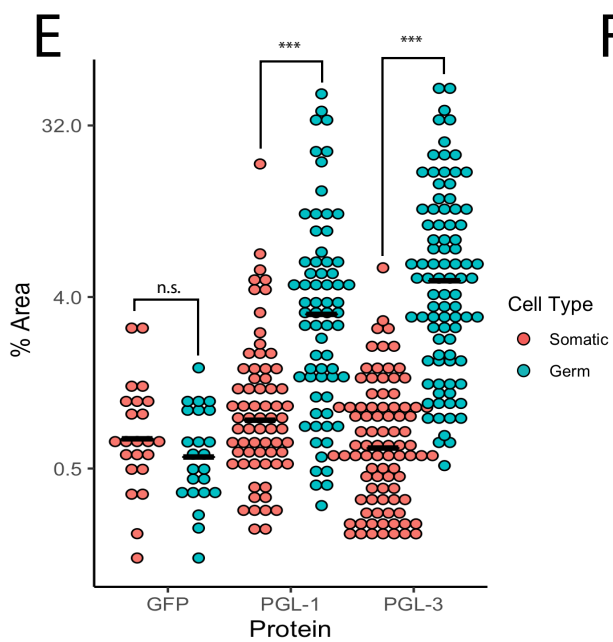
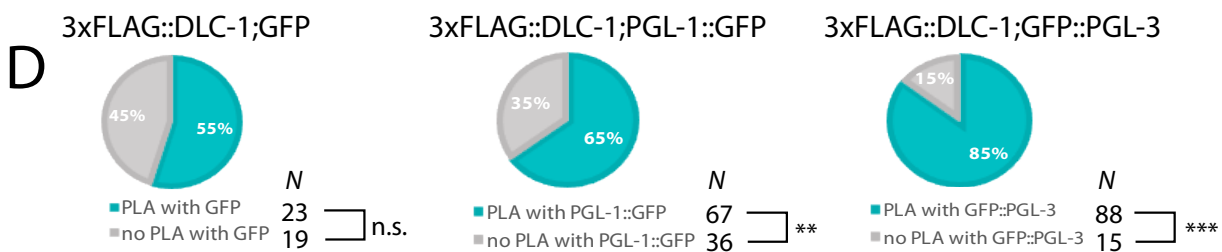
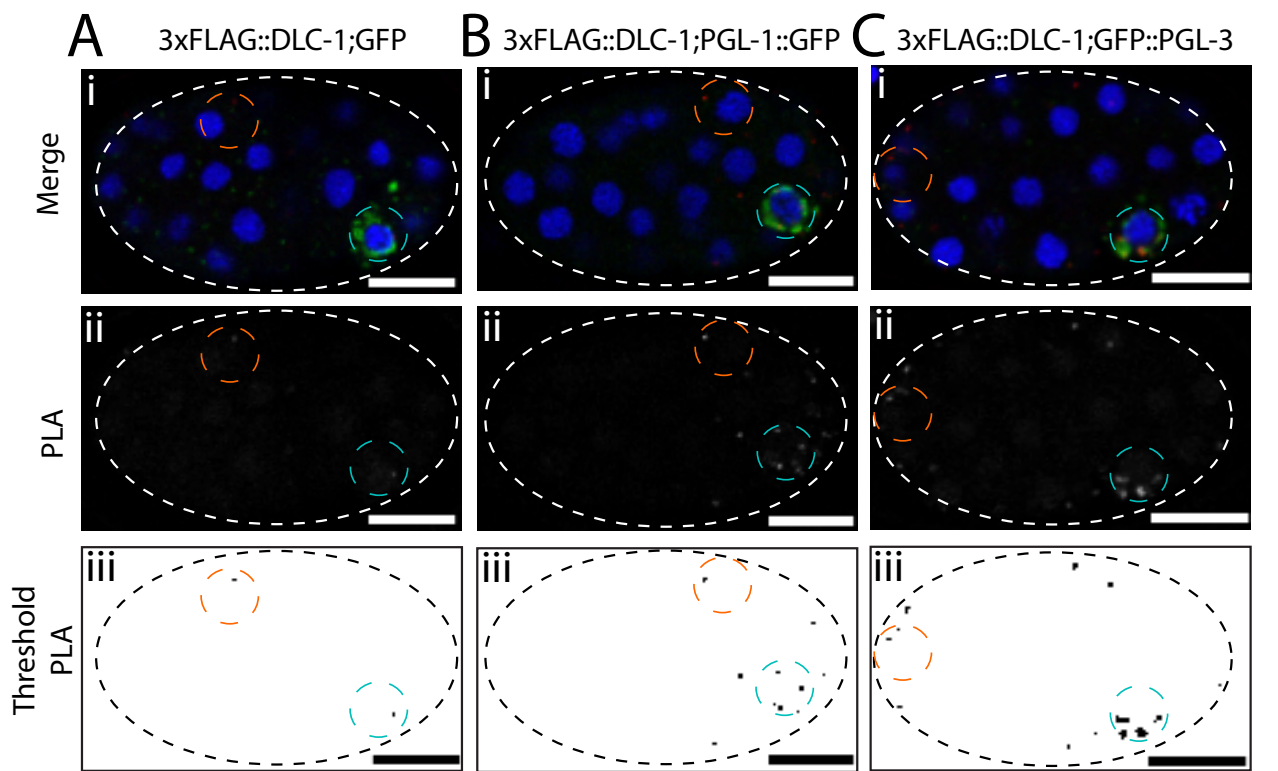


Figure 4.6: DLC-1/PGL complexes are enriched within P granules

- A-C) Representative images of PLA (red) in 3xFLAG::DLC-1; GFP (A), 3xFLAG::DLC-1; PGL-1::GFP (B), and 3xFLAG::DLC-1; GFP::PGL-3 (C) cross sections of extruded embryos at approximately the 40-cell stage. DNA is labeled with DAPI (blue). P granules (green) are immunostained by anti-PGL-1. The PLA channels are also shown in grayscale (Aii, Bii, Cii) for better contrast. For quantification, the PLA foci in the grayscale PLA channels of each embryo image are subject to the particle thresholding procedure described in Chapter 3 (Aiii, Biii, Ciii). The light blue circle designates the germ cell region of interest (ROI), while the orange circle designates the somatic cell. The area that the PLA foci occupy in the germ cell or somatic cell ROIs (% Area) is measured using the FIJI/ImageJ analysis workflow. Images were acquired using a confocal microscope. Scale bars = 10 μ M.
- D-F) Quantitative analysis of PLA results. PLA signal in test and control strains was evaluated using three different metrics. The same embryo images were used for all analyses. PGL-1::GFP and GFP::PGL-3 data are representative of 3 biological replicates, while GFP represents 1 replicate.
- D) DLC-1/PGL complexes are frequently observed at P granules. Pie charts represent proportions of embryos that had PLA foci present in germ cells. The number of observations (N) for each group are shown next to each pie chart legend. The distribution of embryonic germ cells where PLA signal was present versus those without PLA was analyzed by a Chi-square test. (***, $P < 0.0005$; **, $P < 0.005$; n.s. = not significant, $P > 0.05$).

- E) The relative area occupied by PLA signal of DLC-1/PGL complexes is greater in the germ cells than in the somatic cells. Dot plots representing % Area of PLA measurements in somatic or germ cells. The average of each dot plot column is represented by the horizontal bar. The embryos with no signal in the germ cells were excluded from this data set. Comparison of PLA area observed in somatic versus germ cells for each strain was performed using a paired, students *t*-test. (***, $P < 0.0005$; n.s.=not significant, $P > 0.05$).
- F) The germ cell enrichment of DLC-1/PGL-3 complex is greater than that of DLC-1/PGL-1 complex. Bar graphs represent average ratios of % Area of PLA observed in germ cell relative to that observed in somatic cell. Data derived from (E) are an aggregate of embryos across all stages of development, starting with the 13-cell stage when PLA is first observed at condensed P granules. The total number of embryos observed (*N*) for each strain is shown under the bar graphs. Differences in average germ cell/somatic cell relative PLA ratio for each protein analyzed were evaluated by one-way ANOVA followed by *t*-test with Bonferroni correction post-test. Asterisks denote statistical significance (***, $P < 0.0001$; **, $P < 0.001$; n.s.= not significant, $P > 0.0167$). Error bars represent standard deviation from the mean.

To quantify PLA at P granules, we measured the relative area (% Area) that PLA occupies in germ (light blue circle, Figure 4.6A-C) and somatic (orange circle, Figure 4.6A-C) cells of the same embryo. This metric better represented the differences among each strain as opposed to PLA density, which does not account for changes in the size of

PLA foci. These measurements were only performed on embryos where PLA was present in the germ cells (Figure 4.6D). The average % Area of PLA in somatic versus germ cells were not significantly different in the GFP control (Figure 4.6E). By contrast, in both PGL-1 and PGL-3 embryos, the difference in mean relative PLA between somatic and germ cells was significantly different. These observations suggest that germ cells are enriched in DLC-1/PGL-containing RNPs, confirming initial observations that DLC-1 interacts with PGLs at P granules. To determine whether specific DLC-1/PGL complexes might be more enriched in germ cells, we calculated the ratios (Figure 4.6F) for relative area of PLA between the germ and somatic cell for each embryo as plotted in Figure 4.6E. Using this metric, we determined the PLA signal enrichment in P granules of each embryo individually. Quantification of PLA enrichment showed that 3xFLAG::DLC-1; GFP::PGL-3 had significantly higher germline/soma PLA enrichment compared to the 3xFLAG::DLC-1; GFP negative control and 3xFLAG::DLC-1; PGL-1::GFP (Figure 4.6F). Based on this comparison, we conclude that PGL-3/DLC-1 complexes are significantly more enriched in the germ cells than PGL-1/DLC-1 complexes.

Loss of DLC-1 Disrupts P Granule Assembly in the Embryo

Previous work has proposed a role for DLC-1 in assembly of P granules, based on an observation that knockdown of *dlc-1* disrupted localization or expression of PGL-1 transgene [234]. Based on the GST pulldown results (Figure 4.2E), DLC-1 interacts with multiple core P granule components. Additionally, we confirmed incorporation of DLC-1 into RNP complexes with PGL-1 and PGL-3 at P granules in embryos using *in situ* PLA. Since DLC-1 directly interacts with several core P granule components, we hypothesized

that loss of DLC-1 might disrupt P granule assembly rather than simply interfere with expression or localization of PGL-1. To test this hypothesis, we monitored assembly and localization of several P granule components that interact with DLC-1. Using a strain that expresses GFP-tagged PGL-3 in conjunction with immunostaining of endogenous PGL-1, the localization and assembly of PGL-1 and PGL-3 into P granules in embryos was analyzed. Knocking down *dlc-1* with RNAi yields a similar effect as the *dlc-1* mutant, where worms are sterile at 24°C, but embryonic lethal at 20°C. Analysis of control RNAi-treated embryos (Figure 4.7A, C) showed that PGL-1/PGL-3-containing P granules segregate to the germ cell precursor at the 2-cell stage and become perinuclear by the 20-cell stage. In *dlc-1(RNAi)* treated embryos, the segregation of PGL-1/PGL-3-containing P granules in similar, early cell stage embryos was disrupted (Figure 4.7B). At approximately the 20-cell stage, P granules are still not perinuclear at the germ cell and remain dispersed in *dlc-1(RNAi)* embryos (Figure 4.7D). Higher magnification images reveal that formation of PGL-1-PGL-3-containing P granules is disrupted in *dlc-1(RNAi)* embryos (rows v-vii, Figure 4.7B, D) compared to control RNAi embryos (rows v-vii, Figure 4.7A, C). The P granules that do form in *dlc-1(RNAi)* are reduced in size compared to control RNAi embryos and in some instances contain only one of the PGL proteins. Colocalization of PGL-1 with PGL-3 was evaluated by Pearson Correlation using Costes Automatic threshold using the JACoP plugin in FIJI [238]. Colocalization analysis revealed that the average PGL-1/PGL-3 correlation coefficient was significantly reduced in *dlc-1(RNAi)* embryos compared to the control (Figure 4.7E). The reduction in PGL-1/PGL-3 colocalization upon loss of *dlc-1* was intriguing, given that these proteins

directly interact *in vitro* [232]. These findings suggest that DLC-1 promotes P granule assembly and localization of PGL-1 and PGL-3 in developing embryos.

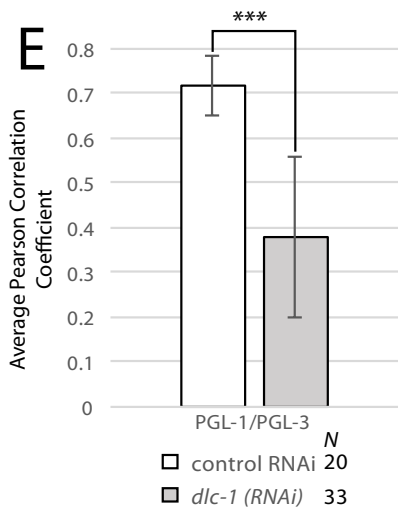
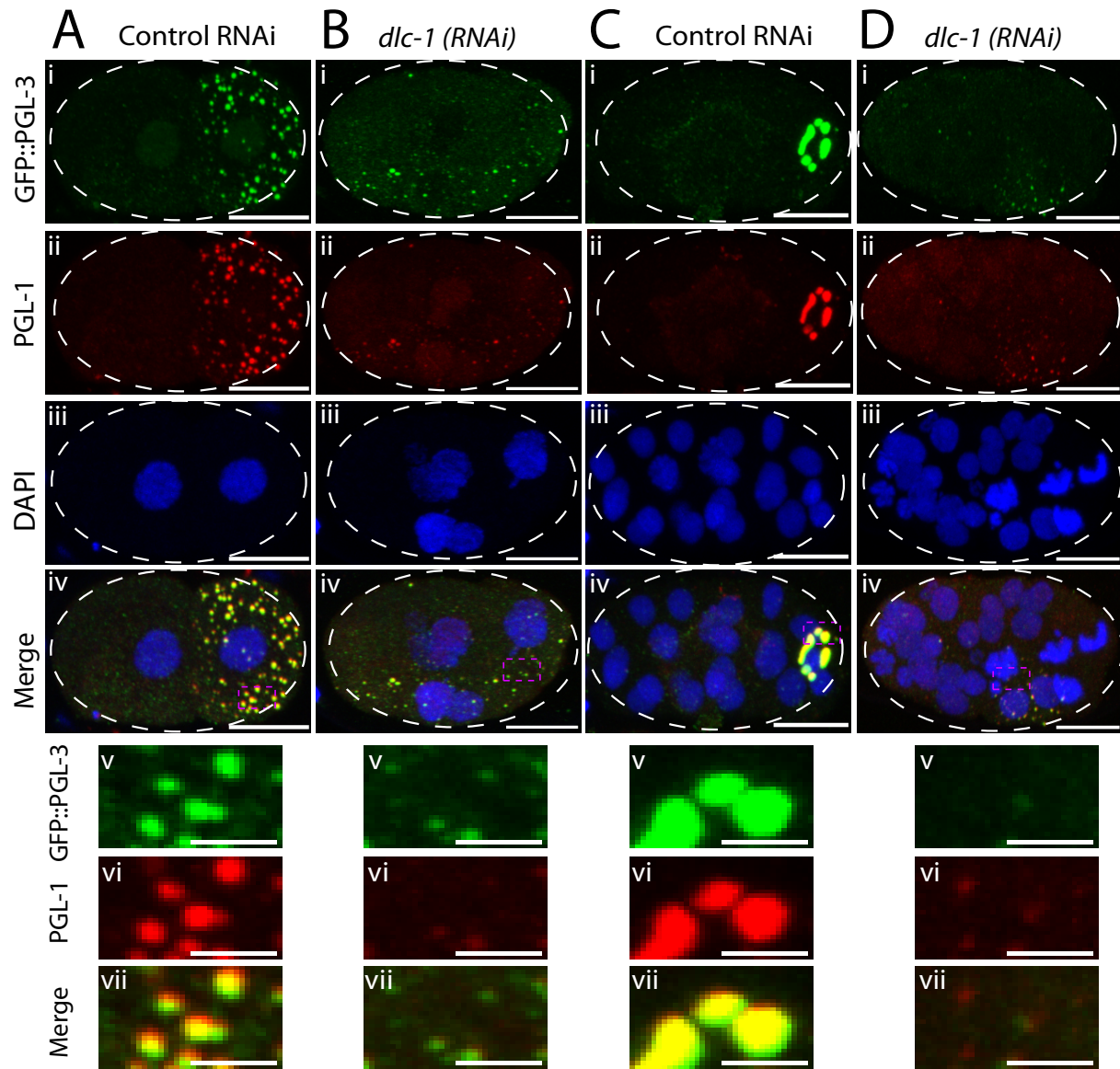


Figure 4.7: *dlc-1* is required for PGL-1 and PGL-3 assembly into embryonic P granules

- A-D) Representative maximum projection images of extruded control or *dlc-1(RNAi)* embryos co-immunostained for the P granule components PGL-1 (red) and GFP::*PGL-3* (green). A-B: 2-4-cell stage embryos. C-D: 21-24-cell stage embryos. DNA is labeled with DAPI (blue). Rows v-vii are zoomed in regions (boxed magenta outline) of images in row iv that are split into single channels to highlight differences in P granule assembly and size between control RNAi or *dlc-1(RNAi)*-treated embryos. Images were acquired using a confocal microscope. Scale bars: 10 μ M (i-iv); 2 μ M (v-vii).
- E) Bar plot representing the average colocalization (Pearson Correlation) coefficient between PGL-1 and GFP::*PGL-3* in wild type and *dlc-1(RNAi)* embryos. The difference between the control and *dlc-1(RNAi)* was significantly different. The *P*-values were determined using a two-tailed/equal variance *t*-test where *** = *P*<0.0005. Error bars represent the standard deviation from the mean. The number of embryos observed (*N*) in each RNAi experiment are denoted in the bar plot legend. Images and data are representative of one replicate.

To test whether loss of DLC-1 disrupts the localization and assembly of additional P granule components, we used a strain of worm that expresses CRISPR-tagged MEG-3::*OLLAS* and MEG-4::*3xFLAG*. By GST pulldown, MEG-3 weakly interacted with DLC-1 (Figure 4.2E), therefore it was not clear whether its localization and assembly with P granules might be disrupted by loss of DLC-1. Both MEG proteins along with the

endogenous PGL-1 were examined in wild type or embryonic lethal *dlc-1* deletion loss of function mutant embryos at 20°C (*dlc-1* mutants are sterile at 24°C, but embryonic lethal at 20°C). In wild type embryos, P granules containing MEG-4, MEG-3, and PGL-1 segregate to the posterior cell at the 2-cell stage (Figure 4.8A) and become perinuclear by the 20-cell stage (Figure 4.8C). In contrast, segregation and perinuclear localization of P granules containing MEG-4, MEG-3, and PGL-1 in *dlc-1* mutants are disrupted in both early and 20-cell stage embryos (Figure 4.8B, D). Close up images of these P granule proteins in both wild type and *dlc-1* mutants highlights the differences in their localization and assembly (images vi-ix, Figure 4.8A-D). While large P granules in wild type embryos contain all three core P granule components (row ix, Figure 4.8A, C), P granules that form in *dlc-1* mutants appear smaller in size and occasionally lack some components (rows vi-ix, Figure 4.8B, D), suggesting that P granule components fail to assemble into the normal complex. For each pair of P granule proteins tested, there was a significant decrease in the colocalization coefficient between the wild type and *dlc-1* mutant (Figure 4.8E) in agreement with this observation. Interestingly, colocalization of MEG-3 and MEG-4 with PGL-1 was affected in *dlc-1* mutant embryos, even though these proteins directly interact *in vitro* [103]. Taken together, these data suggest that DLC-1 serves an important role in both assembly and localization of multiple P granule components in developing embryos, including those that do not directly interact with DLC-1.

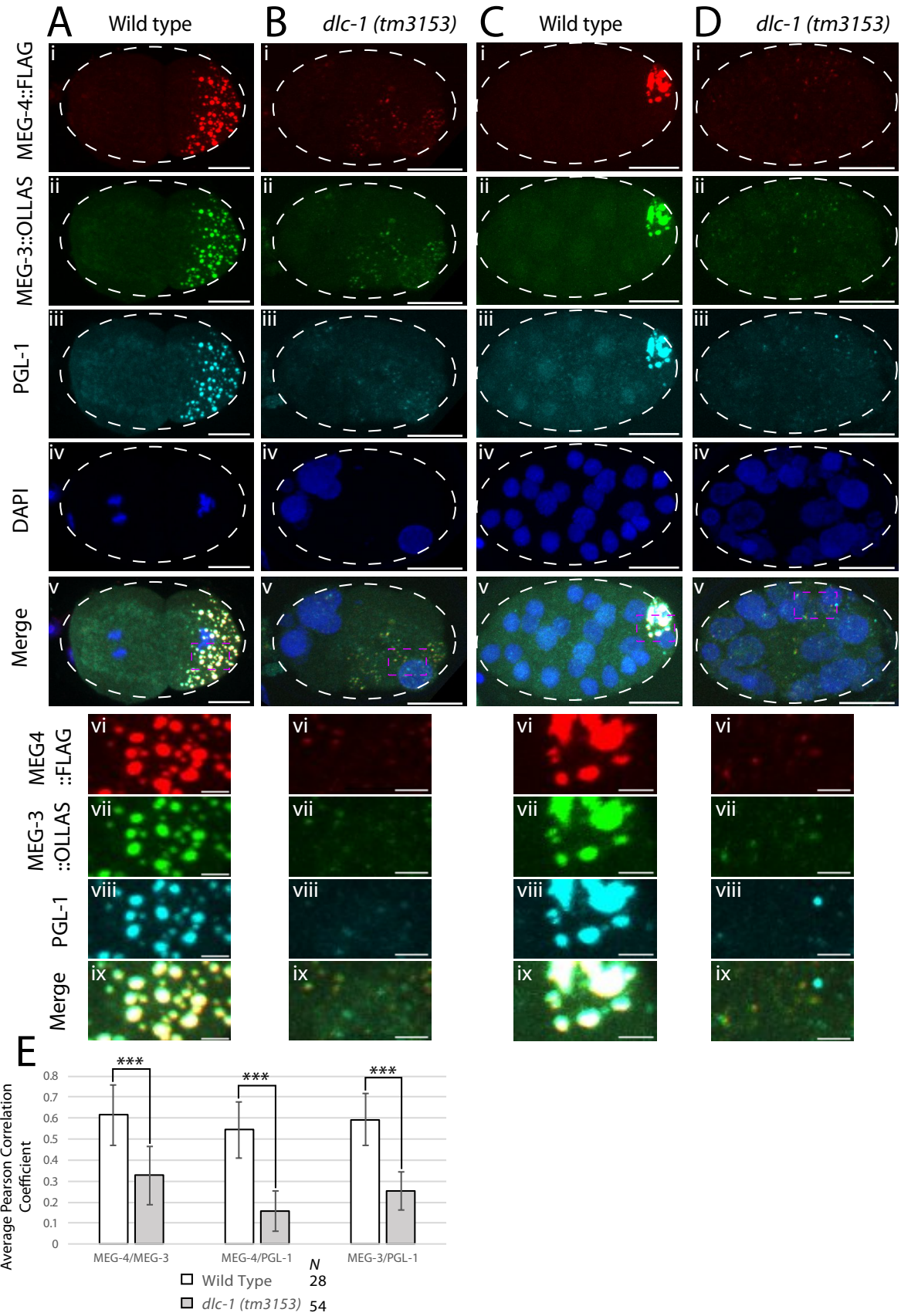


Figure 4.8: *dlc-1* is required for embryonic P granule integrity

A-D) Representative maximum projection images of wild type or *dlc-1* mutant extruded embryos co-immunostained for P granule components MEG-4::3xFLAG (red), MEG-3::OLLAS (green), and PGL-1 (cyan), respectively. DNA was labeled with DAPI (blue). A-B: 2-4-cell stage embryos. C-D: 23-24-cell stage embryos. Rows vi-ix are zoomed-in regions (boxed magenta outline) of images in row v split into single channels for clarity. Images were acquired using a confocal microscope. Scale bars: 10 μ M (i-v); 2 μ M (vi-ix).

E) Bar plot representing the average colocalization (Pearson Correlation) coefficient for each specified pair of P granule proteins in wild type and *dlc-1* mutant embryos. For each pair of P granule proteins examined, the difference between the wild type and mutant was significantly different. The *P*-values were determined using a two-tailed/equal variance *t*-test where *** = $P < 0.0005$. Error bars represent standard deviation from the mean. The number of wild type or *dlc-1* mutant embryos observed (*N*) are denoted in the bar plot legend. Images and data are representative of 3 biological replicates.

Discussion

In this study, we report discovery of interactions between several P granule components and DLC-1. Data from both PLA and analysis of embryos with *dlc-1* knockdown or knockout emphasizes that DLC-1 interacts with these P granule components predominantly in the embryo. Loss of DLC-1 disrupts the assembly and localization of multiple P granule proteins essential for assembly of large P granules. Taken together,

our findings suggest that DLC-1 is a critical component in P granule assembly in *C. elegans* embryos.

Bioinformatics Identifies New DLC-1 Binding Partners

The interaction motif scan identified a number of RBPs that could putatively interact with DLC-1, including several P granule components. Using GST pulldowns, we confirmed direct interaction between DLC-1 and PGL-1, PGL-3, GLH-4, and MEG-4 (Figure 4.2E). This provides insight into the sensitivity of the motif scanning approach, where we confirmed 4 out of 6 potential interactors, suggesting the set of putative interacting proteins is enriched with real interactors. These true interactors were recovered using a combination of three different interaction motifs to scan the proteome, suggesting there is diversity in the protein sequences recognized by DLC-1, which cannot be captured in a single degenerate motif. Diversity of DLC-1 or other types of interaction sites is important to consider in future scan experiments as the overrepresented interaction motif may not accurately reflect the variety of potential binding sites.

To assess the selectivity of interactor predictions, paralogs of the direct interactors that were not recovered from the motif scan (PGL-2, GLH-1, MEG-3), were also tested for direct interaction with DLC-1; however, only MEG-3 weakly interacted with DLC-1 (Figure 4.2E). This demonstrates the sensitivity and specificity of bioinformatic approaches to generate biologically relevant information and discover new interaction networks. While there are more than 40 known P granule proteins in *C. elegans* [108], our motif scan identified several specific RBPs as putative interactors that were later

confirmed experimentally. Further work is needed to identify the binding sites as this information can direct mutagenesis of these RBPs to prevent DLC-1 binding in order to observe how loss of DLC-1 binding affects P granules *in vivo*.

Preferential Interaction of DLC-1 with PGL-1 in the Germline

While DLC-1 is to a large extent co-expressed with its interaction partners, PLA data highlights where specific interactions occur in the germline. Quantification of PLA in germlines shows that DLC-1 predominantly interacts with PGL-1 throughout the germline and moderately with PGL-3 in the mid to late pachytene region of the germline. Previous reports found that *dlc-1(RNAi)* had no effect on localization or stability of PGL-1 in the germline [171,234], suggesting that the interactions detected by PLA may indicate a different role for DLC-1. Since DLC-1 may serve a hub-like role, it could be involved in recruiting client proteins to P granules in the germline. Indeed, DLC-1 was required for localization of the RBP FBF-2 to PGL-1 (used to mark P granules) in the distal region of the germline to facilitate its function as a translational repressor [171]. Future work is needed to test whether recruitment occurs through direct interaction between DLC-1 with PGL-1 and FBF-2.

DLC-1 is Found in Complex with PGLs in the Embryo

The interactions of PGL-1 and PGL-3 with DLC-1 are more prevalent in embryos than in the germlines, which points towards DLC-1's potential importance during this stage of worm development. Quantification of PLA in embryos revealed that PLA densities for PGLs were higher than their respective densities in germlines (compare Figure 4.3G with

Figure 4.5P). The higher prevalence of interactions implies that formation of DLC-1/PGL RNP complexes serves a more prominent role during embryo development. Notably, the presence of PLA signal in embryonic somatic cells suggests that DLC-1 is interacting with PGL-1 and to a lesser extent, PGL-3, that remain in the somatic cell after the first asymmetric cell division. Somatic PGL-1/3 proteins are concentrated by LLPS to facilitate their degradation by autophagy [248] and DLC-1 could play a role in this process. Future work is needed to understand the interaction between DLC-1 and somatic PGL-1/3 and whether it relates to degradation of PGL proteins.

Are DLC-1 Interactions with its Partners Subject to Regulation?

Overall, PLA in germlines and embryos suggests that interactions between DLC-1 and PGLs could be subject to temporal and spatial regulation. The drop in PLA density observed for both PGL-1/DLC-1 and PGL-3/DLC-1 in the oocytes compared to the mid to late pachytene is an example of temporal regulation. Oogenesis and oocyte maturation are a timepoint in development where P granules lose their perinuclear localization and become cytoplasmic. This remodeling of P granules could influence the interaction between DLC-1 and either PGL protein. In the embryo, DLC-1 appears to interact more with PGL-3 over PGL-1 at P granules (Figure 4.6F). It will be interesting to look at this result over time during embryo development as P granules condense and become perinuclear, to see if enrichment of DLC-1/PGL complexes correlates with these changes in P granules. Additional work will also be needed to understand whether the distinction between PGL-1 and PGL-3 is an artefact resulting from differences in the rate of autophagy of PGL-1 versus PGL-3 in somatic cells, that could affect calculation of the

relative PLA ratios. It also remains to be determined how enrichment of DLC-1/PGL-3 complexes might be involved in assembly and localization of P granules in germ cells. It will be interesting to analyze embryonic P granule assembly in PGL-3 mutants that cannot bind DLC-1, as this may provide insight into the role that DLC-1/PGL-3 complexes play in this process.

Does DLC-1 Have a Role in P Granule Assembly?

Previous reports have demonstrated that core P granule proteins can form P granule-like condensates in the absence of other proteins, which conflicts with the model of hierarchical assembly (see Introduction of this chapter). *In vitro* liquid droplet assays using only MEG-3 [35,105] or PGL-3 [249] demonstrate that these proteins can phase separate on their own to reconstitute condensates similar to P granules. Ectopic expression of PGL-3 in both mammalian cells and somatic *C. elegans* cells also results in formation of condensates in the absence of other P granule components [231]. Despite these observations, *glh* mutants compromise assembly of PGL-containing P granules [229] *in vivo*. Interestingly, knockdown of *pgl-1* and *pgl-3* by RNAi revealed that GLH-1 protein requires PGLs to localize to embryonic P granules [231] and ectopic expression of GLH-1 alone in *C. elegans* somatic cells does not result in formation of P granule-like condensates [250], suggesting mutual dependence of these proteins to properly localize to P granules. These findings suggest that depending on what model system and proteins are used, reductionist-based *in vitro* approaches can mimic P granule assembly. However, these approaches do not fully recapitulate the complexity of P granule assembly *in vivo*.

As previously mentioned above, *dlc-1* was identified by an RNAi screen as a gene that disrupted localization of transgenic PGL-1 in embryos [234]. Our results provide a more robust analysis of *dlc-1*'s contribution to P granule assembly than was previously reported. First, we used a *dlc-1* mutant strain, which has a consistent phenotype and eliminates concern over ineffective knockdown of *dlc-1* by RNAi. Second, with the exception of transgenic GFP-tagged PGL-3, our analysis focused on the localization and assembly of CRISPR-tagged or endogenous MEG-3/4 and PGL-1 proteins, which eliminates concern that transgenic strains may not accurately reflect their endogenous counterparts. We observed that these proteins fail to condense and form large P granules upon loss of *dlc-1*, suggesting that DLC-1 has an important, biologically relevant role in P granule assembly. Finally, we provide quantitative data to support our finding that loss of *dlc-1* disrupts assembly of 4 P granule proteins as opposed to a previous, qualitative observation made for a single protein. Through colocalization analysis, the correlation between different pairs of P granule proteins analyzed was found to significantly decrease in embryos lacking *dlc-1*, compared to the control/wild type. Surprisingly, loss of *dlc-1* affected the colocalization of MEG-3 with other P granule proteins, even though MEG-3 and DLC-1 do not directly interact. Together, these results suggested complete failure of P granule assembly and phase separation rather than selective loss of DLC-1-interacting components from a stable resilient structure. Furthermore, *in vitro* experiments have demonstrated direct interaction between MEG-3 and PGL-1 [103], MEG-4 and PGL-1 [103], PGL-1 and PGL-3 [232], and MEG-4 and PGL-3 (N.D., unpublished). While several P granule proteins can interact without intermediaries *in vitro*, our data implies

that P granule assembly *in vivo* requires additional factors such as *dlc-1*. This suggests that assembly of P granules *in vivo* is not driven by association of core components alone.

Based on our findings, we propose that *dlc-1* has an important role in promoting efficient phase-separation of core P granule components. There are several mechanisms through which DLC-1 could contribute to this process. Like other LC8-family hub proteins, DLC-1 interacts with proteins through their IDRs, which are found in many RBPs that are associated with P granules, including those identified in this study as direct interactors with DLC-1. Therefore, DLC-1 could serve a scaffold-like role that promotes and/or stabilizes complex formation among different disordered P granule components that is necessary for their assembly *in vivo*. Another possibility is that this scaffold can promote recruitment of additional proteins to P granules. DLC-1 was also speculated to serve as a linker that promotes perinuclear localization of P granules based on observation that its yeast homolog Dyn2, an LC8 protein, binds to the yeast Nup159 nucleoporin and promotes assembly of the nuclear pore complex [145]. It remains to be determined whether DLC-1 exhibits a punctate pattern of localization at the nuclear envelope as does Dyn2, which would suggest that DLC-1 could have a similar role in nuclear pore complex assembly. On a related note, DLC-1 interacts with GLH-4, which contains phenylalanine-glycine (FG) repeats [230] that are necessary for interaction with nucleoporins [251]. DLC-1 binding to GLH-4 could promote GLH-4's association with nucleoporins and establish a link where DLC-1 can contribute to perinuclear localization of P granules. Finally, *dlc-1*'s genetic requirement for P granule assembly could be related to the motor function of dynein, since DLC-1 protein associates with the dynein motor complex and is required for the motor function. Total loss of function dynein

heavy chain (*dhc-1*) mutants are unable to produce embryos, therefore we have been unable to determine whether the dynein motor is involved in P granule assembly. A previous study found that embryos treated with nocodazole or colcemid, which disrupt microtubule assembly, resulted in no effect on coalescence or asymmetry of P granules [252]. Despite these findings, it still remains to be determined whether loss of dynein motor complex has an effect on P granule assembly. Additional work is needed to test which of these potential molecular mechanisms is behind *dlc-1*'s role in P granule assembly and localization; these approaches are described further in the Future Directions section of Chapter 5.

Chapter 5

Conclusions and Future Directions

LC8 family dynein light chains are emerging as hubs that interact with other proteins beyond the originally characterized dynein motor complex. Among the diverse group of LC8-interacting proteins, are RBPs that facilitate post-transcriptional regulation of gene expression. Using the *C. elegans* germline as a model system, our lab previously found that the LC8 homolog DLC-1 interacted with 2 dissimilar RBPs and promoted their function and localization independent of the dynein motor [171,172]. This led to the proposal that DLC-1 functions as an RBP cofactor that may facilitate the function of multiple germline RBPs. Cofactor binding can affect the stability and localization of an RBP, therefore it is important to study their impact on RBP function. Little is known about how widespread LC8's RBP cofactor function may be or how DLC-1 and its LC8 homologs contribute to mRNA regulation in any organism. The goal of this dissertation was to investigate DLC-1's role in post-transcriptional mRNA regulation through its interactions with RBPs in *C. elegans*. To address this goal, the dissertation research focused on 2 areas: identification of mRNAs regulated by DLC-1 and identification of RBPs that interact with DLC-1. Findings from this dissertation show that DLC-1 is important for both the mRNA regulatory role and assembly of ribonucleoprotein (RNP) complexes, which might suggest a similar function for LC8 in other organisms, including humans.

DLC-1 Contributes to Post-Transcriptional mRNA Regulation

Research presented in chapter 2 has provided further insight into DLC-1's incorporation into RNP complexes through the use of a RIPseq approach to identify what mRNAs are potentially regulated by DLC-1. Based on the recovery of a large number of DLC-1-associated mRNAs, we inferred that DLC-1 contributes to the regulatory activity of many RBPs. Furthermore, we found that DLC-1-associated mRNAs depend on DLC-1 for regulation of their expression, suggesting DLC-1 has a role as an RBP cofactor. Most mRNAs are predominantly associated with regulating the oogenic transcriptome, which further expands upon DLC-1's previously reported roles in regulation of stem cell maintenance and initiation of meiosis.

DLC-1 Might Function as a Cofactor of OMA-1 RBPs

Since DLC-1 has many associated mRNAs and regulates their expression in the germline, we were also interested in identifying what other RBPs are in complex with DLC-1. OMA-1 was among the several RBPs that had significant target mRNA overlap with DLC-1. Additionally, *oma-1;oma-2* double mutant germlines fail to activate expression of *meg-1* in oocytes [100], which is similar to the decrease in MEG-1 expression in *dlc-1(RNAi)* germlines (chapter 2). The similarity in these phenotypes suggested that DLC-1 may associate with OMA-1 to promote its activity. Indeed, OMA-1 directly interacted with DLC-1 *in vitro*, however an *in vivo* pulldown of OMA-1/DLC-1 complexes was not successful and could be the result of weak or transient interactions *in vivo*. The overlapping patterns of expression for both OMA-1 and DLC-1 suggest that they might interact, so we developed a protocol that uses PLA to probe for protein-

protein interactions *in situ* in the germline (chapter 3). This powerful tool allowed us to quantify and visualize OMA-1/DLC-1 interactions in the germline and may prove to be useful for future protein-protein interaction experiments, especially to uncover developmentally-regulated interactions. PLA detected a significant number of interactions between DLC-1 and OMA-1 in the oocytes where OMA-1 is expressed (chapter 3), suggesting that these proteins are in complex *in vivo*. In the future, to test whether DLC-1 binding promotes OMA-1's function, we will create a strain of worm that expresses an OMA-1 mutant protein that does not bind to DLC-1. We will cross this into an *oma-1; oma-2* double mutant strain that expresses GFP-tagged MEG-1 and use fluorescence microscopy to determine whether loss of DLC-1 binding affects OMA-1-mediated activation of MEG-1 expression. If we observe loss of MEG-1 expression in OMA-1 mutant oocytes, then this would suggest that DLC-1 is a cofactor that promotes OMA-1's function. In contrast, no change in MEG-1 expression in the oocytes would suggest that DLC-1 does not contribute to OMA-1-mediated activation of its targets and may serve a different role.

Since RIPseq identified DLC-1 associated mRNAs, we expected to recover multiple RBPs by analysis of target mRNA overlap. However, OMA-1 was the only new RBP identified in this study to interact with and require DLC-1 for mRNA regulation. This analysis was constrained by the limited number of existing datasets that have documented what mRNAs are targeted by *C. elegans* RBPs. While there are estimated to be at least 594 *C. elegans* RBPs [26], we were only able to compare target mRNAs from 10 RBPs, which limited our ability to detect new interactors. As a result, identification of

RBPs that interact with DLC-1 still remained unresolved, therefore we sought to use an alternate bioinformatic method to identify other RBPs that interact with DLC-1.

DLC-1-Binding Sites in P Granule Components

In chapter 4, we implemented an *in silico* motif scanning approach to predict what RBPs interact with DLC-1 as this approach has been effective in identifying new interaction partners [161]. By scanning the *C. elegans* proteome for RBPs that contain LC8 interaction sequences, we identified more than 100 candidate interactors.

Remarkably, many of the RBPs that directly interacted with DLC-1 are also core components of P granules, which are subcellular protein-RNA complexes that are important for post-transcriptional regulation. P granule assembly in one cell-staged embryos has been under intensive investigation (see chapter 4 introduction) and we speculated that DLC-1's function as a hub protein could be involved in this process. While we have found that several core P granule components directly interact with DLC-1, the specific interaction sites on the binding partners remain unknown. The bioinformatic scan in chapter 4 denoted the putative interaction sequences in these interacting partners, however initial attempts to mutate these sites to ablate binding *in vitro* were not successful. As an alternate approach to identify the actual binding sites, future work will generate truncations of DLC-1 binding partners to isolate the regions that interact with DLC-1 using *in vitro* GST pulldowns. If DLC-1 interacts with these truncations, we can further test for the specific binding site in the truncated protein by site-directed mutagenesis of amino acids that resemble putative binding motifs. After swapping putative binding sequences with alanines, binding can be tested using the same

assay to determine if the interaction is ablated. If we observe that more than one truncation of the same protein binds to DLC-1, then this interacting partner has more than one DLC-1 binding site. If no truncations for a specific protein bind, then we have disrupted a protein conformation that is recognized by DLC-1. If some truncations are unable to express, then we will focus on other interactors identified in chapter 4. Determination of DLC-1 interaction sequences on these binding partners will be critical for additional downstream experiments described below that aim to characterize phenotypes that result from loss of DLC-1 binding.

PGL/DLC-1 Interaction in Somatic Cells

PLA data in chapter 4 suggests that DLC-1 predominantly interacts with PGL-1/3 proteins during embryogenesis. While PGL proteins are more abundant in the germ cell, numerous PLA foci were observed in somatic cells, suggesting that DLC-1 interacts with PGLs that remain in the somatic cells. The function of DLC-1/PGL interactions in somatic cells is still unclear, however it might be of relevance that PGLs in somatic cells form granules that are removed by autophagy as the embryo continues to develop [247]. PGL clearance is facilitated by a pathway that involves several autophagy-related proteins. The receptor protein SEPA-1 is necessary for both formation and degradation of PGL granules through its interaction with PGL-3, while LGG-1, the *C. elegans* Atg8 ortholog, is important for forming the autophagosome [247]. Recent work has determined that SEPA-1 and post-translational modifications (PTMs) of PGLs, including phosphorylation and arginine methylation, modulate LLPS-mediated assembly of somatic PGL granules [253]. This LLPS-mediated assembly is necessary for subsequent

degradation of PGL granules by autophagy. Since IDRs are important drivers of LLPS and both PGL-1/3 contain IDRs, it is possible that DLC-1 binding to SLiMs in IDRs may have a role in LLPS-mediated assembly of somatic PGL granules. To test whether DLC-1 has a role in LLPS of somatic PGL granules, future experiments will determine if loss of DLC-1 binding has an effect on this process. By generating strains of worms that express fluorescently tagged mutant PGL-1 and PGL-3 proteins that are unable to bind DLC-1, we can observe any effects that may arise from the absence of DLC-1 binding to PGLs *in vivo*. To induce formation of somatic PGL granules in the embryo, we will knock down *lgg-1* by RNAi [247] in worms expressing these PGL mutants and look for presence of PGL granules in somatic cells by fluorescence microscopy. If we do not observe mutant PGL granules in somatic cells, then this would suggest that DLC-1 is important for LLPS of PGLs *in vivo*. On the other hand, if we observe persistence of somatic mutant PGL granules, then this would suggest that DLC-1 is not important for their LLPS-mediated assembly.

If DLC-1 is important for formation of somatic PGL granules, we can perform additional experiments to further probe its role in this process. To test whether DLC-1 is important for directly promoting phase separation of PGL-1/3, we will use phase separation assays, which are often used to test whether proteins undergo LLPS *in vitro*. These assays monitor formation of visible condensates that appear as liquid droplets and resemble *in vivo* P granules. The size and/or quantity per given area of droplets can be quantified and are used as metrics to interpret changes when conditions are modified, such as the inclusion of a cofactor or substrate. Previous work has shown that PGL-1 and PGL-3 are capable of phase separating and forming liquid droplets *in vitro* [248,249].

Using bacterially expressed and purified PGL-1, PGL-3, and DLC-1, we will test whether inclusion of DLC-1 enhances phase separation of PGL-1 and PGL-3 individually as well as co-condensates of PGL-1/3. As a control, we will compare these condensates to those that form without DLC-1. If we observe an increase in size or number of PGL condensates with the inclusion of DLC-1, then this would suggest that DLC-1 promotes phase separation of PGLs. If no change in size or number of PGL condensates is observed, then DLC-1 does not directly promote phase separation of PGLs in somatic cells.

Another potential role for DLC-1 in promoting LLPS could be through modulation PTMs of PGLs. PTMs can control how proteins condense through LLPS [40,254] and recent work has shown that arginine methylation of PGLs prevents LLPS, while heat stress causes elevated mTORC1-mediated phosphorylation that induces PGL condensation into autophagy-resistant somatic PGL granules [248]. Loss of DLC-1 binding could cause PGLs to have an altered state of PTMs, where DLC-1 binding might prevent methylation of PGLs to promote their LLPS. We will use *in vitro* phase separation assays as described above to test whether DLC-1 binding affects methylation of PGL proteins *in vitro*. Methylation results in reduced number and size of droplets, compared to PGL droplets that form in the absence of the EPG-11 methyltransferase [248]. Therefore, we will test whether inclusion of DLC-1 affects EPG-11-mediated methylation of PGLs by measuring the size and number of PGL condensates that form. We can further isolate these condensates by phase sedimentation and probe for methylated arginines by Western blot to determine whether these droplets contain methylated PGLs as in [248]. If we observe that inclusion of DLC-1 leads to an increase

in the number or size of PGL condensates that are not methylated, then this would suggest that DLC-1 binding promotes LLPS of PGLs by preventing their methylation. If no change is observed, then DLC-1 is not involved in modulating methylation of PGLs and may be involved with a different PTM of PGLs. Since phosphorylation promotes LLPS of PGLs, we can also test whether DLC-1 binding affects this PTM. We will use the same *in vitro* phase separation assay, however the *C. elegans* MTOR ortholog LET-363 will be used to phosphorylate PGLs *in vitro*. We will test whether inclusion of DLC-1 enhances LLPS and phosphorylation of PGL condensates. These condensates will be isolated by sedimentation and phosphorylation of PGLs will be evaluated by Western blot using an antibody against phosphorylated PGL-1 as in [248]. If we observe that inclusion of DLC-1 results in an increase in the number or size of phosphorylated PGL condensates, then we will conclude that DLC-1 promotes LLPS of PGLs through modulation of PTMs. In contrast, if we observe no change in these condensates, then DLC-1 binding to somatic PGLs serves a different role that remains to be determined.

DLC-1 Function in Embryonic P Granule Assembly

In the embryonic germ cells, P granules failed to assemble into large condensates when *dlc-1* was knocked down or knocked out *in vivo*. This was a striking finding given that some of these core P granule components directly interact with each other in the absence of DLC-1, *in vitro* (see chapter 4 discussion). These findings underlie the importance of DLC-1 and likely other LC8 family orthologs in promoting assembly of large protein and protein-RNA complexes, such as RNA granules. During the 1-cell stage of *C. elegans* embryogenesis, P granules re-assemble in the posterior region through

LLPS and hierarchical assembly of core proteins (see chapter 4 introduction). MEG-3 and its redundant paralog MEG-4 are phosphoproteins that are important for nucleating the assembly of P granules. *meg-3* or *meg-4* single mutants have no effect on P granule assembly, however P granules in *meg-3 meg-4* double mutants fail to assemble [103]. We found that DLC-1 directly interacted with MEG-4 (Figure 4.2E) and MEG-4 migrates as a higher molecular weight protein in *dlc-1(RNAi)*-treated worms (Figure 2.4G), which might indicate a different splice isoform of MEG-4 or an alteration of its PTMs. If DLC-1 binding does affect the PTMs of MEG-4, it could affect MEG-4's ability to facilitate P granule assembly. Previous work has shown that phosphorylation of MEG-3 destabilizes P granule assembly [103], which may also be relevant for MEG-4. To test whether loss of DLC-1 binding on MEG-4 has an effect on P granule assembly, future work will create a transgenic strain of worm that expresses a 3xFLAG tagged MEG-4 mutant that is unable to bind DLC-1 and cross it into a *meg-3 meg-4* double mutant. Using this strain, we can test whether loss of DLC-1 binding to MEG-4 has an effect on P granule assembly by immunostaining for endogenous PGL-1 as a marker of P granules. If P granules fail to assemble or condense in the P cell, this would suggest that DLC-1 is an important cofactor for MEG-4-mediated P granule assembly. If we find by western blot that this MEG-4 mutant has an altered state of PTMs similar to the wild type MEG-4 in the absence of *dlc-1*, we will further characterize these PTMs. Using mass spectrometry, we will analyze what PTMs are present on mutant MEG-4 proteins that do not bind DLC-1. This may provide insight into how the presence or absence of DLC-1 binding affects MEG-4's PTMs, which may in turn modulate MEG-4's function. However, if P granules

do assemble, this would suggest that DLC-1 is not important for promoting MEG-4's function in P granule assembly and may serve a different role for MEG-4.

An alternate hypothesis is that DLC-1 promotes MEG-4's interaction with different P granule proteins. To test this, we will use *in vitro* GST pulldowns to test whether inclusion of DLC-1 promotes the interaction between MEG-4 and another P granule protein such as GLH-4 that does not normally bind to MEG-4. If we observe that DLC-1 promotes the interaction between these proteins, then this would support the hypothesis. We can also test whether DLC-1 affects proteins that can interact with their partners independent of DLC-1. While MEG-4 binds with PGL-1 *in vitro*, we observed a reduction in the colocalization of these proteins *in vivo* when *dlc-1* was knocked down or knocked out, suggesting that they are interacting less often. As a follow up experiment, we can test whether colocalization of these proteins is impacted by loss of DLC-1 binding *in vivo*. We will create a strain of worms that expresses the following mutant P granule proteins that do not bind DLC-1: GFP tagged PGL-1, OLLAS tagged PGL-3, and 3xFLAG tagged MEG-4. PGL-3 will be included as its colocalization with PGL-1 was disrupted by *dlc-1(RNAi)* and it also interacts with MEG-4 *in vitro*. Colocalization of these proteins will be measured using the same approach as shown in Figures 4.7 and 4.8. If we observe a statistically significant reduction in colocalization of MEG-4 with PGL-1 or PGL-3, then this would suggest that DLC-1 binding is important for promoting assembly of these proteins *in vivo*. Using *in vitro* GST pulldowns, we can test whether inclusion of DLC-1 facilitates these interactions by monitoring changes in abundance of these proteins in pulldown eluents by Western blot band density analysis. In the case that colocalization of MEG-4 with PGL-1 or PGL-3 does not change when DLC-1 binding is

removed, then DLC-1 does not promote MEG-4's interaction with other core P granule proteins and serves a different purpose.

In addition to reduced colocalization of different P granule proteins, embryonic P granules are reduced in size when *dlc-1* is knocked down or knocked out. This could result from inefficient phase separation of these proteins in the absence of *dlc-1*. Using phase separation assays, we can test whether DLC-1 promotes the efficiency of PGL and MEG proteins to phase separate *in vitro*. Besides PGL-1 and PGL-3 mentioned earlier, MEG-3 has also previously been found to phase separate *in vitro* and form liquid droplets [35]. The redundant paralog of MEG-3, MEG-4, has not been shown to undergo LLPS *in vitro*, however it is presumed to have similar properties like MEG-3 that allow it phase separate. Using bacterially expressed and purified MEG-4, PGL-1/3, and DLC-1 proteins, we will reconstitute P granule assembly *in vitro* using phase separation assays. We will test whether inclusion of DLC-1 stimulates formation of more liquid droplets or an increase in their size. Droplet formation of DLC-1 with PGL-1, PGL-3, or MEG-4 individually or paired (PGL-1/3, PGL-1/MEG-4, PGL-3/MEG-4) will be compared to control liquid droplets where DLC-1 is excluded. If we observe an increase in the number of droplets or size, then this would suggest that DLC-1 promotes efficient phase separation of P granule proteins. If no change in size or number of condensates is observed, then DLC-1 is not needed for promoting LLPS.

Another potential role for DLC-1 is that it recruits transient RBP components to the P granules. Our lab has previously shown that DLC-1 is needed for localization of FBF-2 to P granules [171]. Using GST pulldowns, we will determine whether DLC-1 binding promotes interaction between PGL-1 or PGL-3 and FBF-2. If these experiments

show that DLC-1 is needed for FBF-2 to interact with core P granule components, then this would support DLC-1's role in recruiting RBPs to P granules. On the contrary, if DLC-1 does not promote the interaction between FBF-2 and PGL-1 or PGL-3, then DLC-1 serves a different role for P granules that remains to be determined.

The Dynein Motor Function of DLC-1 in P Granule Assembly is Not Yet Ruled Out

The putative functions of DLC-1 described above are based on its function independent of the dynein motor. However, DLC-1's putative role in P granule assembly may involve the dynein motor complex. Currently, no research has established nor ruled out the dynein motor as a contributor to P granule assembly. Using drugs that disrupt polymerization of the microtubule network, such as nocodazole or colcemid, segregation and formation of P granules into the P cell were not disrupted [252], suggesting that P granule asymmetry and assembly do not involve transport along microtubules. Despite these findings, it remains to be determined whether loss of dynein motor function affects embryonic P granule assembly. The dynein motor is essential for many functions in the cell, therefore constitutive loss of function mutants or knockdown by RNAi of dynein heavy chain 1 *dhc-1* are embryonic lethal. To overcome this issue and study loss of dynein function in the embryo, future experiments will use a temperature sensitive (ts) *dhc-1* mutant that causes the dynein motor to lose function within seconds upon shifting the animals to a higher temperature [255]. Using a *dhc-1(ts)* strain of worm that expresses GFP-tagged PGL-1 and RFP-tagged MEG-4, we can shift 1-cell stage embryos from a permissive temperature (16°C) to a restrictive temperature (25°C) to inactivate the dynein motor. Colocalization of MEG-4 and PGL-1 will be quantified and compared with

control embryos at the same temperature with active, wild type *dhc-1*. If we observe a significant reduction in the colocalization of MEG-4 and PGL-1 in embryos with inactive *dhc-1*, then DLC-1's role in P granule assembly likely involves the dynein motor. In contrast, no change in colocalization would mean that DLC-1 likely functions independently of the dynein motor to promote P granule assembly.

Concluding Remarks

Previous research from our lab together with the work presented in this dissertation has pointed to DLC-1 as a germline RBP cofactor. Additionally, the findings presented in chapter 4 illuminated another critical function of DLC-1 in promoting embryonic P granule assembly. Since DLC-1 is a member of the conserved LC8 protein family, our findings that describe its functions in RNA regulation may be relevant to LC8 in other model systems. The proposed future work will help to better understand and define DLC-1's role in P granule assembly. As a result, these studies may cause the field to consider the importance of cofactors such as DLC-1 and how they influence processes such as mRNA regulation and assembly of biomolecular condensates in the cell.

References

- [1] Morris, A.R., Mukherjee, N. and Keene, J.D. (2010). Systematic analysis of posttranscriptional gene expression. *Wiley Interdiscip Rev Syst Biol Med* 2, 162-180.
- [2] Dassi, E. (2017). Handshakes and Fights: The Regulatory Interplay of RNA-Binding Proteins. *Front Mol Biosci* 4, 67.
- [3] Halbeisen, R.E., Galgano, A., Scherrer, T. and Gerber, A.P. (2008). Post-transcriptional gene regulation: from genome-wide studies to principles. *Cell Mol Life Sci* 65, 798-813.
- [4] Neelamraju, Y., Gonzalez-Perez, A., Bhat-Nakshatri, P., Nakshatri, H. and Janga, S.C. (2018). Mutational landscape of RNA-binding proteins in human cancers. *RNA Biol* 15, 115-129.
- [5] Thelen, M.P. and Kye, M.J. (2019). The Role of RNA Binding Proteins for Local mRNA Translation: Implications in Neurological Disorders. *Front Mol Biosci* 6, 161.
- [6] Corbett, A.H. (2018). Post-transcriptional regulation of gene expression and human disease. *Curr Opin Cell Biol* 52, 96-104.
- [7] Mayr, C. (2019). What Are 3' UTRs Doing? *Cold Spring Harb Perspect Biol* 11
- [8] Araujo, P.R., Yoon, K., Ko, D., Smith, A.D., Qiao, M., Suresh, U., Burns, S.C. and Penalva, L.O. (2012). Before It Gets Started: Regulating Translation at the 5' UTR. *Comp Funct Genomics* 2012, 475731.
- [9] Leppek, K., Das, R. and Barna, M. (2018). Functional 5' UTR mRNA structures in eukaryotic translation regulation and how to find them. *Nat Rev Mol Cell Biol* 19, 158-174.
- [10] Theil, K., Herzog, M. and Rajewsky, N. (2018). Post-transcriptional Regulation by 3' UTRs Can Be Masked by Regulatory Elements in 5' UTRs. *Cell Rep* 22, 3217-3226.
- [11] Prasad, A., Porter, D.F., Kroll-Conner, P.L., Mohanty, I., Ryan, A.R., Crittenden, S.L., Wickens, M. and Kimble, J. (2016). The PUF binding landscape in metazoan germ cells. *RNA* 22, 1026-43.
- [12] Merritt, C., Rasoloson, D., Ko, D. and Seydoux, G. (2008). 3' UTRs are the primary regulators of gene expression in the *C. elegans* germline. *Curr Biol* 18, 1476-82.
- [13] Hentze, M.W., Castello, A., Schwarzl, T. and Preiss, T. (2018). A brave new world of RNA-binding proteins. *Nat Rev Mol Cell Biol* 19, 327-341.
- [14] Järvelin, A.I., Noerenberg, M., Davis, I. and Castello, A. (2016). The new (dis)order in RNA regulation. *Cell Commun Signal* 14, 9.
- [15] Corley, M., Burns, M.C. and Yeo, G.W. (2020). How RNA-Binding Proteins Interact with RNA: Molecules and Mechanisms. *Mol Cell* 78, 9-29.
- [16] Glisovic, T., Bachorik, J.L., Yong, J. and Dreyfuss, G. (2008). RNA-binding proteins and post-transcriptional gene regulation. *FEBS Lett* 582, 1977-86.

- [17] Müller-McNicoll, M., Rossbach, O., Hui, J. and Medenbach, J. (2019). Auto-regulatory feedback by RNA-binding proteins. *J Mol Cell Biol* 11, 930-939.
- [18] Young, C.L., Khoshnevis, S. and Karbstein, K. (2013). Cofactor-dependent specificity of a DEAD-box protein. *Proc Natl Acad Sci U S A* 110, E2668-76.
- [19] Heininger, A.U. et al. (2016). Protein cofactor competition regulates the action of a multifunctional RNA helicase in different pathways. *RNA Biol* 13, 320-30.
- [20] Wheeler, E.C., Van Nostrand, E.L. and Yeo, G.W. (2018). Advances and challenges in the detection of transcriptome-wide protein-RNA interactions. *Wiley Interdiscip Rev RNA* 9
- [21] Wang, M., Ogé, L., Perez-Garcia, M.D., Hamama, L. and Sakr, S. (2018). The PUF Protein Family: Overview on PUF RNA Targets, Biological Functions, and Post Transcriptional Regulation. *Int J Mol Sci* 19
- [22] Tamburino, A.M., Ryder, S.P. and Walhout, A.J. (2013). A compendium of *Caenorhabditis elegans* RNA binding proteins predicts extensive regulation at multiple levels. *G3 (Bethesda)* 3, 297-304.
- [23] Si, J., Cui, J., Cheng, J. and Wu, R. (2015). Computational Prediction of RNA-Binding Proteins and Binding Sites. *Int J Mol Sci* 16, 26303-17.
- [24] Bressin, A., Schulte-Sasse, R., Figini, D., Urdaneta, E.C., Beckmann, B.M. and Marsico, A. (2019). TriPepSVM: de novo prediction of RNA-binding proteins based on short amino acid motifs. *Nucleic Acids Res* 47, 4406-4417.
- [25] Zheng, J., Zhang, X., Zhao, X., Tong, X., Hong, X., Xie, J. and Liu, S. (2018). Deep-RBPPred: Predicting RNA binding proteins in the proteome scale based on deep learning. *Sci Rep* 8, 15264.
- [26] Matia-González, A.M., Laing, E.E. and Gerber, A.P. (2015). Conserved mRNA-binding proteomes in eukaryotic organisms. *Nat Struct Mol Biol* 22, 1027-33.
- [27] Castello, A., Horos, R., Strein, C., Fischer, B., Eichelbaum, K., Steinmetz, L.M., Krijgsveld, J. and Hentze, M.W. (2013). System-wide identification of RNA-binding proteins by interactome capture. *Nat Protoc* 8, 491-500.
- [28] Castello, A. et al. (2017). Identification of RNA-binding domains of RNA-binding proteins in cultured cells on a system-wide scale with RBDmap. *Nat Protoc* 12, 2447-2464.
- [29] Castello, A. et al. (2012). Insights into RNA biology from an atlas of mammalian mRNA-binding proteins. *Cell* 149, 1393-406.
- [30] Baltz, A.G. et al. (2012). The mRNA-bound proteome and its global occupancy profile on protein-coding transcripts. *Mol Cell* 46, 674-90.
- [31] Balcerak, A., Trebinska-Stryjewska, A., Konopinski, R., Wakula, M. and Grzybowska, E.A. (2019). RNA-protein interactions: disorder, moonlighting and junk contribute to eukaryotic complexity. *Open Biol* 9, 190096.

- [32] Panhale, A., Richter, F.M., Ramírez, F., Shvedunova, M., Manke, T., Mittler, G. and Akhtar, A. (2019). CAPRI enables comparison of evolutionarily conserved RNA interacting regions. *Nat Commun* 10, 2682.
- [33] Zagrovic, B., Bartonek, L. and Polyansky, A.A. (2018). RNA-protein interactions in an unstructured context. *FEBS Lett* 592, 2901-2916.
- [34] Lee, C.S., Putnam, A., Lu, T., He, S., Ouyang, J.P.T. and Seydoux, G. (2020). Recruitment of mRNAs to P granules by condensation with intrinsically-disordered proteins. *Elife* 9
- [35] Smith, J., Calidas, D., Schmidt, H., Lu, T., Rasoloson, D. and Seydoux, G. (2016). Spatial patterning of P granules by RNA-induced phase separation of the intrinsically-disordered protein MEG-3. *Elife* 5
- [36] Anderson, P. and Kedersha, N. (2009). RNA granules: post-transcriptional and epigenetic modulators of gene expression. *Nat Rev Mol Cell Biol* 10, 430-6.
- [37] Banani, S.F., Lee, H.O., Hyman, A.A. and Rosen, M.K. (2017). Biomolecular condensates: organizers of cellular biochemistry. *Nat Rev Mol Cell Biol* 18, 285-298.
- [38] Boeynaems, S. et al. (2018). Protein Phase Separation: A New Phase in Cell Biology. *Trends Cell Biol* 28, 420-435.
- [39] Brangwynne, C.P., Eckmann, C.R., Courson, D.S., Rybarska, A., Hoege, C., Gharakhani, J., Jülicher, F. and Hyman, A.A. (2009). Germline P granules are liquid droplets that localize by controlled dissolution/condensation. *Science* 324, 1729-32.
- [40] Shin, Y. and Brangwynne, C.P. (2017). Liquid phase condensation in cell physiology and disease. *Science* 357
- [41] Yoshizawa, T., Nozawa, R.S., Jia, T.Z., Saio, T. and Mori, E. (2020). Biological phase separation: cell biology meets biophysics. *Biophys Rev*
- [42] Hyman, A.A., Weber, C.A. and Jülicher, F. (2014). Liquid-liquid phase separation in biology. *Annu Rev Cell Dev Biol* 30, 39-58.
- [43] Shin, Y., Berry, J., Pannucci, N., Haataja, M.P., Toettcher, J.E. and Brangwynne, C.P. (2017). Spatiotemporal Control of Intracellular Phase Transitions Using Light-Activated optoDroplets. *Cell* 168, 159-171.e14.
- [44] Wang, Y., Lomakin, A., Kanai, S., Alex, R. and Benedek, G.B. (2017). Liquid-Liquid Phase Separation in Oligomeric Peptide Solutions. *Langmuir* 33, 7715-7721.
- [45] Gomes, E. and Shorter, J. (2019). The molecular language of membraneless organelles. *J Biol Chem* 294, 7115-7127.
- [46] Zhou, H.X., Nguemaha, V., Mazarakos, K. and Qin, S. (2018). Why Do Disordered and Structured Proteins Behave Differently in Phase Separation? *Trends Biochem Sci* 43, 499-516.
- [47] Uversky, V.N. (2017). Intrinsically disordered proteins in overcrowded milieu: Membrane-less organelles, phase separation, and intrinsic disorder. *Curr Opin Struct Biol* 44, 18-30.

- [48] Mittag, T. and Parker, R. (2018). Multiple Modes of Protein-Protein Interactions Promote RNP Granule Assembly. *J Mol Biol* 430, 4636-4649.
- [49] Protter, D.S.W., Rao, B.S., Van Treeck, B., Lin, Y., Mizoue, L., Rosen, M.K. and Parker, R. (2018). Intrinsically Disordered Regions Can Contribute Promiscuous Interactions to RNP Granule Assembly. *Cell Rep* 22, 1401-1412.
- [50] Lin, Y., Protter, D.S., Rosen, M.K. and Parker, R. (2015). Formation and Maturation of Phase-Separated Liquid Droplets by RNA-Binding Proteins. *Mol Cell* 60, 208-19.
- [51] Van Treeck, B. and Parker, R. (2018). Emerging Roles for Intermolecular RNA-RNA Interactions in RNP Assemblies. *Cell* 174, 791-802.
- [52] Van Treeck, B., Protter, D.S.W., Matheny, T., Khong, A., Link, C.D. and Parker, R. (2018). RNA self-assembly contributes to stress granule formation and defining the stress granule transcriptome. *Proc Natl Acad Sci U S A* 115, 2734-2739.
- [53] Rhine, K., Vidaurre, V. and Myong, S. (2020). RNA Droplets. *Annu Rev Biophys*
- [54] Elbaum-Garfinkle, S. (2019). Matter over mind: Liquid phase separation and neurodegeneration. *J Biol Chem* 294, 7160-7168.
- [55] Thomas, M.G., Loschi, M., Desbats, M.A. and Boccaccio, G.L. (2011). RNA granules: the good, the bad and the ugly. *Cell Signal* 23, 324-34.
- [56] Ivanov, P., Kedersha, N. and Anderson, P. (2019). Stress Granules and Processing Bodies in Translational Control. *Cold Spring Harb Perspect Biol* 11
- [57] Anderson, P. and Kedersha, N. (2006). RNA granules. *J Cell Biol* 172, 803-8.
- [58] Buchan, J.R. (2014). mRNP granules. Assembly, function, and connections with disease. *RNA Biol* 11, 1019-30.
- [59] Luo, Y., Na, Z. and Slavoff, S.A. (2018). P-Bodies: Composition, Properties, and Functions. *Biochemistry* 57, 2424-2431.
- [60] Sheth, U. and Parker, R. (2003). Decapping and decay of messenger RNA occur in cytoplasmic processing bodies. *Science* 300, 805-8.
- [61] Hubstenberger, A. et al. (2017). P-Body Purification Reveals the Condensation of Repressed mRNA Regulons. *Mol Cell* 68, 144-157.e5.
- [62] Stoecklin, G. and Kedersha, N. (2013). Relationship of GW/P-bodies with stress granules. *Adv Exp Med Biol* 768, 197-211.
- [63] Kedersha, N. et al. (2005). Stress granules and processing bodies are dynamically linked sites of mRNP remodeling. *J Cell Biol* 169, 871-84.
- [64] Kiebler, M.A. and Bassell, G.J. (2006). Neuronal RNA granules: movers and makers. *Neuron* 51, 685-90.
- [65] Pushpalatha, K.V. and Besse, F. (2019). Local Translation in Axons: When Membraneless RNP Granules Meet Membrane-Bound Organelles. *Front Mol Biosci* 6, 129.

- [66] Cagnetta, R., Frese, C.K., Shigeoka, T., Krijgsveld, J. and Holt, C.E. (2018). Rapid Cue-Specific Remodeling of the Nascent Axonal Proteome. *Neuron* 99, 29-46.e4.
- [67] Formicola, N., Vijayakumar, J. and Besse, F. (2019). Neuronal ribonucleoprotein granules: Dynamic sensors of localized signals. *Traffic* 20, 639-649.
- [68] Das, S., Singer, R.H. and Yoon, Y.J. (2019). The travels of mRNAs in neurons: do they know where they are going? *Curr Opin Neurobiol* 57, 110-116.
- [69] Voronina, E., Seydoux, G., Sassone-Corsi, P. and Nagamori, I. (2011). RNA granules in germ cells. *Cold Spring Harb Perspect Biol* 3
- [70] Strome, S. and Updike, D. (2015). Specifying and protecting germ cell fate. *Nat Rev Mol Cell Biol* 16, 406-16.
- [71] Updike, D.L., Knutson, A.K., Egelhofer, T.A., Campbell, A.C. and Strome, S. (2014). Germ-granule components prevent somatic development in the *C. elegans* germline. *Curr Biol* 24, 970-5.
- [72] Sengupta, M.S. and Boag, P.R. (2012). Germ granules and the control of mRNA translation. *IUBMB Life* 64, 586-94.
- [73] Friday, A.J. and Keiper, B.D. (2015). Positive mRNA Translational Control in Germ Cells by Initiation Factor Selectivity. *Biomed Res Int* 2015, 327963.
- [74] Fan, A.C. and Leung, A.K. (2016). RNA Granules and Diseases: A Case Study of Stress Granules in ALS and FTL. *Adv Exp Med Biol* 907, 263-96.
- [75] Wolozin, B. and Apicco, D. (2015). RNA binding proteins and the genesis of neurodegenerative diseases. *Adv Exp Med Biol* 822, 11-5.
- [76] Lehtiniemi, T. and Kotaja, N. (2018). Germ granule-mediated RNA regulation in male germ cells. *Reproduction* 155, R77-R91.
- [77] Corsi, A.K., Wightman, B. and Chalfie, M. (2015). A Transparent Window into Biology: A Primer on *Caenorhabditis elegans*. *Genetics* 200, 387-407.
- [78] Apfeld, J. and Alper, S. (2018). What Can We Learn About Human Disease from the Nematode *C. elegans*? *Methods Mol Biol* 1706, 53-75.
- [79] Meneely, P.M., Dahlberg, C.L. and Rose, J.K. (2019). Working with Worms: *Caenorhabditis elegans* as a Model Organism. *Current Protocols* 19
- [80] Hubbard, E.J.A. and Schedl, T. (2019). Biology of the *Caenorhabditis elegans* germline stem cell system. *Genetics* 213, 1145-1188.
- [81] Kimble, J. and Crittenden, S.L. (2007). Controls of germline stem cells, entry into meiosis, and the sperm/oocyte decision in *Caenorhabditis elegans*. *Annu Rev Cell Dev Biol* 23, 405-33.
- [82] Wang, X. and Voronina, E. (2020). Diverse Roles of PUF Proteins in Germline Stem and Progenitor Cell Development in. *Front Cell Dev Biol* 8, 29.

- [83] Lee, M.H., Mamillapalli, S.S., Keiper, B.D. and Cha, D.S. (2016). A systematic mRNA control mechanism for germline stem cell homeostasis and cell fate specification. *BMB Rep* 49, 93-8.
- [84] Lamont, L.B., Crittenden, S.L., Bernstein, D., Wickens, M. and Kimble, J. (2004). FBF-1 and FBF-2 regulate the size of the mitotic region in the *C. elegans* germline. *Dev Cell* 7, 697-707.
- [85] Ariz, M., Mainpal, R. and Subramaniam, K. (2009). *C. elegans* RNA-binding proteins PUF-8 and MEX-3 function redundantly to promote germline stem cell mitosis. *Dev Biol* 326, 295-304.
- [86] Mainpal, R., Priti, A. and Subramaniam, K. (2011). PUF-8 suppresses the somatic transcription factor PAL-1 expression in *C. elegans* germline stem cells. *Dev Biol* 360, 195-207.
- [87] Suh, N., Crittenden, S.L., Goldstrohm, A., Hook, B., Thompson, B., Wickens, M. and Kimble, J. (2009). FBF and its dual control of *gld-1* expression in the *Caenorhabditis elegans* germline. *Genetics* 181, 1249-60.
- [88] Eckmann, C.R., Crittenden, S.L., Suh, N. and Kimble, J. (2004). *GLD-3* and control of the mitosis/meiosis decision in the germline of *Caenorhabditis elegans*. *Genetics* 168, 147-60.
- [89] Francis, R., Maine, E. and Schedl, T. (1995). Analysis of the multiple roles of *gld-1* in germline development: interactions with the sex determination cascade and the *glp-1* signaling pathway. *Genetics* 139, 607-30.
- [90] Ellis, R. and Schedl, T. (2007). Sex determination in the germ line. *WormBook*, 1-13.
- [91] Barton, M.K. and Kimble, J. (1990). *fog-1*, a regulatory gene required for specification of spermatogenesis in the germ line of *Caenorhabditis elegans*. *Genetics* 125, 29-39.
- [92] Noble, D.C., Aoki, S.T., Ortiz, M.A., Kim, K.W., Verheyden, J.M. and Kimble, J. (2016). Genomic Analyses of Sperm Fate Regulator Targets Reveal a Common Set of Oogenic mRNAs in *Caenorhabditis elegans*. *Genetics* 202, 221-34.
- [93] Aoki, S.T., Porter, D.F., Prasad, A., Wickens, M., Bingman, C.A. and Kimble, J. (2018). An RNA-Binding Multimer Specifies Nematode Sperm Fate. *Cell Rep* 23, 3769-3775.
- [94] Ellis, R.E. and Kimble, J. (1995). The *fog-3* gene and regulation of cell fate in the germ line of *Caenorhabditis elegans*. *Genetics* 139, 561-77.
- [95] Kim, K.W., Nykamp, K., Suh, N., Bachorik, J.L., Wang, L. and Kimble, J. (2009). Antagonism between *GLD-2* binding partners controls gamete sex. *Dev Cell* 16, 723-33.
- [96] Kim, K.W., Wilson, T.L. and Kimble, J. (2010). *GLD-2/RNP-8* cytoplasmic poly(A) polymerase is a broad-spectrum regulator of the oogenesis program. *Proc Natl Acad Sci U S A* 107, 17445-50.

- [97] Kaymak, E. and Ryder, S.P. (2013). RNA recognition by the *Caenorhabditis elegans* oocyte maturation determinant OMA-1. *J Biol Chem* 288, 30463-72.
- [98] Detwiler, M.R., Reuben, M., Li, X., Rogers, E. and Lin, R. (2001). Two zinc finger proteins, OMA-1 and OMA-2, are redundantly required for oocyte maturation in *C. elegans*. *Dev Cell* 1, 187-99.
- [99] Lin, R. (2003). A gain-of-function mutation in *oma-1*, a *C. elegans* gene required for oocyte maturation, results in delayed degradation of maternal proteins and embryonic lethality. *Dev Biol* 258, 226-39.
- [100] Tsukamoto, T., Gearhart, M.D., Spike, C.A., Huelgas-Morales, G., Mews, M., Boag, P.R., Beilharz, T.H. and Greenstein, D. (2017). LIN-41 and OMA Ribonucleoprotein Complexes Mediate a Translational Repression-to-Activation Switch Controlling Oocyte Meiotic Maturation and the Oocyte-to-Embryo Transition in *Caenorhabditis elegans*. *Genetics* 206, 2007-2039.
- [101] Spike, C.A., Coetzee, D., Eichten, C., Wang, X., Hansen, D. and Greenstein, D. (2014). The TRIM-NHL protein LIN-41 and the OMA RNA-binding proteins antagonistically control the prophase-to-metaphase transition and growth of *Caenorhabditis elegans* oocytes. *Genetics* 198, 1535-58.
- [102] Leacock, S.W. and Reinke, V. (2008). MEG-1 and MEG-2 are embryo-specific P-granule components required for germline development in *Caenorhabditis elegans*. *Genetics* 178, 295-306.
- [103] Wang, J.T. et al. (2014). Regulation of RNA granule dynamics by phosphorylation of serine-rich, intrinsically disordered proteins in *C. elegans*. *Elife* 3, e04591.
- [104] Griffin, E.E., Odde, D.J. and Seydoux, G. (2011). Regulation of the MEX-5 gradient by a spatially segregated kinase/phosphatase cycle. *Cell* 146, 955-68.
- [105] Putnam, A., Cassani, M., Smith, J. and Seydoux, G. (2019). A gel phase promotes condensation of liquid P granules in *Caenorhabditis elegans* embryos. *Nat Struct Mol Biol* 26, 220-226.
- [106] Keene, J.D. (2007). RNA regulons: coordination of post-transcriptional events. *Nat Rev Genet* 8, 533-43.
- [107] Blackinton, J.G. and Keene, J.D. (2014). Post-transcriptional RNA regulons affecting cell cycle and proliferation. *Semin Cell Dev Biol* 34, 44-54.
- [108] Updike, D. and Strome, S. (2010). P granule assembly and function in *Caenorhabditis elegans* germ cells. *J Androl* 31, 53-60.
- [109] Strome, S. and Wood, W.B. (1982). Immunofluorescence visualization of germ-line-specific cytoplasmic granules in embryos, larvae, and adults of *Caenorhabditis elegans*. *Proc Natl Acad Sci U S A* 79, 1558-62.

- [110] Knutson, A.K., Egelhofer, T., Rechtsteiner, A. and Strome, S. (2017). Germ Granules Prevent Accumulation of Somatic Transcripts in the Adult. *Genetics* 206, 163-178.
- [111] Gallo, C.M., Wang, J.T., Moteji, F. and Seydoux, G. (2010). Cytoplasmic partitioning of P granule components is not required to specify the germline in *C. elegans*. *Science* 330, 1685-9.
- [112] Gao, M. and Arkov, A.L. (2013). Next generation organelles: structure and role of germ granules in the germline. *Mol Reprod Dev* 80, 610-23.
- [113] Arkov, A.L. and Ramos, A. (2010). Building RNA-protein granules: insight from the germline. *Trends Cell Biol* 20, 482-90.
- [114] Schmidt, H. and Carter, A.P. (2016). Review: Structure and mechanism of the dynein motor ATPase. *Biopolymers* 105, 557-67.
- [115] Allan, V.J. (2011). Cytoplasmic dynein. *Biochem Soc Trans* 39, 1169-78.
- [116] Roberts, A.J., Kon, T., Knight, P.J., Sutoh, K. and Burgess, S.A. (2013). Functions and mechanics of dynein motor proteins. *Nat Rev Mol Cell Biol* 14, 713-26.
- [117] Cole, D.G. (2003). The intraflagellar transport machinery of *Chlamydomonas reinhardtii*. *Traffic* 4, 435-42.
- [118] Wickstead, B. and Gull, K. (2007). Dyneins across eukaryotes: a comparative genomic analysis. *Traffic* 8, 1708-21.
- [119] Bhabha, G., Johnson, G.T., Schroeder, C.M. and Vale, R.D. (2016). How Dynein Moves Along Microtubules. *Trends Biochem Sci* 41, 94-105.
- [120] Tsai, N.P., Tsui, Y.C. and Wei, L.N. (2009). Dynein motor contributes to stress granule dynamics in primary neurons. *Neuroscience* 159, 647-56.
- [121] Loschi, M., Leishman, C.C., Berardone, N. and Boccaccio, G.L. (2009). Dynein and kinesin regulate stress-granule and P-body dynamics. *J Cell Sci* 122, 3973-82.
- [122] Kwon, S., Zhang, Y. and Matthias, P. (2007). The deacetylase HDAC6 is a novel critical component of stress granules involved in the stress response. *Genes Dev* 21, 3381-94.
- [123] Ivanov, P.A., Chudinova, E.M. and Nadezhdina, E.S. (2003). Disruption of microtubules inhibits cytoplasmic ribonucleoprotein stress granule formation. *Exp Cell Res* 290, 227-33.
- [124] Sweet, T.J., Boyer, B., Hu, W., Baker, K.E. and Coller, J. (2007). Microtubule disruption stimulates P-body formation. *RNA* 13, 493-502.
- [125] Aizer, A., Brody, Y., Ler, L.W., Sonenberg, N., Singer, R.H. and Shav-Tal, Y. (2008). The dynamics of mammalian P body transport, assembly, and disassembly in vivo. *Mol Biol Cell* 19, 4154-66.
- [126] Strasser, M.J., Mackenzie, N.C., Dumstrei, K., Nakkrasae, L.I., Stebler, J. and Raz, E. (2008). Control over the morphology and segregation of Zebrafish germ cell granules during embryonic development. *BMC Dev Biol* 8, 58.

- [127] Schiavo, G., Greensmith, L., Hafezparast, M. and Fisher, E.M. (2013). Cytoplasmic dynein heavy chain: the servant of many masters. *Trends Neurosci* 36, 641-51.
- [128] Pfister, K.K., Shah, P.R., Hummerich, H., Russ, A., Cotton, J., Annuar, A.A., King, S.M. and Fisher, E.M. (2006). Genetic analysis of the cytoplasmic dynein subunit families. *PLoS Genet* 2, e1.
- [129] King, S.J. and Schroer, T.A. (2000). Dynactin increases the processivity of the cytoplasmic dynein motor. *Nat Cell Biol* 2, 20-4.
- [130] McKenney, R.J., Huynh, W., Tanenbaum, M.E., Bhabha, G. and Vale, R.D. (2014). Activation of cytoplasmic dynein motility by dynactin-cargo adapter complexes. *Science* 345, 337-41.
- [131] Rao, L., Romes, E.M., Nicholas, M.P., Brenner, S., Tripathy, A., Gennerich, A. and Slep, K.C. (2013). The yeast dynein Dyn2-Pac11 complex is a dynein dimerization/processivity factor: structural and single-molecule characterization. *Mol Biol Cell* 24, 2362-77.
- [132] Trokter, M., Mücke, N. and Surrey, T. (2012). Reconstitution of the human cytoplasmic dynein complex. *Proc Natl Acad Sci U S A* 109, 20895-900.
- [133] Pfister, K.K., Fay, R.B. and Witman, G.B. (1982). Purification and polypeptide composition of dynein ATPases from *Chlamydomonas* flagella. *Cell Motil* 2, 525-47.
- [134] King, S.M. and Patel-King, R.S. (1995). The M(r) = 8,000 and 11,000 outer arm dynein light chains from *Chlamydomonas* flagella have cytoplasmic homologues. *J Biol Chem* 270, 11445-52.
- [135] Wilson, M.J., Salata, M.W., Susalka, S.J. and Pfister, K.K. (2001). Light chains of mammalian cytoplasmic dynein: identification and characterization of a family of LC8 light chains. *Cell Motil Cytoskeleton* 49, 229-40.
- [136] Kamath, R.S. et al. (2003). Systematic functional analysis of the *Caenorhabditis elegans* genome using RNAi. *Nature* 421, 231-7.
- [137] Dick, T., Ray, K., Salz, H.K. and Chia, W. (1996). Cytoplasmic dynein (*ddlc1*) mutations cause morphogenetic defects and apoptotic cell death in *Drosophila melanogaster*. *Mol Cell Biol* 16, 1966-77.
- [138] King, A., Hoch, N.C., McGregor, N.E., Sims, N.A., Smyth, I.M. and Heierhorst, J. (2019). Dynll1 is essential for development and promotes endochondral bone formation by regulating intraflagellar Dynein function in primary cilia. *Hum Mol Genet*
- [139] Rapali, P., Szenes, Á., Radnai, L., Bakos, A., Pál, G. and Nyitray, L. (2011). DYNLL/LC8: a light chain subunit of the dynein motor complex and beyond. *FEBS J* 278, 2980-96.
- [140] Reck-Peterson, S.L., Redwine, W.B., Vale, R.D. and Carter, A.P. (2018). The cytoplasmic dynein transport machinery and its many cargoes. *Nat Rev Mol Cell Biol* 19, 382-398.

- [141] Singh, P.K., Weber, A. and Häcker, G. (2018). The established and the predicted roles of dynein light chain in the regulation of mitochondrial apoptosis. *Cell Cycle* 17, 1037-1047.
- [142] Barbar, E. (2008). Dynein light chain LC8 is a dimerization hub essential in diverse protein networks. *Biochemistry* 47, 503-8.
- [143] Singh, P.K., Roukounakis, A., Weber, A., Das, K.K., Sohm, B., Villunger, A., Garcia-Saez, A.J. and Häcker, G. (2020). Dynein light chain binding determines complex formation and posttranslational stability of the Bcl-2 family members Bmf and Bim. *Cell Death Differ* 27, 434-450.
- [144] Jurado, S. et al. (2012). ATM substrate Chk2-interacting Zn²⁺ finger (ASCIZ) Is a bi-functional transcriptional activator and feedback sensor in the regulation of dynein light chain (DYNLL1) expression. *J Biol Chem* 287, 3156-64.
- [145] Stelter, P., Kunze, R., Flemming, D., Höpfner, D., Diepholz, M., Philippsen, P., Böttcher, B. and Hurt, E. (2007). Molecular basis for the functional interaction of dynein light chain with the nuclear-pore complex. *Nat Cell Biol* 9, 788-96.
- [146] Jespersen, N. et al. (2019). Systematic identification of recognition motifs for the hub protein LC8. *Life Sci Alliance* 2
- [147] King, S.M., Barbarese, E., Dillman, J.F., Patel-King, R.S., Carson, J.H. and Pfister, K.K. (1996). Brain cytoplasmic and flagellar outer arm dyneins share a highly conserved Mr 8,000 light chain. *J Biol Chem* 271, 19358-66.
- [148] Jespersen, N. and Barbar, E. (2020). Emerging Features of Linear Motif-Binding Hub Proteins. *Trends Biochem Sci* 45, 375-384.
- [149] Liang, J., Jaffrey, S.R., Guo, W., Snyder, S.H. and Clardy, J. (1999). Structure of the PIN/LC8 dimer with a bound peptide. *Nat Struct Biol* 6, 735-40.
- [150] Clark, S.A., Jespersen, N., Woodward, C. and Barbar, E. (2015). Multivalent IDP assemblies: Unique properties of LC8-associated, IDP duplex scaffolds. *FEBS Lett* 589, 2543-51.
- [151] Wang, L., Hare, M., Hays, T.S. and Barbar, E. (2004). Dynein light chain LC8 promotes assembly of the coiled-coil domain of swallow protein. *Biochemistry* 43, 4611-20.
- [152] Kidane, A.I., Song, Y., Nyarko, A., Hall, J., Hare, M., Löhr, F. and Barbar, E. (2013). Structural features of LC8-induced self-association of swallow. *Biochemistry* 52, 6011-20.
- [153] Van Roey, K., Uyar, B., Weatheritt, R.J., Dinkel, H., Seiler, M., Budd, A., Gibson, T.J. and Davey, N.E. (2014). Short linear motifs: ubiquitous and functionally diverse protein interaction modules directing cell regulation. *Chem Rev* 114, 6733-78.
- [154] Rodríguez-Crespo, I., Yélamos, B., Roncal, F., Albar, J.P., Ortiz de Montellano, P.R. and Gavilanes, F. (2001). Identification of novel cellular

- proteins that bind to the LC8 dynein light chain using a pepscan technique. FEBS Lett 503, 135-41.
- [155] Martínez-Moreno, M., Navarro-Lérida, I., Roncal, F., Albar, J.P., Alonso, C., Gavilanes, F. and Rodríguez-Crespo, I. (2003). Recognition of novel viral sequences that associate with the dynein light chain LC8 identified through a pepscan technique. FEBS Lett 544, 262-7.
- [156] Navarro-Lérida, I., Martínez Moreno, M., Roncal, F., Gavilanes, F., Albar, J.P. and Rodríguez-Crespo, I. (2004). Proteomic identification of brain proteins that interact with dynein light chain LC8. Proteomics 4, 339-46.
- [157] Rapali, P. et al. (2011). Directed evolution reveals the binding motif preference of the LC8/DYNLL hub protein and predicts large numbers of novel binders in the human proteome. PLoS One 6, e18818.
- [158] Benison, G., Karplus, P.A. and Barbar, E. (2007). Structure and dynamics of LC8 complexes with KXTQT-motif peptides: swallow and dynein intermediate chain compete for a common site. J Mol Biol 371, 457-68.
- [159] Lo, K.W., Naisbitt, S., Fan, J.S., Sheng, M. and Zhang, M. (2001). The 8-kDa dynein light chain binds to its targets via a conserved (K/R)XTQT motif. J Biol Chem 276, 14059-66.
- [160] Clark, S., Nyarko, A., Löhr, F., Karplus, P.A. and Barbar, E. (2016). The Anchored Flexibility Model in LC8 Motif Recognition: Insights from the Chica Complex. Biochemistry 55, 199-209.
- [161] Erdős, G., Szaniszló, T., Pajkos, M., Hajdu-Soltész, B., Kiss, B., Pál, G., Nyitray, L. and Dosztányi, Z. (2017). Novel linear motif filtering protocol reveals the role of the LC8 dynein light chain in the Hippo pathway. PLoS Comput Biol 13, e1005885.
- [162] Gagnon, J.A. and Mowry, K.L. (2011). Molecular motors: directing traffic during RNA localization. Crit Rev Biochem Mol Biol 46, 229-39.
- [163] Fu, X.F., Cheng, S.F., Wang, L.Q., Yin, S., De Felici, M. and Shen, W. (2015). DAZ Family Proteins, Key Players for Germ Cell Development. Int J Biol Sci 11, 1226-35.
- [164] Lee, K.H., Lee, S., Kim, B., Chang, S., Kim, S.W., Paick, J.S. and Rhee, K. (2006). Dazl can bind to dynein motor complex and may play a role in transport of specific mRNAs. EMBO J 25, 4263-70.
- [165] Hall, J., Karplus, P.A. and Barbar, E. (2009). Multivalency in the assembly of intrinsically disordered Dynein intermediate chain. J Biol Chem 284, 33115-21.
- [166] Williams, J.C., Roulhac, P.L., Roy, A.G., Vallee, R.B., Fitzgerald, M.C. and Hendrickson, W.A. (2007). Structural and thermodynamic characterization of a cytoplasmic dynein light chain-intermediate chain complex. Proc Natl Acad Sci U S A 104, 10028-33.
- [167] Bergen, J.M. and Pun, S.H. (2007). Evaluation of an LC8-binding peptide for the attachment of artificial cargo to dynein. Mol Pharm 4, 119-28.

- [168] Bullock, S.L. and Ish-Horowicz, D. (2001). Conserved signals and machinery for RNA transport in *Drosophila* oogenesis and embryogenesis. *Nature* 414, 611-6.
- [169] Navarro, C., Puthalakath, H., Adams, J.M., Strasser, A. and Lehmann, R. (2004). Egalitarian binds dynein light chain to establish oocyte polarity and maintain oocyte fate. *Nat Cell Biol* 6, 427-35.
- [170] Goldman, C.H., Neiswender, H., Veeranan-Karmegam, R. and Gonsalvez, G.B. (2019). The Egalitarian binding partners Dynein light chain and Bicaudal-D act sequentially to link mRNA to the Dynein motor. *Development* 146
- [171] Wang, X., Olson, J.R., Rasoloson, D., Ellenbecker, M., Bailey, J. and Voronina, E. (2016). Dynein light chain DLC-1 promotes localization and function of the PUF protein FBF-2 in germline progenitor cells. *Development* 143, 4643-4653.
- [172] Ellenbecker, M., Osterli, E., Wang, X., Day, N.J., Baumgarten, E., Hickey, B. and Voronina, E. (2019). Dynein Light Chain DLC-1 Facilitates the Function of the Germline Cell Fate Regulator GLD-1 in. *Genetics* 211, 665-681.
- [173] Imig, J., Kanitz, A. and Gerber, A.P. (2012). RNA regulons and the RNA-protein interaction network. *Biomol Concepts* 3, 403-14.
- [174] Nusch, M. and Eckmann, C.R. (2013). Translational control in the *Caenorhabditis elegans* germ line. *Adv Exp Med Biol* 757, 205-47.
- [175] Pazdernik, N. and Schedl, T. (2013). Introduction to germ cell development in *Caenorhabditis elegans*. *Adv Exp Med Biol* 757, 1-16.
- [176] Zhang, B., Gallegos, M., Puoti, A., Durkin, E., Fields, S., Kimble, J. and Wickens, M.P. (1997). A conserved RNA-binding protein that regulates sexual fates in the *C. elegans* hermaphrodite germ line. *Nature* 390, 477-84.
- [177] Crittenden, S.L. et al. (2002). A conserved RNA-binding protein controls germline stem cells in *Caenorhabditis elegans*. *Nature* 417, 660-3.
- [178] Hansen, D., Wilson-Berry, L., Dang, T. and Schedl, T. (2004). Control of the proliferation versus meiotic development decision in the *C. elegans* germline through regulation of GLD-1 protein accumulation. *Development* 131, 93-104.
- [179] Kadyk, L.C. and Kimble, J. (1998). Genetic regulation of entry into meiosis in *Caenorhabditis elegans*. *Development* 125, 1803-13.
- [180] Tocchini, C., Keusch, J.J., Miller, S.B., Finger, S., Gut, H., Stadler, M.B. and Ciosk, R. (2014). The TRIM-NHL protein LIN-41 controls the onset of developmental plasticity in *Caenorhabditis elegans*. *PLoS Genet* 10, e1004533.
- [181] Seydoux, G. (2018). The P Granules of *C. elegans*: A Genetic Model for the Study of RNA-Protein Condensates. *J Mol Biol*

- [182] Wright, J.E., Gaidatzis, D., Senften, M., Farley, B.M., Westhof, E., Ryder, S.P. and Ciosk, R. (2011). A quantitative RNA code for mRNA target selection by the germline fate determinant GLD-1. *EMBO J* 30, 533-45.
- [183] Jungkamp, A.C., Stoeckius, M., Mecnas, D., Grün, D., Mastrobuoni, G., Kempa, S. and Rajewsky, N. (2011). In vivo and transcriptome-wide identification of RNA binding protein target sites. *Mol Cell* 44, 828-40.
- [184] Spike, C.A., Coetzee, D., Nishi, Y., Guven-Ozkan, T., Oldenbroek, M., Yamamoto, I., Lin, R. and Greenstein, D. (2014). Translational control of the oogenic program by components of OMA ribonucleoprotein particles in *Caenorhabditis elegans*. *Genetics* 198, 1513-33.
- [185] Epstein, E. et al. (2000). Dynein light chain binding to a 3'-untranslated sequence mediates parathyroid hormone mRNA association with microtubules. *J Clin Invest* 105, 505-12.
- [186] Rom, I., Faicevici, A., Almog, O. and Neuman-Silberberg, F.S. (2007). *Drosophila* Dynein light chain (DDLC1) binds to *gurken* mRNA and is required for its localization. *Biochim Biophys Acta* 1773, 1526-33.
- [187] Brenner, S. (1974). The genetics of *Caenorhabditis elegans*. *Genetics* 77, 71-94.
- [188] Novak, P., Wang, X., Ellenbecker, M., Feilzer, S. and Voronina, E. (2015). Splicing Machinery Facilitates Post-Transcriptional Regulation by FBFs and Other RNA-Binding Proteins in *Caenorhabditis elegans* Germline. *G3 (Bethesda)* 5, 2051-9.
- [189] Voronina, E., Paix, A. and Seydoux, G. (2012). The P granule component PGL-1 promotes the localization and silencing activity of the PUF protein FBF-2 in germline stem cells. *Development* 139, 3732-40.
- [190] Krueger, F. (2015) Trim Galore!: A wrapper tool around Cutadapt and FastQC to consistently apply quality and adapter trimming to FastQ files. <https://github.com/krueger/trim-galore>
- [191] Langmead, B. and Salzberg, S.L. (2012). Fast gapped-read alignment with Bowtie 2. *Nat Methods* 9, 357-9.
- [192] Dobin, A. et al. (2013). STAR: ultrafast universal RNA-seq aligner. *Bioinformatics* 29, 15-21.
- [193] Love, M.I., Huber, W. and Anders, S. (2014). Moderated estimation of fold change and dispersion for RNA-seq data with DESeq2. *Genome Biol* 15, 550.
- [194] Bailey, T.L. (2011). DREME: motif discovery in transcription factor ChIP-seq data. *Bioinformatics* 27, 1653-9.
- [195] Grant, C.E., Bailey, T.L. and Noble, W.S. (2011). FIMO: scanning for occurrences of a given motif. *Bioinformatics* 27, 1017-8.
- [196] Dorsett, M. and Schedl, T. (2009). A role for dynein in the inhibition of germ cell proliferative fate. *Mol Cell Biol* 29, 6128-39.
- [197] Kershner, A.M., Shin, H., Hansen, T.J. and Kimble, J. (2014). Discovery of two GLP-1/Notch target genes that account for the role of GLP-1/Notch

- signaling in stem cell maintenance. *Proc Natl Acad Sci U S A* 111, 3739-44.
- [198] Morthorst, T.H. and Olsen, A. (2013). Cell-nonautonomous inhibition of radiation-induced apoptosis by dynein light chain 1 in *Caenorhabditis elegans*. *Cell Death Dis* 4, e799.
- [199] Angeles-Albores, D., N Lee, R.Y., Chan, J. and Sternberg, P.W. (2016). Tissue enrichment analysis for *C. elegans* genomics. *BMC Bioinformatics* 17, 366.
- [200] Ortiz, M.A., Noble, D., Sorokin, E.P. and Kimble, J. (2014). A new dataset of spermatogenic vs. oogenic transcriptomes in the nematode *Caenorhabditis elegans*. *G3 (Bethesda)* 4, 1765-72.
- [201] Sharifnia, P. and Jin, Y. (2014). Regulatory roles of RNA binding proteins in the nervous system of *C. elegans*. *Front Mol Neurosci* 7, 100.
- [202] Kiltschewskij, D. and Cairns, M. (2017) Post-Transcriptional Mechanisms of Neuronal Translational Control in Synaptic Plasticity, *InTech*
- [203] Antonacci, S. et al. (2015). Conserved RNA-binding proteins required for dendrite morphogenesis in *Caenorhabditis elegans* sensory neurons. *G3 (Bethesda)* 5, 639-53.
- [204] Bernstein, D., Hook, B., Hajarnavis, A., Opperman, L. and Wickens, M. (2005). Binding specificity and mRNA targets of a *C. elegans* PUF protein, FBF-1. *RNA* 11, 447-58.
- [205] Li, W., Yi, P. and Ou, G. (2015). Somatic CRISPR-Cas9-induced mutations reveal roles of embryonically essential dynein chains in *Caenorhabditis elegans* cilia. *J Cell Biol* 208, 683-92.
- [206] Clark, S. et al. (2018). Multivalency regulates activity in an intrinsically disordered transcription factor. *Elife* 7
- [207] Berggård, T., Linse, S. and James, P. (2007). Methods for the detection and analysis of protein-protein interactions. *Proteomics* 7, 2833-42.
- [208] Nooren, I.M. and Thornton, J.M. (2003). Diversity of protein-protein interactions. *EMBO J* 22, 3486-92.
- [209] Patil, A., Kinoshita, K. and Nakamura, H. (2010). Hub promiscuity in protein-protein interaction networks. *Int J Mol Sci* 11, 1930-43.
- [210] De Las Rivas, J. and Fontanillo, C. (2010). Protein-protein interactions essentials: key concepts to building and analyzing interactome networks. *PLoS Comput Biol* 6, e1000807.
- [211] Vangindertael, J., Camacho, R., Sempels, W., Mizuno, H., Dedeker, P. and Janssen, K.P.F. (2018). An introduction to optical super-resolution microscopy for the adventurous biologist. *Methods Appl Fluoresc* 6, 022003.
- [212] Veeraraghavan, R. and Gourdie, R.G. (2016). Stochastic optical reconstruction microscopy-based relative localization analysis (STORM-RLA) for quantitative nanoscale assessment of spatial protein organization. *Mol Biol Cell* 27, 3583-3590.

- [213] Thymiakou, E. and Episkopou, V. (2011). Detection of signaling effector-complexes downstream of bmp4 using PLA, a proximity ligation assay. *J Vis Exp*
- [214] Wang, S., Yoo, S., Kim, H.Y., Wang, M., Zheng, C., Parkhouse, W., Krieger, C. and Harden, N. (2015). Detection of in situ protein-protein complexes at the Drosophila larval neuromuscular junction using proximity ligation assay. *J Vis Exp*, 52139.
- [215] Algar, W.R., Hildebrandt, N., Vogel, S.S. and Medintz, I.L. (2019). FRET as a biomolecular research tool - understanding its potential while avoiding pitfalls. *Nat Methods* 16, 815-829.
- [216] Kodama, Y. and Hu, C.D. (2012). Bimolecular fluorescence complementation (BiFC): a 5-year update and future perspectives. *Biotechniques* 53, 285-98.
- [217] Piston, D.W. and Kremers, G.J. (2007). Fluorescent protein FRET: the good, the bad and the ugly. *Trends Biochem Sci* 32, 407-14.
- [218] Hiatt, S.M., Shyu, Y.J., Duren, H.M. and Hu, C.D. (2008). Bimolecular fluorescence complementation (BiFC) analysis of protein interactions in *Caenorhabditis elegans*. *Methods* 45, 185-91.
- [219] Söderberg, O., Leuchowius, K.J., Gullberg, M., Jarvius, M., Weibrecht, I., Larsson, L.G. and Landegren, U. (2008). Characterizing proteins and their interactions in cells and tissues using the in situ proximity ligation assay. *Methods* 45, 227-32.
- [220] Day, N.J., Ellenbecker, M. and Voronina, E. (2018). *Caenorhabditis elegans* DLC-1 associates with ribonucleoprotein complexes to promote mRNA regulation. *FEBS Lett* 592, 3683-3695.
- [221] Hird, S.N. and White, J.G. (1993). Cortical and cytoplasmic flow polarity in early embryonic cells of *Caenorhabditis elegans*. *J Cell Biol* 121, 1343-55.
- [222] Golden, A. (2000). Cytoplasmic flow and the establishment of polarity in *C. elegans* 1-cell embryos. *Curr Opin Genet Dev* 10, 414-20.
- [223] Tenlen, J.R., Molk, J.N., London, N., Page, B.D. and Priess, J.R. (2008). MEX-5 asymmetry in one-cell *C. elegans* embryos requires PAR-4- and PAR-1-dependent phosphorylation. *Development* 135, 3665-75.
- [224] Wu, Y., Han, B., Li, Y., Munro, E., Odde, D.J. and Griffin, E.E. (2018). Rapid diffusion-state switching underlies stable cytoplasmic gradients in the. *Proc Natl Acad Sci U S A* 115, E8440-E8449.
- [225] Wu, Y., Zhang, H. and Griffin, E.E. (2015). Coupling between cytoplasmic concentration gradients through local control of protein mobility in the *Caenorhabditis elegans* zygote. *Mol Biol Cell* 26, 2963-70.
- [226] Wu, Y., Han, B., Gauvin, T.J., Smith, J., Singh, A. and Griffin, E.E. (2019). Single-molecule dynamics of the P granule scaffold MEG-3 in the *Caenorhabditis elegans* zygote. *Mol Biol Cell* 30, 333-345.
- [227] Spike, C.A., Bader, J., Reinke, V. and Strome, S. (2008). DEPS-1 promotes P-granule assembly and RNA interference in *C. elegans* germ cells. *Development* 135, 983-93.

- [228] Kawasaki, I., Shim, Y.H., Kirchner, J., Kaminker, J., Wood, W.B. and Strome, S. (1998). PGL-1, a predicted RNA-binding component of germ granules, is essential for fertility in *C. elegans*. *Cell* 94, 635-45.
- [229] Spike, C. et al. (2008). Genetic analysis of the *Caenorhabditis elegans* GLH family of P-granule proteins. *Genetics* 178, 1973-87.
- [230] Kuznicki, K.A., Smith, P.A., Leung-Chiu, W.M., Estevez, A.O., Scott, H.C. and Bennett, K.L. (2000). Combinatorial RNA interference indicates GLH-4 can compensate for GLH-1; these two P granule components are critical for fertility in *C. elegans*. *Development* 127, 2907-16.
- [231] Hanazawa, M., Yonetani, M. and Sugimoto, A. (2011). PGL proteins self associate and bind RNPs to mediate germ granule assembly in *C. elegans*. *J Cell Biol* 192, 929-37.
- [232] Kawasaki, I. et al. (2004). The PGL family proteins associate with germ granules and function redundantly in *Caenorhabditis elegans* germline development. *Genetics* 167, 645-61.
- [233] Amiri, A., Keiper, B.D., Kawasaki, I., Fan, Y., Kohara, Y., Rhoads, R.E. and Strome, S. (2001). An isoform of eIF4E is a component of germ granules and is required for spermatogenesis in *C. elegans*. *Development* 128, 3899-912.
- [234] Updike, D.L. and Strome, S. (2009). A genomewide RNAi screen for genes that affect the stability, distribution and function of P granules in *Caenorhabditis elegans*. *Genetics* 183, 1397-419.
- [235] Voronina, E. and Seydoux, G. (2010). The *C. elegans* homolog of nucleoporin Nup98 is required for the integrity and function of germline P granules. *Development* 137, 1441-50.
- [236] Bailey, T.L. and Elkan, C. (1994). Fitting a mixture model by expectation maximization to discover motifs in biopolymers. *Proc Int Conf Intell Syst Mol Biol* 2, 28-36.
- [237] Park, Y.N., Glover, R.A., Daniels, K.J. and Soll, D.R. (2016). Generation and Validation of Monoclonal Antibodies Against the Maltose Binding Protein. *Monoclon Antib Immunodiagn Immunother* 35, 104-8.
- [238] Bolte, S. and Cordelières, F.P. (2006). A guided tour into subcellular colocalization analysis in light microscopy. *J Microsc* 224, 213-32.
- [239] Day, N.J., Wang, X. and Voronina, E. (2020). In Situ Detection of Ribonucleoprotein Complex Assembly in the *C. elegans* Germline using Proximity Ligation Assay. *J Vis Exp*
- [240] Simonis, N. et al. (2009). Empirically controlled mapping of the *Caenorhabditis elegans* protein-protein interactome network. *Nat Methods* 6, 47-54.
- [241] Li, S. et al. (2004). A map of the interactome network of the metazoan *C. elegans*. *Science* 303, 540-3.
- [242] Jones, A.R., Francis, R. and Schedl, T. (1996). GLD-1, a cytoplasmic protein essential for oocyte differentiation, shows stage- and sex-specific

- expression during *Caenorhabditis elegans* germline development. *Dev Biol* 180, 165-83.
- [243] Wang, L., Eckmann, C.R., Kadyk, L.C., Wickens, M. and Kimble, J. (2002). A regulatory cytoplasmic poly(A) polymerase in *Caenorhabditis elegans*. *Nature* 419, 312-6.
- [244] Tabara, H., Hill, R.J., Mello, C.C., Priess, J.R. and Kohara, Y. (1999). *pos-1* encodes a cytoplasmic zinc-finger protein essential for germline specification in *C. elegans*. *Development* 126, 1-11.
- [245] Patterson, J.R., Wood, M.P. and Schisa, J.A. (2011). Assembly of RNP granules in stressed and aging oocytes requires nucleoporins and is coordinated with nuclear membrane blebbing. *Dev Biol* 353, 173-85.
- [246] Hird, S.N., Paulsen, J.E. and Strome, S. (1996). Segregation of germ granules in living *Caenorhabditis elegans* embryos: cell-type-specific mechanisms for cytoplasmic localisation. *Development* 122, 1303-12.
- [247] Zhang, Y. et al. (2009). SEPA-1 mediates the specific recognition and degradation of P granule components by autophagy in *C. elegans*. *Cell* 136, 308-21.
- [248] Zhang, G., Wang, Z., Du, Z. and Zhang, H. (2018). mTOR Regulates Phase Separation of PGL Granules to Modulate Their Autophagic Degradation. *Cell* 174, 1492-1506.e22.
- [249] Saha, S. et al. (2016). Polar Positioning of Phase-Separated Liquid Compartments in Cells Regulated by an mRNA Competition Mechanism. *Cell* 166, 1572-1584.e16.
- [250] Updike, D.L., Hachey, S.J., Kreher, J. and Strome, S. (2011). P granules extend the nuclear pore complex environment in the *C. elegans* germ line. *J Cell Biol* 192, 939-48.
- [251] Aramburu, I.V. and Lemke, E.A. (2017). Floppy but not sloppy: Interaction mechanism of FG-nucleoporins and nuclear transport receptors. *Semin Cell Dev Biol* 68, 34-41.
- [252] Strome, S. and Wood, W.B. (1983). Generation of asymmetry and segregation of germ-line granules in early *C. elegans* embryos. *Cell* 35, 15-25.
- [253] Li, S., Yang, P., Tian, E. and Zhang, H. (2013). Arginine methylation modulates autophagic degradation of PGL granules in *C. elegans*. *Mol Cell* 52, 421-33.
- [254] Hofweber, M. and Dormann, D. (2019). Friend or foe-Post-translational modifications as regulators of phase separation and RNP granule dynamics. *J Biol Chem* 294, 7137-7150.
- [255] Schmidt, D.J., Rose, D.J., Saxton, W.M. and Strome, S. (2005). Functional analysis of cytoplasmic dynein heavy chain in *Caenorhabditis elegans* with fast-acting temperature-sensitive mutations. *Mol Biol Cell* 16, 1200-12.